Mass Spectrometry-Based Investigation of the Adaptive Response of Membrane Lipids to Glucose Stress in *C. elegans*

by

Mark Andy Xatse

A dissertation submitted to the faculty of
WORCESTER POLYTECHNIC INSTITUTE
In partial fulfillment of the requirements for the
Doctor of Philosophy in Biochemistry

Approved by

Carissa Perez Olsen, Ph.D. Advisor (WPI, CBC)	**Suzanne Scarlata, Ph.D**. Chairperson (WPI, CBC)
José Argüello, Ph.D. (WPI, CBC)	**Amy Walker, Ph.D.** (UMASS)

ACKNOWLEDGMENTS

Completing this dissertation is a testament to the collective support and guidance I've received from advisors, colleagues, friends, and family during my journey as a graduate student. I am deeply grateful for each individual who has shaped my academic and personal growth.

I want to express profound gratitude and thanks to my advisor, Dr. Carissa Olsen, whose unwavering encouragement and inspiration have been the bedrock of my academic pursuits. Thank you for giving me the opportunity to be in WPI and providing steadfast mentorship through my successes and failures. I would also like to thank my thesis committee members, Dr. Suzanne Scarlata, Dr. José Argüello, and Dr. Amy Walker, for their invaluable insight and perspectives regarding all aspects of my projects over the years.

I would like to appreciate and thank past and present members of the Olsen group who have not only been valuable colleagues in the lab but have also become amazing friends. Enormous thanks to Dr. Andre Vieira, who guided me in my early years in graduate school and gave me the foundation necessary to complete these projects. Thanks to Dr. Nadia Sultana, who trained me in mass spectrometry instrumentation and analysis. Thank you to my fellow graduate students, Alvan Okechukwu and Paige Silvia, who have contributed to my projects. Thanks to the many undergraduates who contributed to this work and provided me with opportunities to become a mentor myself.

Finally, I would like to thank my family for their unconditional love, support, and sacrifice. I would like to express my profound gratitude to my wife, Tiffany, for her unwavering support for me to pursue this degree. My heartfelt gratitude to my little Jayne, who has endured many nights without her "daddy" around. I am incredibly grateful to my family in California, who have provided tremendous support for me. Their encouragement has been a constant source of motivation, propelling me forward in my studies. I am grateful to my family in Ghana for their encouragement and help. Their words and actions have crossed continents to uplift and sustain me. I am highly thankful to my brother Jerome for all his sacrifices for my education.

TABLE OF CONTENTS

LIST OF FIGURES

LIST OF ABBREVIATIONS

Cer	Ceramide
CGT	Ceramide glucosyltransferase
CI	Chemical Ionization
DDA	Data dependent acquisition
EI	Electron impact
ESI	Electrospray ionization
FA	Fatty acids
GC/MS	Gas chromatograph coupled with mass spectrometer
GlcCer	Glucosylceramide
HG	High growth media
HPLC-MS/MS	High performance liquid chromatography tandem mass spectrometer
IGLR-2	Immunoglobulin (Ig)-like domain and several leucine-rich repeats
mmBCFA	Monomethyl branched-chain fatty acids
MUFA	Monounsaturated fatty acids
NGM+CI	Nematode growth media with carbenicillin and Isopropyl ß-D-1-thiogalactopyranoside
oxL	Oxidized lipids
PAQR-2	Progestin and adipoQ receptor
PC	Phosphatidylcholine
PE	Phosphatidylethanolamine
PI	Phosphatidylinositol

PL	Phospholipid
PS	Phosphatidylserine
PUFA	Polyunsaturated fatty acids
RNAi	RNA interference
SFA	Saturated fatty acids
SM	Sphingomyelin
TORC	Target of rapamycin complex
UFA	Unsaturated fatty acids

DISSERTATION ABSTRACT

The unique composition of lipids that build biological membranes dramatically impacts an organism's cellular function and physiology. Environmental and dietary changes can influence the membrane lipid composition, leading to either perturbations in the membrane composition or adaptive changes to preserve membrane integrity and optimal cellular function. One of such typical stress is an elevated glucose diet, which is linked with alterations in lipid metabolism. This thesis employed targeted mass spectrometry, isotope labeling strategies, lifespan assays, and other biochemical methodologies to elucidate the membrane response mechanisms to glucose-induced stress in *C. elegans.* In doing so, we have uncovered novel adaptive responses to glucose stress in the nematodes critical for maintaining membrane homeostasis. We demonstrated that monomethyl branched-chain fatty acids are essential for the response to glucose stress by serving as precursors to glucosylceramide production. Using targeted lipidomics, we identified a specific glucosylceramide significantly upregulated with glucose stress in wild-type animals. Notably, compromising the production of glucosylceramides leads to premature death in glucose-fed animals. We posit that glucosylceramides mediate signaling events, potentially through the TORC complex. Furthermore, we investigated the underlying stress caused by glucose and uncovered the critical need for active polyunsaturated fatty acid (PUFA) synthesis under glucose-induced stress conditions. This is attributed to the damage of PUFAs caused by glucose-induced oxidative stress, leading to the accumulation of oxidized lipids. Notably, the accumulation of oxidized lipids is selectively higher in phosphatidylethanolamine (PE), suggesting that oxidative stress induced by glucose occurs in specific localizations where PE is particularly enriched. This dissertation underscores the intricate interplay between glucose stress, membrane lipid dynamics, and physiological outcomes, providing a mechanistic understanding of metabolic adaptability in response to nutritional stress.

CHAPTER 1 - GENERAL INTRODUCTION

1.1 The membrane bilayer

The tendency for lipids to self-aggregate to form a membrane barrier is the basis for the formation of cells and discrete organelles [1,2]. The amphipathic nature of the lipids that make up the membranes drives their self-assembly into a bilayer where the hydrophilic head group of the lipid faces the environment, and the hydrophobic core is embedded within the bilayer. Beyond serving as a protective barrier, cell membranes function as a dynamic interface facilitating several cellular functions [3,4]. The membrane mainly comprises proteins and a diverse pool of lipids, including phospholipids, sphingolipids, and sterols (Figure 1.1). The diverse pool of lipids significantly contributes to the structure and function of membranes by influencing the membrane's biophysical properties, such as fluidity, thickness, viscosity, curvature, packing, and surface charge [5,6]. Consequently, alterations in membrane lipid composition can influence the membranes' functionality [7,8].

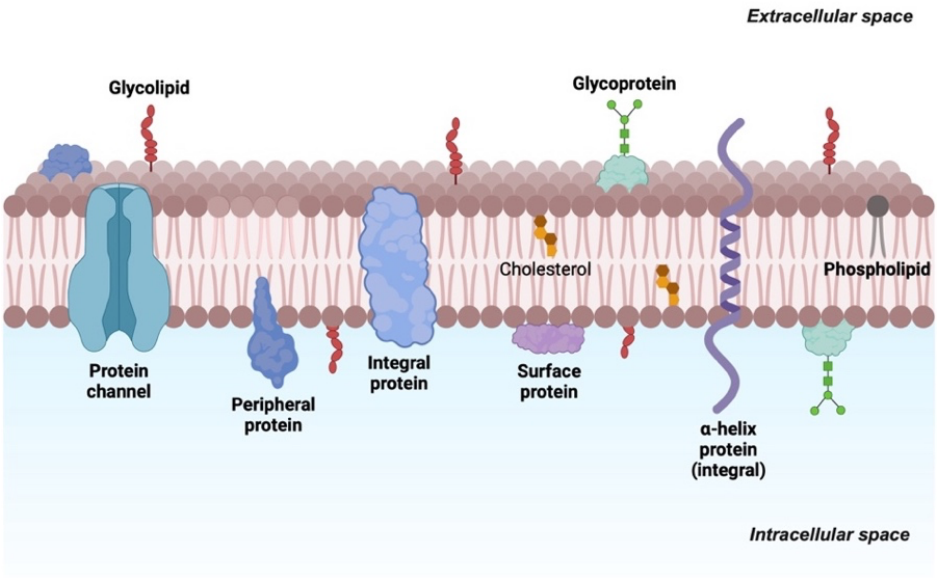

Figure 1.1 Structure of membrane bilayer.
Lipids self-assemble to form a bilayer. The membrane consists of phospholipids, glycolipids, cholesterol, and several proteins that facilitate various chemical reactions. This figure was made using BioRender.

The membrane lipid composition is not only established on formation but must be maintained throughout the life of an organism because membrane lipids are constantly consumed by processes such as vesicle trafficking, damage, and degradation [9–11]. In addition to maintaining a membrane over time, the lipid composition of cell membranes is influenced by dietary conditions such as high glucose or high saturated fat diet and environmental conditions such as hypoxia, cold, heat, osmotic, or oxidative stress. Therefore, organisms have complex mechanisms, including membrane sensors and transcriptional factors that maintain the composition of membrane lipids for optimal function [4,7,12–15]. Without these mechanisms in place, membrane integrity will be severely compromised, impacting cellular activity and increasing the vulnerability of organisms to diseases and death [16,17]. In fact, in many diseased states, such as cancer, diabetes, and Alzheimer's, membrane lipid composition is severely compromised [18–21]. Delving into the intricacies of membrane biology holds the promise of unveiling novel perspectives on the role of membrane lipids in diseases. This pursuit opens avenues for identifying new therapeutic targets and paves the way for enhanced drug delivery strategies.

1.2 Diversity of membrane lipids

Membrane structure, organization, and plasticity are impacted by the diverse lipid species that make up the membranes [4,5]. The diversity in the lipid composition of membranes can be defined in two main ways. Firstly, the chemical diversity which arises from the different combinations of amphipathic heads with various kinds of fatty acids via different chemical linkages [11,18]. Secondly, the compositional diversity which stems from the distribution of lipids across organelles, cells, tissue, or organs that confer a unique membrane composition necessary for optimal function [22–24]. Both chemical and compositional diversity are critical for the overall functionality of the membrane. As elegantly stated in a review by Harayama and Riezman, "Chemical diversity confers specific properties on lipids, and compositional diversity affects the collective behavior of lipids in membranes" [25].

1.2.1 Chemical diversity of membrane lipids

Membrane lipids exhibit remarkable chemical diversity, which is fundamental to their role in forming the structure and influencing the biophysical properties of cellular membranes. This diversity arises from the various chemical building blocks that make up these lipids. This section describes the chemical diversity of major membrane lipids and how they impact the structure and biophysical properties of the membrane [2,26].

Phospholipids are major components of the membrane and are amphipathic molecules with a hydrophobic tail composed of two fatty acyl chains linked to the *sn*-1 and *sn*-2 positions of a glycerol backbone. The hydrophilic head group of a phospholipid is linked to the *sn*-3 position of the glycerol via a phosphodiester bond [11,18]. There are a few polar molecules that can constitute the headgroup, with phosphatidylcholine (PC) and phosphatidylethanolamine (PE) being the major species in most organisms [5,10,27](Figure 1.2). In addition, other headgroups, such as serine, inositol, and glycerol, are also present, albeit at a relatively low abundance, and play specialized roles in signaling and apoptotic pathways [2,4]. The type of headgroup present in the membrane confers unique properties and functionality to the membrane. PC lipids generally have a cylindrical geometry and tend to self-assemble in bilayers (Figure 1.3). PE lipids have a smaller headgroup to fatty acyl ratio and tend to form a cone that induces a negative curvature on the membrane (Figure 1.3). This curvature is essential for processes such as exocytosis and membrane fusion events[4,28,29]. Phosphatidylserine (PS) and phosphatidylinositol (PI) are negatively charged and determine the overall surface charge of the membrane, making them essential for membrane protein interactions [28,30].

In addition, the type of linkage to the headgroup also accounts for a degree of variations in the membrane lipids. In a typical phospholipid, an ester linkage connects FA to the glycerol backbone at the *sn*-1 position. However, in some cases, this is an ether linkage, generating a class of phospholipids known as plasmalogens [31,32]. Depending on the type of ether linkage, plasmalogen can either be a plasmanyl, -O (alkyl ether) or a plasmenyl, -P (vinyl-ether) phospholipid (Figure 1.2). Plasmalogens within cellular membranes are posited to serve as sacrificial antioxidants. Unlike phospholipids, plasmalogens react faster and form less vicious oxidative products when

attacked by reactive oxygen species. This unique property highlights their significance in cellular defense mechanisms against oxidative stress [33,34].

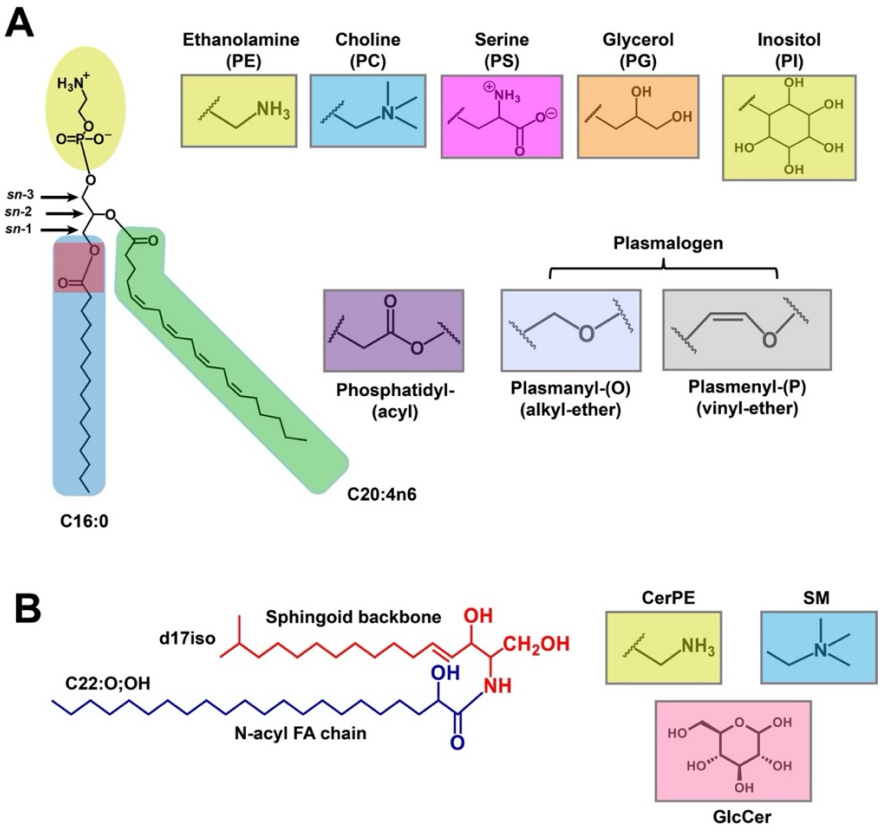

Figure 1.2 Chemical diversity of membrane lipids.
A) Phospholipids are made up of glycerol backbone with two fatty acids at the *sn-1* and *sn-2* position and a headgroup at *sn-3*. The FA can be saturated (e.g., C16:0) or unsaturated (e.g., C20:4n6). FA is notated with the nomenclature CX:YnZ where X indicates the number of carbons in the FA, and Y shows the number of double bonds at position Z. The headgroup comprises different chemical groups such as ethanolamine, choline, serine, glycerol, and inositol. Additional diversity occurs from the type of linkage in the *sn-1* position with an acyl linkage in canonical phospholipids and ether linkages in plasmalogens. **B)** Sphingolipids are made up of a sphingoid backbone attached to an N-acyl FA to form ceramide. FA and sphingoid backbone can have one or more hydroxyl groups. Headgroups can be made of chemical groups such as glucose, ethanolamine, and choline.

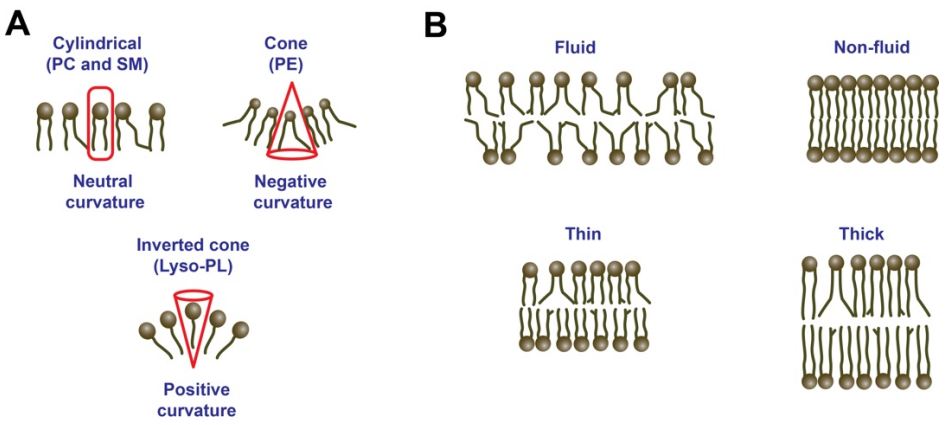

Figure 1.3 The impact of chemical diversity on membrane biophysical properties.
A) Lipids with an equal area ratio of headgroup to fatty acyl chains, such as phosphatidylcholine (PC) and sphingomyelin (SM), have a neutral shape in the membrane. Conversely, lipids with a smaller headgroup to fatty acyl chain area ratio, such as phosphatidylethanolamine (PE), have a cone shape that induces a negative curvature on the membrane. Lysophospholipids have an inverted cone shape because the large head group area relative to the fatty acyl tail induces a positive curvature on the membrane. **B)** A membrane enriched with UFA tends to pack loosely and form fluid membranes compared to those enriched in SFA, which are less fluid. Additionally, chain length also impacts the membrane thickness, with longer chain FA increasing membrane thickness compared to shorter chain lipids.

Much of the diversity in membrane lipids stems from the type of fatty acid (FA) attached to the glycerol backbone. The FA available in the membrane varies in length from 12 to 22 carbons and in degree of unsaturation from 0 to 6 double bonds in most organisms [3,35]. The FA can be saturated (SFA) with no double bond, monounsaturated (MUFA) with one double bond, or polyunsaturated (PUFA) with two or more double bonds. PUFA can further be divided into two subclasses, omega-3 (n-3) and omega-6 (n-6), depending on the position of the double bond. Lipids with SFA pack at higher densities and tend to form non-fluid gel phases, while a cis-double bond in the acyl chain generates a kink or bend that reduces the packing density of acyl chains. The reduced acyl packing promotes the formation of fluid membranes at physiological temperature (Figure 1.3) [3,7]. Therefore, maintaining an appropriate ratio of SFA, MUFA, and PUFA is critical for maintaining the optimum physicochemical properties such as membrane fluidity, packing, and lateral pressure that is critical for many membrane activities such as protein-protein interactions and membrane permeability [4,36]. Finally, in addition to intact PL, lysophospholipids (present at low concentrations) contain only one acyl chain and are produced by partial hydrolysis of intact PL by

phospholipases. Lysophospholipids typically have a large ratio of head group area to acyl chain area and, therefore, display different properties than their original phospholipids [37]. Lysophospholipids pack in highly curved structures and introduce packing stress that can impact membrane integrity and influence processes such as membrane protein insertion and conformation (Figure 1.3) [38,39].

Sphingolipids are also a highly diverse group of lipids in the membrane lipid landscape. Sphingolipids are characterized by a sphingoid backbone made up of a hydrocarbon chain attached to an amino and hydroxyl group (Figure 1.2) [40,41]. The sphingoid backbone is typically linked to fatty acids that form ceramides. The fatty acyl chain attached to the sphingoid backbone can range from 14-36 carbons and are usually saturated or monounsaturated [42,43]. Ceramides can further be derivatized by adding chemical groups to form simple sphingolipids such as sphingomyelin, glucosylceramides, and galactosylceramides (Figure 1.2). In addition, sphingolipids can further be modified by the additional sugar groups that can generate complex glycosphingolipids [40]. Glycosphingolipids are enriched in lipid raft domains, which serve as a platform for the recruitment of proteins and signaling molecules critical to several biochemical processes. Therefore, sphingolipids influence many cellular processes, such as cell growth and proliferation, neuronal development, nutrient sensing, cell signaling, apoptosis, intracellular transport, and protein sorting [40,44,45]. Like phospholipids, some lyso-sphingolipids are present in small abundance and are associated with signaling events [40].

In summary, the vast chemical diversity inherent in lipid species culminates in the formation of many distinct lipid molecules. Each lipid's unique chemical structure imparts specific properties to cellular membranes, which are crucial for their optimal functioning.

1.2.2 Compositional diversity

Although the chemical diversity of membrane lipids leads to the generation of more than 1000 different lipid species, these lipids are not distributed homogenously throughout an organism [2,5]. Instead, their distribution is finely tuned to endow subcellular organelles, cells, and organs with specific physicochemical properties critical for optimal function. In this section, I highlight a few examples of how lipids are distributed and impact organisms on the cellular and organ levels.

Each organelle has a unique membrane lipid composition at the subcellular level, as summarized in Figure 1.4. The ER is mainly made of unsaturated lipids and less cholesterol [2,4]. The composition of lipids is ideal for the ER as the loosely packed lipids allow for the insertion of newly synthesized lipids and proteins. In contrast, the plasma membrane comprises tightly packed lipids, such as sphingomyelin and cholesterol, that can resist mechanical stress. In addition, the plasma membrane contains a significant amount of PC and PE as well. Similarly, the Golgi contains significant cholesterol levels and is the main site for the synthesis and trafficking of sphingolipids. In addition, membranes of the Golgi contain substantial amounts of PE and PI lipids. Endosomes derived from plasma membranes are enriched in bis(monoacylglycerol)phosphate (BMP) and PIs, essential for vesicle trafficking and protein-lipid interactions [2,5,24]. Finally, compared to other organelles, the mitochondria are particularly enriched in PE, which is ideal for the highly curved structure of the mitochondrial membrane.

The compositional diversity of membrane lipids is not limited to subcellular organelles but is also reflected in tissues and organs (Figure 1.4B). A recent study by Surma et al. (2021) thoroughly characterized the lipid composition of various organs and tissues in mice using mass spectrometry [46]. The study showed a remarkable distinction in the lipid composition of different organs. Specifically, the brain is enriched in cholesterol, PC, and PE plasmalogen (PE O-). In addition to the high PC and cholesterol, the lipid composition of the lungs is enriched with sphingomyelin and PS. The spleen has a significant amount of PC plasmalogen (PC O-), PI, and PS. Interestingly, the intestine is distinctly characterized by a significant amount of lysophospholipids (LPC and LPE) compared to all other organs. The liver and kidney contain substantial amounts of diacylglycerol (DAG). However, the liver has a considerable amount of PIs compared to the kidney and other

organs. The unique lipid signature of each organ further underscores the impact of the compositional diversity of membranes within an organism.

Collectively, the implications of the compositional diversity of membrane lipids are far-reaching. At the subcellular level, it not only influences the fluidity and permeability of membranes but also affects the interactions with proteins and the transport of molecules [2,4,22]. At a higher organizational level, it shapes the mechanical properties of cells and tissues, impacting processes from nutrient absorption to signal transduction and energy conversion [25,46]. Ultimately, the distribution of these lipid species is a pivotal factor in the optimal function of every biological entity, from the smallest organelle to the most complex organ systems.

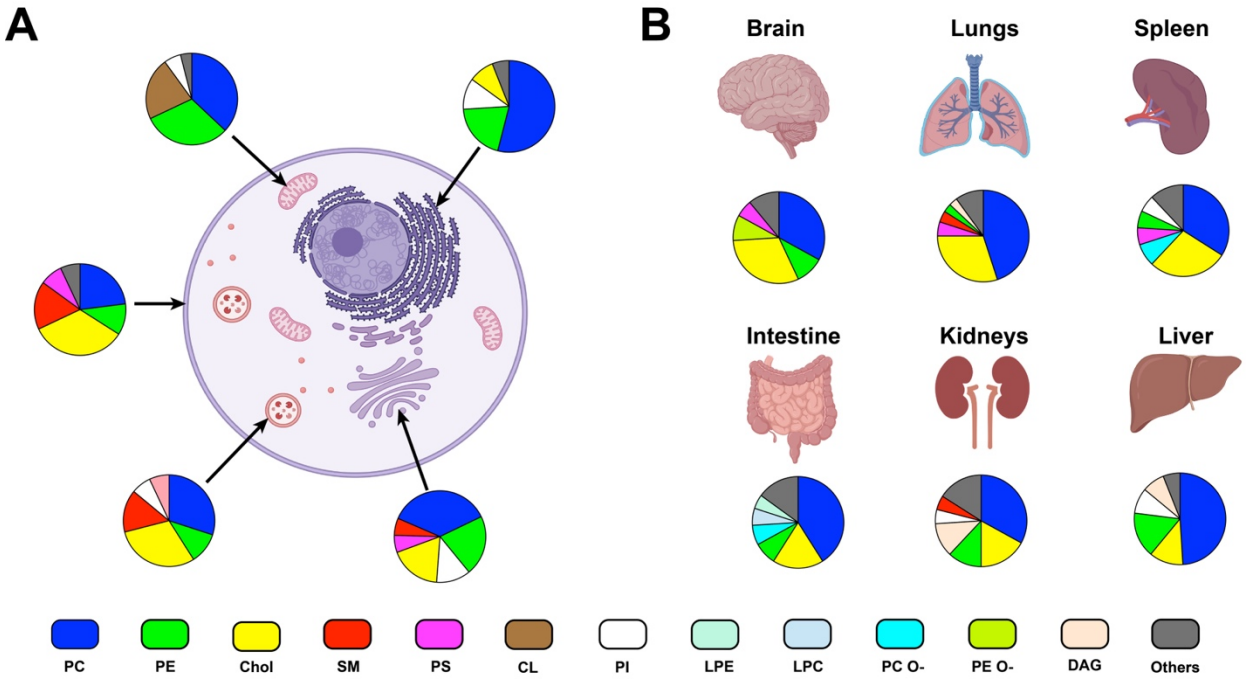

Figure 1.4 Compositional diversity of membrane lipids.
A) Membrane lipid distribution in ER, mitochondria, plasma membrane, endosomes, and Golgi in a mammalian cell. Data was obtained and re-graphed from Van Meer et al. (2009) [2]. **B)** Membrane lipid composition in mice analyzed by mass spectrometry reveals unique lipid signatures in various organs. Adapted from Surma et al. (2021) [46].

1.3 Probing membrane diversity using mass spectrometry

Due to their vast diversity, the membrane lipids are characterized using lipidomics, which combines advanced mass spectrometry, system biology, and biostatistics to address the identification, cellular, and tissue distribution of lipids and related signaling and metabolic pathways [27,47]. Over the last decades, advances in the development of high-resolution and high mass-accuracy mass spectrometry techniques have significantly improved the sensitivity and specificity of lipid detection [48,49]. In addition, coupling MS to gas chromatography (GC) or liquid chromatography (LC) allows the separation of isomeric (species with the same molecular formula but different structure) and isobaric (species that have the same or nearly the same mass but are structurally unrelated). Before subjecting samples to mass spectrometry-based analyses, lipids are typically purified from biological samples. This purification process can be accomplished using either the classical chloroform/methanol extraction method or the more contemporary methyl tert-butyl ether (MTBE) extraction method [42,43]. Further separation of different lipids can be achieved using the solid phase extraction (SPE) column. For sphingolipid analysis, an alkaline hydrolysis step is often carried out after chloroform/methanol or MTBE extraction to hydrolyze all ester bonds, thereby eliminating all phospholipids and glycerolipids that are present in the sample and improving the sensitivity of measuring these sphingolipids [42,43]. This section describes current mass spectrometry techniques employed to map membrane lipid composition and dynamics.

1.3.1 GC/MS analysis of fatty acids

Gas chromatography coupled with mass spectrometry (GC/MS) is a robust analytical technique for analyzing fatty acid composition [11,35]. To analyze fatty acids associated with membrane lipids, total lipids extracted must first be separated using a solid phase extraction (SPE) column, separating the lipids into lipid classes based on their affinity to eluting solvents. Subsequently, fatty acid methyl esters (FAMEs) are generated from each lipid class by the hydrolysis of the head group and glycerol backbone and the subsequent methylation of FA in the presence of methanol and concentrated sulfuric acid [11,35]. This analysis is ideal for thoroughly mapping the FA associated with each lipid class (e.g., FA from phospholipids). However, because the FA are removed from

the parent lipid, the information on head groups and any other FAs attached to the parent lipid is lost [11,35]. Furthermore, FAMEs cannot be generated from sphingolipids and ether-linked lipids as the acidic methylation does not liberate FA from the amide-linked sphingoid backbone and alkyl group [35]. Consequently, analysis of FA is limited to mainly phospholipids and triglycerides.

Following their generation, FAMEs are separated in a GC that uses a very long polar column (e.g., 30 m 5%-phenyl-methylpolysiloxane) that separates FAs based on size and polarity. In addition, this column can also adeptly separate isomeric FAs with the same number of double bonds present within different positions of the carbon chain. Separated FAMEs are detected and quantified in the mass spectrometer, where they are first fragmented in an Electron Impact (EI) or Chemical Ionization (CI) source and subsequently separated by their mass-to-charge ratio (m/z) in a quadrupole mass analyzer. The extensive fragmentation also provides detailed information about the structure of specific FAs, allowing accurate identification [10,11].

1.3.2 LC-MS/MS analysis of intact membrane lipids

The analysis of intact membrane lipids, such as phospholipids and sphingolipids, is typically conducted using liquid chromatography and tandem mass spectrometry (MS/MS) instruments. The use of LC to separate intact lipids before MS analysis is crucial and provides a few advantages. LC separation enables the efficient resolution of multiple lipid species with identical elemental composition and exact mass, which cannot be distinguished in a mass spectrometer alone [27,48]. Furthermore, separating lipid species based on their physicochemical properties reduces ion-suppression effects and matrix interference and improves the reproducibility of the analysis. Various LC methodologies typically employed in lipidomics are normal-phase LC (NPLC), hydrophilic interaction chromatography (HILIC), and reversed-phase LC (RPLC) [27,48].

NPLC utilizes polar stationary and non-polar mobile phases to separate lipid species based on polarity. NPLC is suitable for separating unipolar lipids such as triglycerides, diacylglycerides, and cholesterol. However, some of the non-polar mobile phase (e.g., hexane) utilized in this type of separation makes NPLC unsuitable for electrospray ionization (ESI), typically used for intact lipid analysis because ESI requires a relatively volatile solvent that can accept or donate ions for

efficient ionization [48]. Therefore, for coupling with ESI MS, a mobile phase must be chosen that allows for the formation of ions. HILIC separation offers a better alternative to NPLC as it also separates lipid species based on polarity using a stationary phase made up of silica or functionalized silica and a mobile phase made of water and water-miscible organic solvent [48]. HILIC separation is an effective way to separate various lipid classes within a complex lipid extract. The disadvantage of HILIC separation is that it is not suited for the separation of molecular species within a specific lipid class. RPLC is the most widely adopted technique for lipidomics analysis. RPLC utilizes a non-polar stationary phase and a polar mobile phase to separate lipid species based on their hydrophobicity. RPLC enables the separation of isomeric lipid species based on chain length and unsaturation level. The elution orders of lipids increase as the FA chain length increases, and within lipids with the same fatty acid chain, elution order decreases with an increase in the number of double bonds. Because of the narrow range of elution in RPLC, a mobile phase gradient is typically employed to optimize the separation of several classes of lipids within a single acquisition [11,31,48].

1.3.3 Mass spectrometry of intact membrane lipids

The acquisition of lipidomics data using mass spectrometry can be categorized into untargeted and targeted approaches. Untargeted lipidomics seeks to identify and quantify all the detectable lipids in a sample. This approach allows the identification of novel lipids within a sample, such as lipids related to specific disease conditions. On the other hand, targeted lipidomics is the measurement of a predefined set of lipid species [50,51]. Although targeted lipidomics doesn't allow for the discovery of new lipids, it offers the ability for absolute quantification of a specific lipid. In addition, it is suitable for validating one or several hypotheses based on the predefined lipid list. Lipidomics studies can be carried out in single-stage instruments (such as Time-of-Flight (TOF) and orbitrap) and hybrid instruments (such as quadrupole/QTOF and quadrupole/orbitrap). Hybrid instruments are particularly advantageous for the comprehensive identification of intact membrane lipids, as they offer the capability of tandem mass spectrometry (MS/MS) for characterizing unique lipid species. In these hybrid instruments, lipids separated by LC are first ionized by soft ionization techniques such as ESI, which preserves the intact structure of the lipids. These ionized lipids are

then detected by their intact mass (MS1). Subsequently, in a second round of mass spectrometry (MS2), ionized lipids are fragmented (typically in a collision cell using an inert gas) to generate a unique fingerprint to identify a specific lipid species [52,53].

Tandem mass spectrometry (MS/MS) acquisition provides more detailed information that is ideal for truly identifying and quantifying intact phospholipids and sphingolipids. For instance, the lipid species PE 36:4 is a PE lipid with a total FA carbon length of 36 and a total double bond number of four with a m/z of 738.5094. PE 36:4 can have a FA chain combination comprising several combinations, including, but not limited to, two 18:2 FA or a 16:0 and 20:4 combination. Determining the chain length and combination is impossible with just the m/z of the intact lipid from an MS1 scan. However, with the fragmentation pattern acquired from an MS2 analysis, it is possible to assign chain length combinations for a specific lipid species and the type of headgroup associated with the lipid (Figure 1.5A). Similar to phpspholipids, sphingolipids also exhibit a unique fragmentation pattern that allows the accurate confirmation of the structure of a specific species. For instance, in *C. elegans,* fragmentation of Cer and GlcCer results in a C17iso sphingoid base fragment with a unique product with m/z 250.25 (Figure 1.5B) [54,55]. Because the sphingoid base in *C. elegans* is a C17iso sphingoid base, the *N*-fatty acyl chain can easily be predicted using the intact m/z of GlcCer or Cer species and fragment product of the sphingoid base. Therefore, combining MS1 and MS2 analysis allows us to probe the diversity of membrane lipids thoroughly.

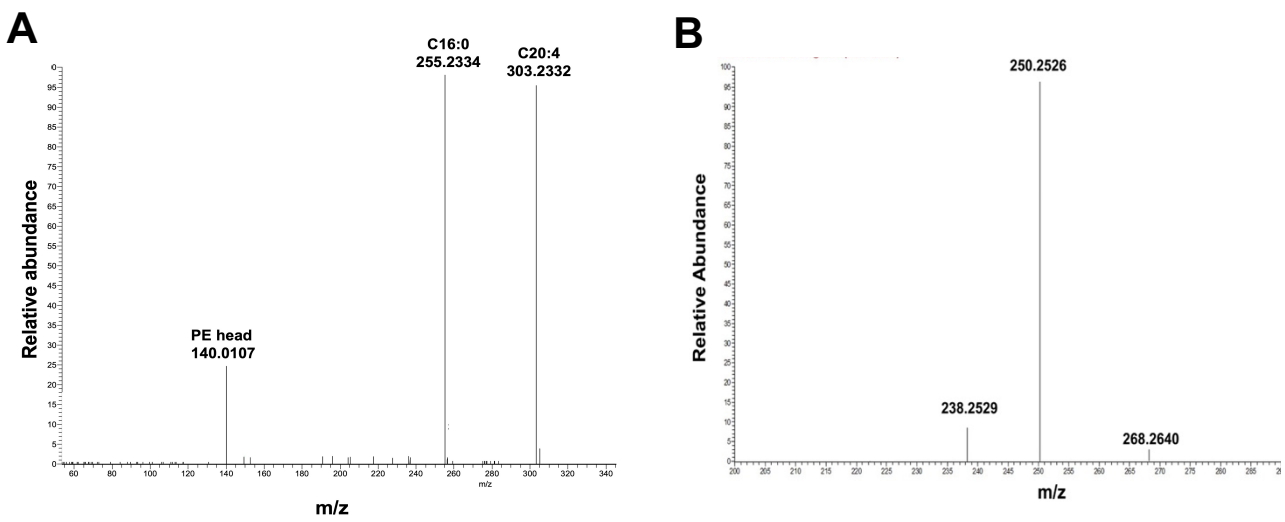

Figure 1.5 Tandem mass spectrometry (MS/MS) provides detailed structure insights of lipids. **A)** The mass spectrum showing the MS2 scan for PE 36:4 (m/z =738.5094). The fragment shows this phospholipid is made up of a 16:0 and 20:4 combination. **B)** The mass spectrum showing the MS2 scan for GlcCer 17:1;O2/22:0;O (m/z = 786.6465). GlcCer (and Cer) fragmentation generates a triplet peak with mass (m/z) 238.2529, 250.2529, and 268.2640, characteristic of a C17:1 sphingoid base found in *C. elegans*. Adapted from Xatse and Olsen 2023 [56].

1.3.4 Stable isotope labeling strategies to monitor membrane dynamics

Advances in mass spectrometry-based techniques have allowed the reliable quantification of membrane lipids. However, changes in the abundance alone of a specific lipid species in the membrane do not provide a complete picture, as these changes can stem from increased production or decreased consumption [57,58]. To understand the dynamic distribution of membrane lipids, flux analysis using stable isotope tracing allows individual lipids' production and consumption rates to be tracked. This approach not only elucidates the dynamics of lipids but also circumvents the dilution effects associated with the vast pool of starting lipids within an organism [11,59]. Consequently, integrating flux measurement with steady measurement provides a comprehensive picture of the composition and dynamics of membrane lipids.

To this end, the Olsen lab and others developed novel ^{13}C and ^{15}N stable isotope labeling strategies to monitor fatty acid tails and intact phospholipid turnover of membrane lipids in *C. elegans,* respectively [10,11,60]. The ^{13}C-label strategy can be used to monitor the dynamics of FA and requires feeding the nematode with a bacteria diet that contains a mixture of ^{12}C and ^{13}C (~1:1). The incorporation of the new carbon in a specific species of FA can be analyzed based on the labeling patterns and correcting for natural abundance of ^{13}C using GC/MS (Figure 1.6A). The labeling pattern describes the shift in mass isotopomer distribution due to the incorporation of ^{13}C isotopes. For example, the FA C16:0, made up of only ^{12}C, has a molecular weight (MW) of 270, which shifts upon being fully labeled with ^{13}C, resulting in a MW of 286. In addition, the isotopomer distribution between 270 – 286 MW indicates C16:0, which is made up of different combinations of ^{12}C and ^{13}C. Using these isotopomer distributions, it is possible to define the origin of FA within the nematode, namely from diet, elongation, maternal, and *de novo* synthesis. Furthermore, using this strategy, the turnover of individual FA into the membrane can be inferred, providing vital information about the dynamics of the membrane. It is worth noting that a limitation of this technique is its dependence on intact parent molecules for monitoring the isotope distribution of a particular fatty acid due to the extensive overlap of isotopically labeled fragment peaks. The use of an Electron Impact (EI) source in the mass spectrometer leads to extensive fragmentation of highly polyunsaturated FA, leading to insufficient detectable parent ions for reliable analysis [59,61].

The dynamics of phospholipids are monitored using a ^{15}N stable isotope labeling strategy (Figure 1.6B). The high diversity of phospholipids and the relatively small difference in MW make the analysis of the ^{13}C stable isotope strategy overly complex for intact phospholipids. Thus, a ^{15}N allows the incorporation of stable isotopes at a single position in the headgroup and facilitates the precise monitoring of the flux of intact phospholipids. To determine the flux of intact phospholipids, the nematodes are fed a diet containing either a 100% ^{14}N or a ^{15}N-labeled diet. The amount of newly incorporated phospholipids is obtained by calculating the enrichment of ^{15}N, derived from the difference in isotopomer distribution between unlabeled and labeled phospholipids [10,11].

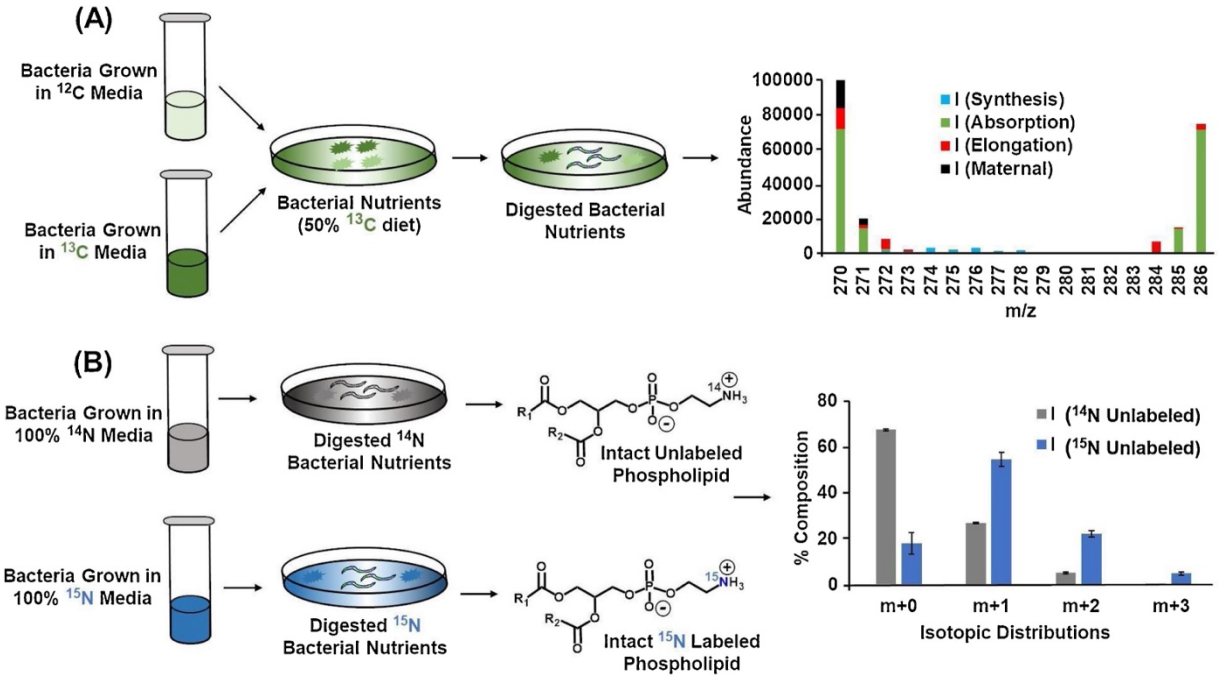

Figure 1.6 Dual ^{13}C and ^{15}N stable isotope labeling strategy to monitor FA and PL dynamics. **A)** Monitoring FA dynamics involves feeding animals with a ^{12}C:^{13}C-labeled diet (50:50). The isotopomer distribution analyzed by GC/MS (example for C16:0 shown here) is used to determine the source and the amount of new FA incorporated into the membrane. **B)** For intact PL, nematodes are fed either a 100 % diet of ^{15}N or ^{14}N. The amount of new PL is deduced from the difference in isotopomer distribution between ^{15}N-labeled lipid and ^{14}N-labeled lipid. Figure adapted from Sultana and Olsen (2020) [11].

1.4 Membrane lipids and disease

Several studies have demonstrated the interplay between aberrant membrane lipid composition and the development of various diseases. While some of these conditions stem directly from disruptions in pathways associated with membrane lipid homeostasis, others may be influenced indirectly. Consequently, it remains unclear whether changes in membrane lipid composition are causal or correlative factors in disease progression [11,25]. Nonetheless, the importance of membrane lipid homeostasis cannot be understated, and this section describes a few examples of membrane-related alterations implicated in some disease conditions, namely diabetes, neurological diseases, and cancers. In addition, I highlight the role of membrane lipid homeostasis in developing resistance to therapies, specifically focusing on cancer studies.

1.4.1 Diabetes

Accumulation of excess SFA has been shown to contribute to the development and progression of diabetes [12,18]. In patients with type II diabetes, a decrease in membrane fluidity due to the accumulation of excess SFA has been observed in several cells [62]. The impact of this increase in membrane saturation includes the activation of ER stress, which can severely disrupt cellular homeostasis by affecting the functionality of membrane channels and transporters [4]. Interestingly, it has been shown that membrane rigidity reduces membrane flexibility for the successful insertion of insulin-dependent glucose transporters that promote the flux of glucose into the cells. The consequence of ineffective glucose transport is increased plasma glucose concentration and overstimulation of pancreatic cells to produce insulin. This vicious cycle contributes β-to cell failure and drives the progression of type II diabetes [18,62].

1.4.2 Neurological diseases

In neurological conditions such as Parkinson's and Alzheimer's, altered membrane composition has been reported [19,21,63]. In patients with Parkinson's, an overall decrease in PE and PC lipids was observed in the brain [19]. A recent study in *C. elegans* shed light on a possible mechanistic role of reduced PE in the progression of Parkinson's disease. The study revealed that low levels of PE

result in ER stress and induce accumulation of α-synuclein protein [64]. Plasmalogens are also a class of lipid species associated with neurogenerative disease, specifically Alzheimer's. Several studies have shown that plasmalogens are significantly decreased in post-mortem brain samples and the cerebrospinal fluid, plasma, serum, and red blood cells of patients with Alzheimer's disease [65–67]. The alteration in plasmalogen is specific to Alzheimer's disease as it is not observed in other neurodegenerative diseases [68]. The role of plasmalogen in the development and progression of Alzheimer's disease is still not clear. A few mechanisms that have been proposed are peroxisome dysfunction, which occurs in the brain of patients with Alzheimer's disease, and an increase in oxidative stress that specifically degrades plasmalogens[68]. The decline in plasmalogen has prompted investigations into the use of plasmalogen as a therapy for treating Alzheimer's disease. Preliminary animal studies have shown improvement in neurogenesis upon supplementation of plasmalogen in diet or injection [68,69]. In human studies, it was shown recently in a randomized clinical study that administrating plasmalogen (1mg/day) improved memory in patients with mild Alzheimer's disease[70]. These are promising progress on the potential for plasmalogen as a therapy, but further studies will be required to ascertain the molecular mechanisms underlying the benefits of plasmalogen on Alzheimer's disease.

1.4.3 Cancers

Altered membrane lipid composition is linked to the progression of various kinds of cancers. Cancer cells are characterized by rapid cellular growth, which requires significant shifts in membrane lipid homeostasis. One of the key membrane lipids that have been linked with cancer is alterations in phosphatidylinositol, which leads to uncontrolled cell growth and proliferation [71]. Sphingolipid metabolism is also a critical mediator for carcinogenesis. Malfunction of ceramide synthesis has been shown to result in cell cycle dysregulation and progression of cancer. Interestingly, increasing ceramide levels inhibits cancer cell proliferation [40,45]. Complex glycosphingolipids on the surfaces of membranes have been suggested to act as tumor-associated antigens. The altered expression of glycosphingolipids has been shown to contribute to cancer development by influencing cell adhesion, motility, and growth [45]. For instance, high levels of the ganglioside GD3 in the membrane bilayer enhance the invasiveness of cancer cells. Interactions

with gangliosides on the surface of the membrane bilayer are postulated to activate signaling pathways, such as the vascular endothelial growth factor (VEGF) signaling pathway, which promotes cellular growth and differentiation [72].

1.4.4 Drug resistance

Changes in membrane composition have also been linked to the development of drug resistance in some cancer cells. Peetla *et al*. 2010 demonstrated that a decrease in membrane fluidity influenced the uptake of the cancer drug doxorubicin in resistant breast cancer cells. The resistant cells were shown to accumulate SFA, sphingolipids, and cholesterol, which form more condensed and tightly packed bilayers, resulting in the ineffective entry of the drug into cell [73]. Another lipid implicated in developing resistance to cancer treatment are glucosylceramides (GlcCer). GlcCer are produced from a highly conserved pathway from the conversation of ceramide to glucosylceramide by the enzyme ceramide glucosyltransferase (CGT). Notably, the overexpression of CGT has been linked to the development of resistance to conventional therapies for many cancerous diseases [74–78]. Consequently, inhibiting CGT activity has emerged as a promising avenue of research targeting therapy-resistant cancer forms. A recent study highlighted in a Nature report supports the potential of targeting GlcCer to combat resistant cancer cells, particularly in Non-Small Cell Lung Cancer (NSCLC) [79]. For patients with advanced NSCLC, Osimertinib, an EGFR tyrosine kinase inhibitor, is the standard first-line treatment. However, resistance to this therapy is observed over time [80]. Lipidomics analysis has shown increased GlcCer levels in lung pleural effusions from NSCLC patients [81]. The study explored whether resistance to Osimertinib in NSCLC is linked to significant changes in sphingolipid metabolism compared to drug-sensitive cells. Using a mice model infected with Osimertinib-resistant cancer cells, researchers inhibited CGT activity using the 1-phenyl-2-decanoylamino-3-morpholino-1-propanol (PDMP) inhibitor. Strikingly, intratumoral administration of PDMP effectively suppressed tumor growth [79]. This study suggests that using a CGT inhibitor could be a viable strategy to treat EGFR-mutant NSCLC patients who are resistant to Osimertinib and other cancers where CGT overexpression is a factor.

In conclusion, the intricate relationship between aberrant membrane lipid composition and the progression of various diseases underscores the need to delve further into membrane lipid studies.

Findings from such studies will provide foundational knowledge that will increase the understanding of membrane biology, which can be applied to studies in these various diseases.

1.5 *Caenorhabditis elegans* as a model to study membrane lipids

Sydney Brenner first introduced the nematode *Caenorhabditis elegans* as a model for research in biology [82]. *C. elegans* is a free-living, transparent, non-infectious, and non-pathogenic soil nematode that is ~1 mm long in adulthood. The nematode exists in 2 sexual forms: the self-fertilizing hermaphrodites (which is the most common form) and males that are rare (~ 0.1-0.2% of the population [83]). The nematode has unique characteristics that make it an excellent model organism that can be used to probe membrane lipid composition. *C. elegans* have a short lifespan (~21 days) and rapid developmental time of ~3 days at 20 ºC with four distinct larval stages (from L1 to L4, Figure 1.7) [35,84,85]. This makes it suitable to characterize the membrane composition in young animals and throughout aging in a relatively short period. *C. elegans* can easily and cheaply be grown on an agar plate in the laboratory. The nematode is a bacterivore and is commonly fed *Escherichia coli* (commonly, the OP50 strain) under standard growth conditions. *C. elegans* can also be fed other bacterial diets, and several studies have probed how different bacterial diets impact the metabolism of the worms [86,87]. Furthermore, the diet can easily be manipulated by supplementing with various metabolites such as lipids, glucose, and oxidants that can tax the worms and allow the probing of membrane lipid response mechanisms [13–15,88–90].

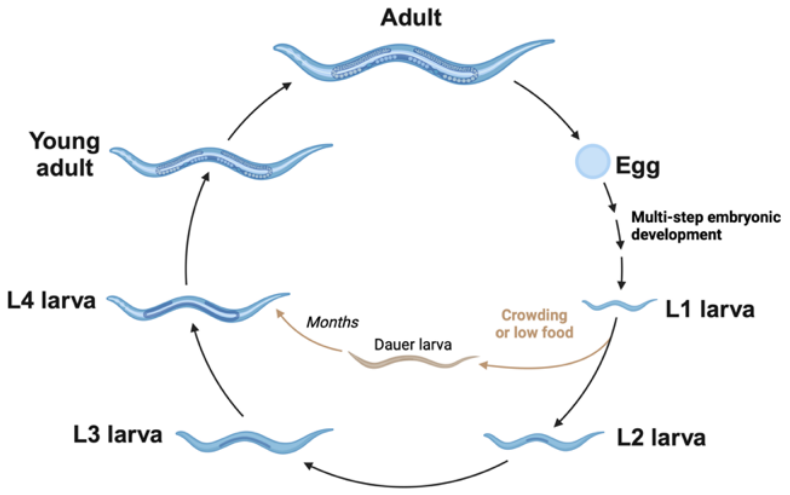

Figure 1.7 The model organism *Caenorhabditis elegans*.
Illustration of various stages of the developmental cycle of *C. elegans*. The figure was generated from BioRender and adapted from WormAtlas.

C. elegans has a versatile genetic system, and most human genes are conserved in the nematode as well [35,91]. The membrane lipid biosynthesis pathway has been comprehensively characterized and shares homology with the mammalian systems [84,92]. The genetic resources available for *C. elegans* include RNA interference (RNAi) and mutants, further enhancing its suitability as a model organism. RNAi allows the study of the reduced expression of genes, while mutants are generated by manipulating the genome of the nematode to eliminate or increase its function. Both mutants and RNAi are used to probe gene function in the nematode, and both have their advantages. RNAi can quickly and easily be performed in the nematode and allows the study of the impact of reduced expression of genes (knockdown) without deleting genes in the organism. Gene knockdown by RNAi is particularly useful for studying genes where the generation of mutants will lead to lethality in the nematodes. Furthermore, RNAi can be performed in various stages in the nematode and offers additional probing gene expression at different life stages [93]. A common challenge in RNAi is the possibility of off-target silencing of closely related genes. In contrast, mutant strains offer specificity, targeting only the gene of interest, thus eliminating the risk of off-target interactions. Furthermore, mutants provide a stable and permanent genetic change that is heritable. This genetic stability is helpful in forward genetics to identify genes that cause a specific phenotype of interest [94]. RNAi can be performed by injection, soaking, or feeding. The typical way by which RNAi is

performed is by feeding, and RNAi libraries have been generated that target most of the genes in *C. elegans* [95,96]. Mutant worms generated by diverse mutations, CRISPR, and other methods are also available at the *Caenorhabditis* Genetics Center (CGC at the University of Minnesota) to facilitate the study of membrane lipid pathways in the nematode [97].

Another important advantage of *C. elegans* as a model to probe membrane lipids is its amenability to stable isotope labeling. The small size of the nematode allows it to be labeled affordably with stable isotopes for very significant enrichment in the organism. The diet can be fully labeled with a general tracer such as ^{13}C or ^{15}N or a metabolite such as ^{13}C-glucose [10,31,54,60]. A general label like ^{13}C is commonly used for lipidomics studies as it easily allows for the simultaneous monitoring of the flux of multiple lipid species. The Olsen lab and others have developed ^{15}N- and ^{13}C- stable isotope feeding strategies in *C. elegans* combined with mass spectrometry to monitor the dynamics of membrane lipids [10,60]. Using this stable isotope labeling strategy, the dynamics of membrane lipid composition of the nematode have been characterized in young animals and along aging. It has been established that most membrane lipids are replaced or modified within 24 hours in young animals, with a tremendous amount of dietary resources funneled to maintain the membrane [10]. Furthermore, there is a general decline in the amount of dietary resources for membrane maintenance along aging (unpublished data from Olsen lab). In addition, we have utilized this stable isotope labeling strategy to uncover a novel response to glucose, which is discussed later. Stable isotopes can also be used to monitor the metabolism of other lipid classes, including sphingolipids. Using stable isotope-labeled amino acids, Hannich *et al.* 2017, were able to show the source of the sphingoid base found in the sphingolipid composition of *C. elegans* [54]. These studies highlight the utility of *C. elegans* for stable isotope tracing, presenting a powerful and cost-effective model for investigating membrane lipid dynamics and flux.

Despite the many advantages of *C. elegans* as a model in studying membrane lipids, some limitations must be noted. Compared to mammalian cell membranes, the membranes of *C. elegans* contain very little amount of cholesterol (~ 20 times less abundant) [98]. Because of this low amount in the membrane, cholesterol is posited to play a role in signaling processes in the worm rather than a structural role in the membrane observed in mammalian systems [98,99]. In addition, because of the small size of nematodes, a large number of animals (> 4000 animals) are required for the

lipid composition analysis using various techniques, and this does not allow us to probe individual organisms [35,59,100]. This composite snapshot of a vast population of worms may overlook the unique metabolic nuances of each organism. Furthermore, lipid analysis is performed on the whole organism, giving a global picture of all the membrane lipids in the nematode. This constraint limits insights into the membrane composition of subcellular organelles and tissues.

1.6 Membrane lipid composition and function in *C elegans*.

Membrane composition in *C. elegans* comprises a diverse pool of lipids. The lipids that make up the membrane have been shown to play critical roles in the development and growth of the nematodes. In this section, I delve into the prominent membrane lipids in the nematode and underscore their pivotal biological roles within the organism.

1.6.1 Fatty Acids (FA)

Fatty acids play a crucial role in shaping the diversity of membrane lipid composition. Typically, FAs do not exist as free fatty acids but are intricately combined with various chemical groups to form complex membrane lipids, including phospholipids and sphingolipids. In *C. elegans*, the FA available in the membrane phospholipids and sphingolipids vary in carbon length from 12 to 27 carbons and in the degree of unsaturation from 0 to 5 double bonds [4,40]. FA is generally notated as CX:YnZ , where X indicates the number of carbons in the FA, and Y shows the number of double bonds at position Z [101]. FA can be divided into three main classes based on the total number of double bonds along the hydrocarbon chain. The FA can be saturated (SFA) with no double bond, monounsaturated (MUFA) with one double bond, or polyunsaturated (PUFA) with two or more double bonds. In addition to the canonical saturated FA (SFA) and unsaturated FA (UFA), the membrane lipids of *C. elegans* contain monomethyl branched-chain fatty acids (mmBCFAs) and cyclopropyl fatty acids that contribute to the intricate lipid landscape of the organism [35,60].

1.6.1.1 Synthesis and maintenance of fatty acids in *C. elegans*

The integration of FA into membrane lipids within *C. elegans* originates from a shared pool generated from four primary sources, i.e., directly from the diet, modification of FA absorbed in

the diet, maternal inheritance, and *de novo* synthesis [10,60]. The *de novo* synthesis in worms is summarized in Figure 1.8. Briefly, fatty acid synthase catalyzes the condensation of malonyl-CoA to acetyl CoA in a series of repeated reactions that result in the generation C16:0 FA. C16:0 is the building block for synthesizing other FAs and is converted to C18:1n7 and C18:1n9 by a set of elongases and desaturases. In addition to being synthesized *de novo*, most of the C18:1n7 is derived from the diet. C18:1n9 serves as the precursor for the synthesis of PUFA. Because the bacteria diet does not contain PUFA, converting C18:0 to C18:1n9 by FAT-7 is critical in maintaining the pool of fatty acids available in the nematode. PUFA is synthesized by a dedicated pool of elongases and desaturases that produce omega-3 and omega-6 PUFA. Furthermore, the bacteria diet of the nematode does not contain mmBCFAs, necessitating the complete synthesis of these FA entirely in the worm [35,96].

Using a stable ^{13}C isotope labeling strategy, our lab successfully elucidated the dynamics of fatty acids incorporated into membrane PL in young animals [10]. This study uncovered that the majority of the membrane FA (70%) are replaced within a 24-hour timeframe. Notably, the turnover rates exhibit species-specific variations; for instance, C16:0 is replaced at a rate of ~ 6% per hour, while C18:2n6 is replaced at a rate of 2.8 % per hour. Furthermore, this tremendous turnover requires funneling a significant amount of dietary resources into maintaining FA incorporated into the PL. This study further identified stearyl CoA desaturases (FAT-7) as a critical regulator of membrane turnover. FAT-7 is required to synthesize PUFAs using C18:0 FA. When compromised, there is a significant accumulation of saturated fat within the pool of FAs available for membrane maintenance. When the expression of FAT-7 is reduced in young animals by RNAi, the rate of membrane turnover is significantly reduced. The reduced membrane maintenance is hypothesized to be a mechanism to protect membrane integrity by preventing the accumulation of excess SFA [10].

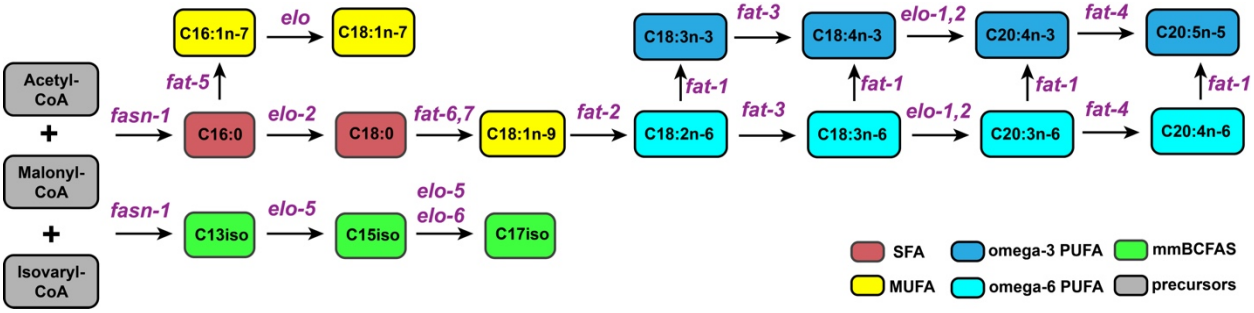

Figure 1.8 Biosynthesis pathway for fatty acids in *C. elegans*.
The synthesis of FA is a complex process involving *de novo* synthesis and dietary absorption. *De novo* synthesis begins with malonyl CoA, which combines with either acetyl CoA or isovaryl CoA to produce C16:0 or C13iso, respectively. These FAs can be converted to other FAs by a set of elongases (elo) that extend the fatty acid chain and desaturases (fat) that add double bonds to FAs. Furthermore, FAs can be absorbed from the diet and utilized to produce other FAs. Adapted from Watts 2017 and Zhang 2015 [35,96].

1.6.1.2 The role of fatty acids in *C. elegans*

1.6.1.2.1 Saturated fatty acids (SFA)

The membrane phospholipids of young adult *C. elegans* are made up of ~ 14 % SFAs with C16:0 and C18:0 (Figure 1.9) comprising the major species present [59,61]. The distinctive molecular shape of SFA significantly increases its melting temperature, causing SFA to pack with a higher density and form non-fluid gel phases [3]. Consequently, the accumulation of excess SFA significantly decreases the fluidity in membrane [2,22]. SFA is typically paired with MUFA or PUFA in phospholipids to maintain optimum membrane fluidity. Many organisms possess inherent mechanisms that prevent the buildup of excess SFA in the membrane [4,7,9].

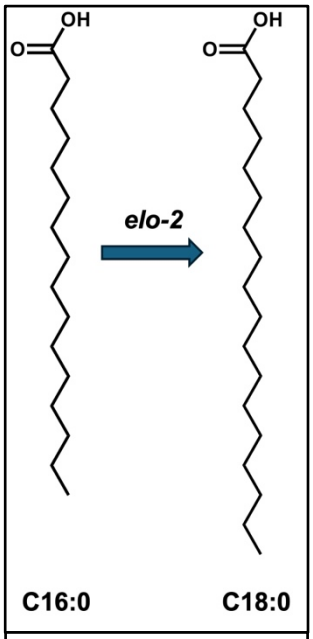

Figure 1.9 SFA in *C. elegans*.

For example, in *C. elegans,* the membrane sensor PAQR-2 (Progestin and adipoQ receptor), in conjunction with its partner IGLR-2 (Immunoglobulin (Ig)-like domain and several leucine-rich repeats), regulates the SFA homeostasis in the membrane. The presence of dietary (SFA-rich diets or glucose) and environmental (cold) perturbations cause the increase in levels of SFA in the

membrane, which decreases the overall fluidity of the membrane [13–15,102]. This change in membrane biophysical property is sensed by the PAQR-2/IGLR-2 complex, which activates downstream signaling events that restore membrane fluidity by promoting fatty acid desaturation via FAT-7 upregulation.

The high melting temperatures of SFA are essential for the adaptation to excessively high fluidity caused by elevated temperatures. In *C. elegans,* elevated temperature (25 ºC) upregulates acyl-CoA dehydratase (ACDH-11), which reduces the expression of FAT-7 and increases the level of SFA in the membrane [103]. The increase in saturation reduces the membrane fluidity and allows the homeoviscous adaptation to heat in the nematode.

1.6.1.2.2 Monounsaturated fatty acids (MUFA)

The membrane phospholipid of *C. elegans* contains ~30 % MUFAs. The most abundant MUFA in young adult animals is C18:1n7 (Figure 1.10), constituting ~25 % of total FAs in PL [59,61]. While predominantly obtained from the diet, C18:1n7 can also be synthesized in the nematode by desaturases that add a double bond to SFA (Figure 1.8).

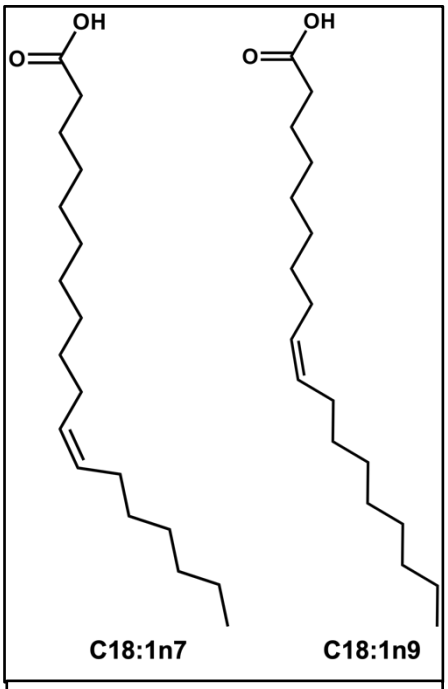

Figure 1.10 Major MUFA in *C. elegans*.

Another MUFA in the nematode is C18:1n9 (Figure 1.10), which is synthesized by the Δ9 desaturases stearyl-CoA desaturases. Although C18:1n9 is present at very low abundance in the membrane (~ 4% of total FAs in the PL of young adult animals), they are important precursors for synthesizing PUFAs [35]. Because PUFAs are not present in the diet of nematodes [35,60,104], the conversion of C18:0 to C18:1n9 is vital for membrane maintenance.

The addition of a double bond in the cis configuration introduces a kink that enables MUFA to exist in a fluid state. Therefore, the presence of MUFA in the membrane significantly increases the overall membrane fluidity [3,105]. It has been shown that an increase in C18:1n9 in the membrane

rescues severe phenotypes of *paqr-2* deficient animals under cold conditions by increasing membrane fluidity [13]. In addition to their biophysical impact on membranes, MUFA has been shown to play critical roles in stress response in *C. elegans*. Using stable isotope labeling technology and time course analysis, the Olsen lab recently showed that C18:1n9 dynamics in membrane phospholipids are essential in glucose stress response in the nematodes. Specifically, C18:1n9 is funneled to maintain the levels of PUFA lost due to the oxidative damage caused by high levels of glucose stress [61].

1.6.1.2.3 Monomethyl branched-chain fatty acids (mmBCFAs)

The mmBCFAs are saturated fatty acids with a methyl group at either the penultimate (iso) or the antepenultimate (anteiso) carbon [106]. In *C. elegans*, the main mmBCFAs are the iso-branched chain 13-methyl myristic acid (C15iso) and 15-methyl hexadecanoic acid (C17iso) (Figure 1.11), collectively constituting ~6 % of the total PL fatty acids [59,106]. In the nematode, mmBCFAs are derived from the amino acid leucine, which is converted to C13iso by the activity of the branched-chain ketoacid dehydrogenase complex (BCKDH), fatty acid synthase (FASN-1) and acetyl-CoA carboxylase (POD-2). ELO-5 then elongates C13iso to make C15iso, which is further elongated by ELO-5 and ELO-6 to produce C17iso [106–108].

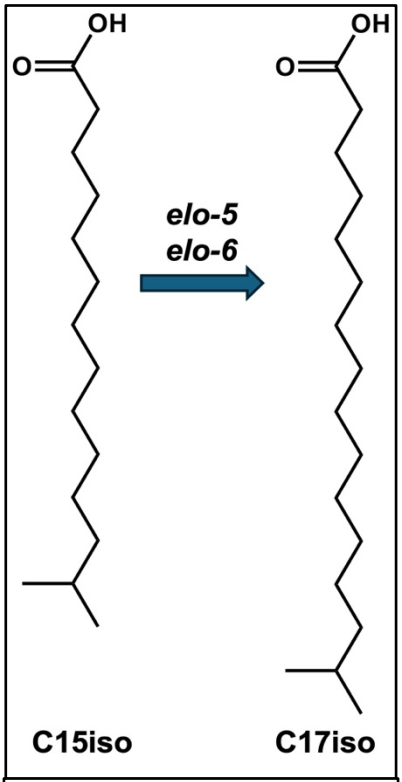

Figure 1.11 Major mmBCFAs in *C. elegans*.

The presence of the methyl group at the iso or anteiso position of mmBCFAs impacts membrane properties such as packing and fluidity [109]. However, in *C elegans*, the role of mmBCFAs has not been linked to their effects on fluidity but through a mechanistic role in the metabolism of the nematode. In the absence of mmBCFAs, the nematode has a variety of developmental, growth, and morphological defects. In addition, mmBCFAs have been linked with signaling processes and the response to nutrient deprivation and nutrient sensing [106,107,110–112]. The mmBCFA, C15iso, is a precursor for the sphingoid backbone required for sphingolipid synthesis in *C. elegans*

[111,113]. Most of the roles of mmBCFAs uncovered in *C. elegans* have been suggested to act through their role in sphingolipid production (see section 1.6.3). However, recent studies have shown additional roles of mmBCFAs in the membrane independent of sphingolipid production. Kniazeva *et al.* showed that mmBCFAs in PL regulate membrane function during embryogenesis by providing optimal conditions for the inositol triphosphate (IP_3) signaling pathway in zygotes [107]. Furthermore, Zhang *et al*. showed that mmBCFA C17iso is crucial for maintaining the morphology and integrity of ER membrane in *C. elegans* [114]. The acyl-CoA synthetase enzyme (*acs-1*) facilitates the incorporation of C17iso into ER membrane PL, ensuring membrane integrity and optimum function. The absence of ACS-1 prevents the incorporation of C17iso into the membrane PL, leading specifically to the dysfunction of the ER [114].

1.6.1.2.4 Polyunsaturated fatty acids (PUFA)

PUFA constitutes the majority of FA in the membrane of young adult *C. elegans,* accounting for ~ 35 % of the total FAs in phospholipids [35,61,104]. PUFAs are divided into two main subclasses, omega-3 (n-3) and omega-6 (n-6), based on the position of the double bond (Figure 1.12). Despite their structural similarity, omega-3 and omega-6 PUFA perform different functions in organisms [104]. In humans, a lower omega-6/omega-3 ratio is suggested to reduce the risk of chronic diseases such as cardiovascular disease and cancer [115,116]. PUFA can be synthesized in an organism or obtained from the diet. In *C. elegans*, the primary dietary food source (OP50) does not contain any PUFA; thus, all the PUFA present in the nematode are synthesized *de novo*. *C. elegans* have a repertoire of elongases and desaturases that intricately orchestrates the synthesis of both n-3 and n-6 PUFA (Figure 1.8), making the nematode a very attractive model to study the biological functions of PUFA *in vivo* [35,104,117].

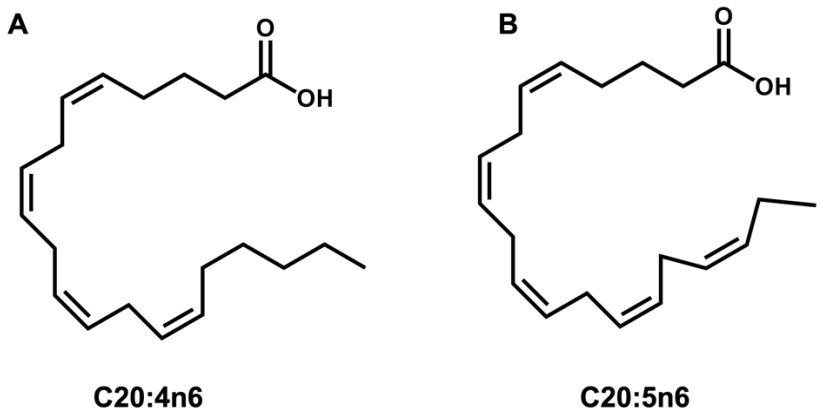

Figure 1.12 Structure of an omega-6 and omega-3 polyunsaturated fatty acid in *C. elegans*. **A)** Arachidonic acid (C20:4n6) is omega-6 PUFA found in the nematode. **B)** Eicosapentaenoic acid (C20:5n3) is an omega-3 PUFA and constitutes the most abundant PUFA in the worm

In membranes, PUFA is predominantly found in phospholipids and significantly impacts the biophysical properties of membranes. The presence of PUFA significantly increases the membrane's overall fluidity, packing disorder, and lateral pressure [25,118]. These biophysical properties allow PUFA to have high structural plasticity, making the membrane more flexible for membrane-fusing events such as endo- and exocytosis [119]. In *C. elegans*, PUFA in the membrane has been shown to play a critical role in synaptic vesicles. Reducing the production and incorporation of arachidonic acid (C20:4n6) in the membrane leads to a defect in touch sensitivity [120]. This effect is attributed to the increase in the bending rigidity of membranes enriched with arachidonic acid (C20:4n6), which impacts the activity and conformation of membrane proteins, including the mechanosensitive channels that are important for touch sensitivity [120].

Despite their critical roles, PUFA increases the overall susceptibility of membranes to lipid peroxidation [121,122]. Compared to SFA and MUFA, PUFAs are highly prone to peroxidation because the C-H bond on the carbon between double bonds is weak and is easily attacked by radicals. The removal of hydrogen from this bond creates a PUFA chain that, in the process of being attacked by the radical, becomes a carbon-centered radical that can attack other lipids and cellular macromolecules (See section 1.7). Lipid peroxidation of PUFA is linked to defects in nematode

reproduction. It has been shown that supplementing the diet of the nematodes with excess dihomogamma linolenic acid (DGLA, 20:3n-6) leads to sterility in the nematodes. The sterility induced by DGLA is suggested to be caused by lipid peroxidation that triggers germ cell death via ferroptosis [123].

1.6.2 Phospholipids (PL)

Phospholipids constitute the primary membrane lipids in *C. elegans,* with PC and PE being the predominant species, collectively accounting for over 85 % of the total pool of phospholipids in the nematode [10]. Additionally, PE plasmalogen species (PE O- and PE P-), lysophospholipids, phosphatidylinositol (PI), and phosphatidylserine (PS) species are present as well, albeit in a lower abundance [35]. In general, phospholipids are illustrated AB X:Y where AB represents the phospholipid class, X represents the total carbon in the fatty acid tails, and Y represents the total number of double bonds within the fatty acid tail [101]. In *C. elegans*, PL ranges from a total of 29 to 40 combined fatty acid chain lengths and a total of 0 to 10 double bonds, reflecting the diversity of membrane landscape in *C. elegans* [10,31,100].

1.6.2.1 Synthesis and maintenance of phospholipid in *C. elegans*

Phospholipids synthesis in *C. elegans* primarily occurs through the Kennedy and CDP-DAG pathways (Figure 1.13) [35,96]. In these pathways, the synthesis of PL is initiated by the addition of two acyl groups to glycerol-3-phosphate (G3P) to form phosphatic acid (PA) through a reaction catalyzed by the acyl-transferase enzymes (GPAT). Subsequently, PA undergoes dephosphorylation to form diacylglycerol (DAG), which enters the Kennedy pathway or CDP DAG pathway. In the CDP-DAG pathway, inositol and glycerol are incorporated into CDP-DAG, producing phosphatidylinositol (PI) and phosphatidylglycerol (PG) through their respective phosphatidyl synthases. Conversely, in the Kennedy pathway, activated CDP-PC and CDP-PE generated by CTP-phosphocholine and CTP-phosphoethanolamine cytidylyl transferase, react with DAG to produce PC and PE, respectively. Phosphatidylserine (PS) is then synthesized from PC and PE by exchanging serine with choline or ethanolamine, facilitated by PS synthase enzymes 1 and 2 (PSSY).

In *C. elegans*, similar to other organisms, PC can be synthesized from PE. This conversion is mediated by methyl transferases that use S-adenosyl methionine (SAMe) as a substrate in a sequential methylation step that converts PE to PC. This process is pivotal in the biosynthesis of PC in *C. elegans,* as animals that have a mutation in the *sams-1* gene have a significant decrease in the overall pool of PC lipids [124]. Finally, the nematode synthesizes plasmalogen in the peroxisomes using the enzymes fatty acyl-CoA reductase (FARD-1), glyceronephosphate O-acyltransferase (ACL-7), and alkylglycerone phosphate synthetase (ADS-1) [31,32]. The plasmalogen synthesis commences with *acl-7* adding an acyl group to dihydroxyacetone phosphate (DHAP). Subsequently, *fard-1* generates a fatty alcohol that is utilized by *ads-1* to replace the acyl group to form the 1-alkyl DHAP, which serves as the backbone for the plasmalogen synthesis. In *C. elegans,* the plasmalogen are mostly species with an ethanolamine headgroup.

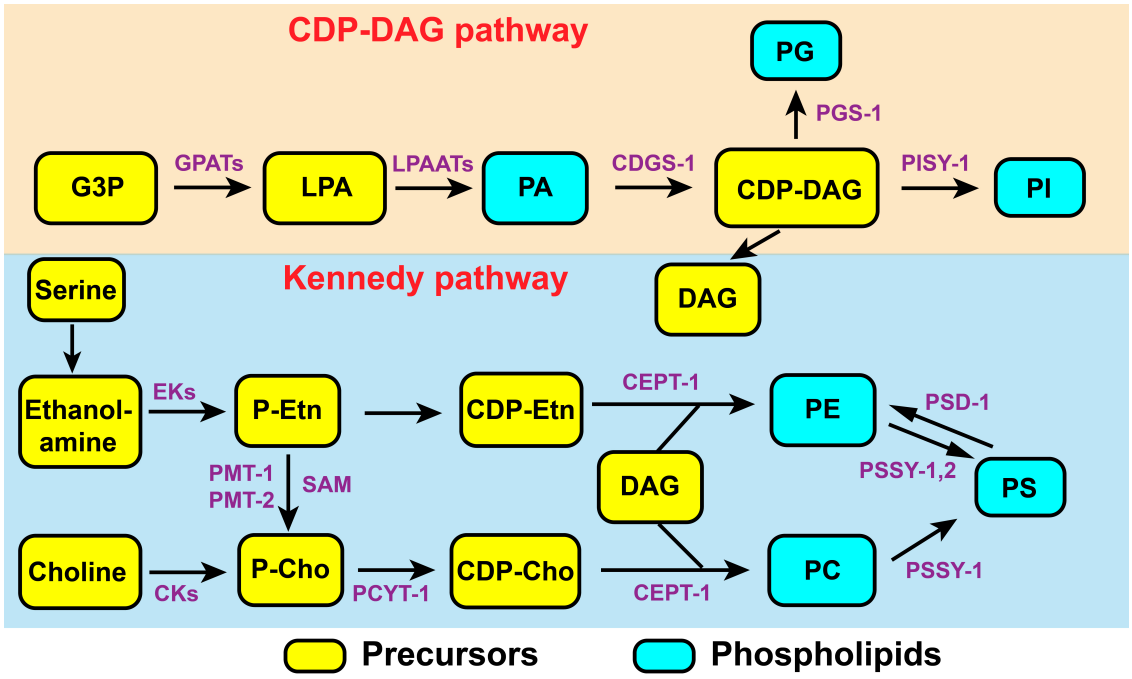

Figure 1.13 Summary of the pathway for synthesizing major phospholipids in *C. elegans*. The biosynthesis of phospholipids occurs in two major pathways – the CDP-DAG pathway (top) and the Kennedy pathway (bottom). Both pathways require diacylglycerol (DAG) as a precursor. The CDP-DAG pathway (top) produces phosphatidylinositol (PI) and phosphatidylglycerol (PG). The Kennedy pathway produces phosphatidylcholine (PC), phosphatidylethanolamine (PE), and phosphatidylserine (PS). Precursors are highlighted in yellow, and membrane lipids are highlighted in blue. Adapted from Watts 2017 and Zhang 2015 [35,96].

Phospholipids play a crucial role in various intrinsic processes within organisms, necessitating their continual maintenance within the cell membrane. Using a novel ^{15}N-isotope labeling feeding strategy, our lab was able to map the membrane dynamics of the major phospholipids (PE and PC) in *C. elegans* [10]. The outcomes revealed intriguing patterns in the turnover of both PL classes and individual lipid species. Similar to FAs, PL maintenance requires a significant funneling of dietary resources. Notably, within the lipid class, PE lipids were replaced at a faster rate compared to PC lipids. Interestingly, this replacement rate varied within PE lipids, with ether-linked PE (PE P-) undergoing a slower replacement rate. These trends were consistent at the lipid species level, where PE with the same tail combination as PC and PE P- were replaced at a faster rate. Additionally, the gene *fat-7* exerted a significant influence on PL maintenance rates. Compromising *fat-7* using RNAi markedly decreased PL turnover, resulting in a paused membrane maintenance state. This paused membrane state prompts a remodeling of the membrane to compensate for the altered pool of FA that is available for PL. This remodeling process included pairing excess SFA with highly polyunsaturated FA and accumulating atypical FAs [10]. Furthermore, our laboratory conducted studies on aging in the nematodes, revealing a general decline in the availability of dietary resources for PL maintenance. We posit that this limitation in resources for membrane maintenance may ultimately contribute to changes in membrane composition during the aging process (unpublished data from Olsen lab). In summary, the innovative use of ^{15}N-isotope labeling provided a window into the dynamic world of membrane lipids in *C. elegans*, revealing differential turnover rates of the major lipids PE and PC. These insights are pivotal, as they deepen our comprehension of PL regulation during growth and aging, highlighting the complexities of membrane PL regulation.

1.6.2.2 The role of phospholipids in the *C. elegans*

The significance of maintaining the proper composition of phospholipids in *C. elegans* cannot be overstated, as they are indispensable for many processes, including development, growth, immunity, embryogenesis, and stress response. When the levels of PC are significantly reduced in nematodes via mutations in the *sams-1* gene, there is a notable accumulation of large lipid droplets, adversely impacting proper growth and reproduction. This accumulation of storage lipids is attributed to the increase in the expression of SREBP-1, which promotes lipogenesis and diverts

excess diacylglycerol (DAG) precursors to triglyceride synthesis. Interestingly, supplementing *sams-1* mutant worms with dietary choline restores the storage lipids to normal levels [124]. Furthermore, a distinct response to low levels of PC is the upregulation of PMK-1-dependent innate immunity, which extends the lifespan of *C. elegans*. PMK-1 is a kinase critical for orchestrating the expression of genes essential for responding to pathogenic infections. The biophysical alterations in the membrane due to low PC is postulated to induce PMK-1-mediated immune response in the nematode [125].

The asymmetric distribution of various lipid species is a characteristic feature of the membrane bilayer, regulated by specific ATPases that translocate lipids between membrane layers [35]. Mutations in *C. elegan*s that lead to the accumulation of PE in the outer membrane of embryos disrupt cell adhesion and morphogenesis during embryogenesis [126]. Maintaining an appropriate pool of membrane lipids is also important for embryogenesis because shifting the production of PC and PE lipids towards lower abundant lipid species PI in *C. elegans* impacts embryonic development. This shift occurs due to a mutation in LIPIN (phosphatidic acid phosphatase), which slows the disassembly of the nuclear envelope during mitosis in the embryos [127].

Plasmalogens play critical roles in the nematodes, with plasmalogen deficiency causing a remodeling of the membrane lipids by increasing the overall levels of SFA and PE lipids [32]. Furthermore, plasmalogen deficiency influences reproduction and increases the sensitivity of the nematodes to oxidative stress and temperature changes [31,128]. Finally, plasmalogen has been suggested to be important in preventing germ cell death that is caused by the accumulation of dihomogamma-linolenic acid (DGLA; 20:3n-6) in the nematode [128].

In summary, the intricate interplay of phospholipids in *C. elegans* underscores the organism's reliance on a finely-tuned membrane composition for its function.

1.6.3 Sphingolipids

Sphingolipids are a class of lipids that play crucial roles as structural components and signaling molecules[40,129]. Sphingolipids are a complex and varied class of lipids characterized by an amino sphingoid base[42]. Although critical components within the membrane, they compromise a fairly small fraction of the total lipid in cells, especially compared to the phospholipid and neutral lipids within an animal [130]. Sphingolipids can be further broken into distinct classes based on the kind of headgroup present, including ceramides (Cer), glucosylceramides (GlcCer), and sphingomyelin (SM). GlcCer can be further derivatized to produce other complex glycolipids by specific glycosyltransferases; therefore, GlcCer are considered vital intermediates of sphingolipid metabolism[40].

Using the stable isotope labeling technique of various amino acids, Hannich *et al*. (2017) found all sphingolipid species contained a d17iso sphingoid base. In addition, feeding worms with different sphingoid bases in the absence of the d17iso sphingoid base leads to severe developmental and digestive defects, suggesting that d17iso is the major, if not the exclusive, sphingoid base incorporated into sphingolipids [54]. The GlcCer pool in *C. elegans* is generated from 7 major species (i.e., comprises more than 4% of the pool). The diversity of GlcCer is generated from the N-acyl FA chain because all GlcCer species in the nematode contain a d17iso sphingoid base. In nematodes, the GlcCer species contain acyl chain lengths ranging from 20–27 with 0 or 1 double bonds and with or without an additional hydroxyl group(s) [55,100,131]. Interestingly, two main GlcCer constitute the majority of the GlcCer pool: specifically, the 22:0;O GlcCer and 24:0;O GlcCer make up ~33% and 36% respectively of the total GlcCer pool (Figure 1.14A) [56,100]. The distribution of GlcCer species indicates the specific regulation of lipids and suggests particular roles for individual species. Intriguingly, this predominance is also reflected, albeit to a lesser extent, in the direct precursors of these GlcCer in the ceramide pool, with 22:0;O Cer and 24:0;O Cer making up ~19% and 25% of the total ceramide population (Figure 1.14B). Although the overall distribution of Cer is similar to the GlcCer pool, distinct differences indicate that the metabolic wiring enriches specific lipids in the GlcCer pool (e.g., 22:0;O GlcCer) while others are depleted (e.g., 22:0 GlcCer). Generally, sphingolipids are represented as AB XX/ YY; O where AB

represents the headgroup, XX represents the sphingoid base, YY represents the N-linked FA, and O represents the hydroxyl group attached to the N-linked FA [101]. Emerging research over the years using the model organism *C. elegans* has provided some insight into the mechanistic role of sphingolipids, which are summarized below.

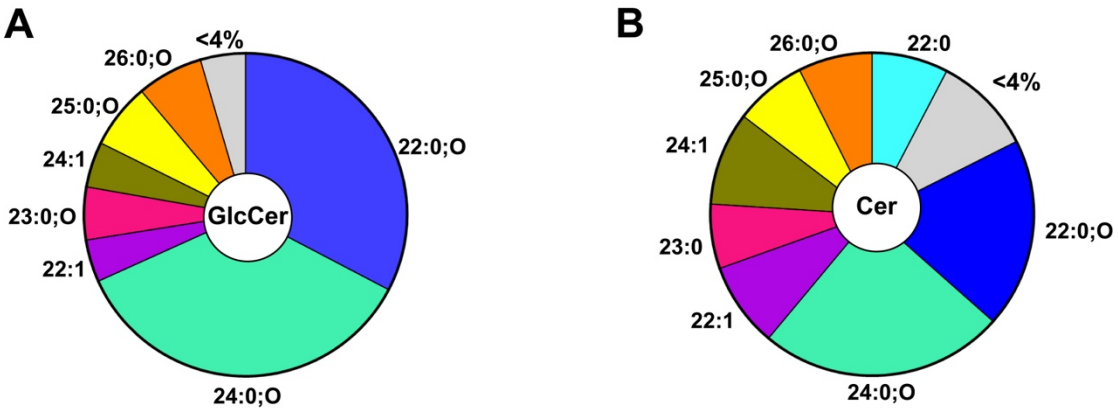

Figure 1.14 Distribution of Ceramide (Cer) and Glucosylceramide (GlcCer) in *C elegans*. **A)** Distribution of the most abundant GlcCer (>4% of total GlcCer) in WT young adult worms. Here, the major GlcCer species are 22:0;O and 24:0;O GlcCer, which account for ~33% and 36% of the total pool of GlcCer. **B)** Distribution of the most abundant ceramides (>4% of total ceramide) in WT young adult worms. The major ceramide species are the 22:0;O and 24:0;O Cer species, which account for ~44% of the total Cer pool.

1.6.3.1 Synthesis and degradation of sphingolipids

In *C. elegans*, the synthesis of sphingolipids has been elucidated and begins with the enzyme ELO-5, which produces two monomethyl-branched fatty acids called C15iso (13-methyl myristic acid) and C17iso (15-methyl hexadecanoic acid) [35,106]. C15iso combines with serine to form the ceramide backbone (d17iso sphinganine) via the enzyme serine palmitoyl transferase (SPTL) [35,54]. In *C. elegans*, three ceramide synthases, HYL-1, HYL-2, and LAGR-1, add a fatty acid to the sphingoid backbone via an amide linkage to form ceramides [132,133]. The fatty acids can range in chain length from 18 to 27 carbons with 0 or 1 double bond, and the specific ceramide synthase used confers chain specificity to sphingolipids [55,131]. For example, the ceramide synthase HYL-1 adds fatty acyl chains of 24–26 carbons, while HYL-2 adds 20–22 carbon fatty acyl chains to the

sphingoid backbone[133]. Ceramide can be converted to sphingomyelin by the addition of a phosphatidylcholine group to sphingomyelin synthase (*sms-1,2, 3*). Finally, the addition of UDP-glucose to an existing ceramide molecule by ceramide glucosyltransferase (CGT) produces glucosylceramide (Figure 1.15). In *C. elegans*, three ceramide glucosyltransferases, CGT-1, CGT-2, and CGT-3, are expressed and function in the intestine [134,135]. GlcCer can be further derivatized to produce other complex glycolipids by specific glycosyltransferases (BRE enzymes) in *C. elegans* [136].

Sphingolipid levels can be impacted by the rates of production and the rates of degradation. Sphingolipids can be degraded into their parent compound via a salvage pathway. GlcCer and SM are broken down to ceramide by glucosyl ceramidases (*gba-1,2,3,4*) and sphingomyelinase (*asm-1,2,3*). The ceramide can then be further degraded to the sphingoid backbone by ceramidase (*asah-1*), and the sphingoid base is phosphorylated by sphingosine kinase (*sphk-1*) to produce sphingosine 1-phosphate, an important signaling molecule. Sphingosine 1-phosphate can be further broken down to ethanolamine phosphate and a C17iso aldehyde by sphingosine 1-phosphate lyase (*spl-1*), which can be used to produce other lipids. The degradation pathway is also critical for nematode health. For example, the loss of SPL-1 causes severe defects in the gut and the reproductive tract of *C. elegans* [35,96,137].

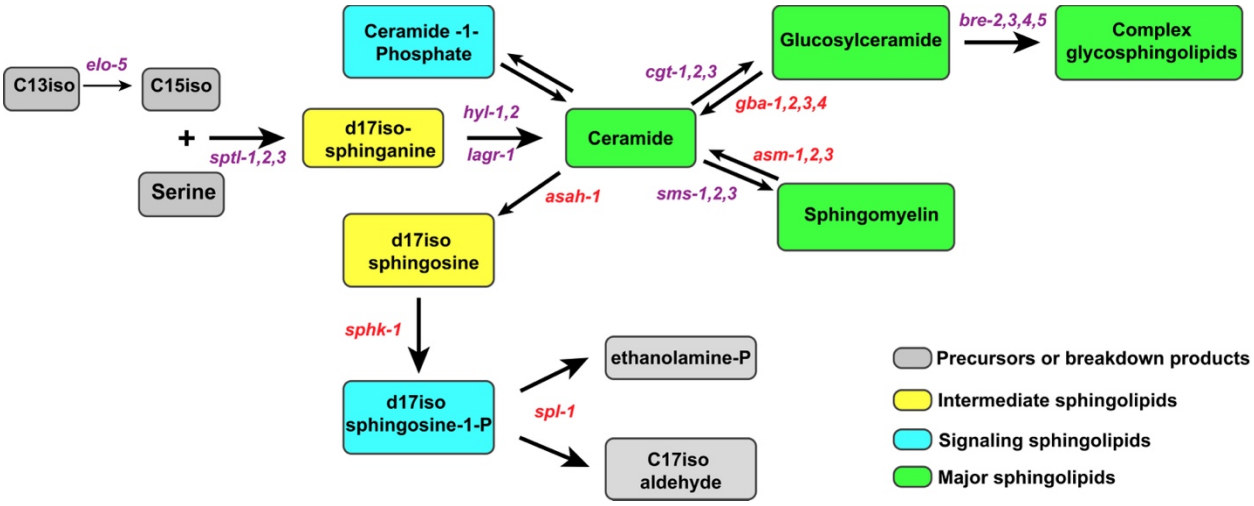

Figure 1.15 Summary of the synthesis and breakdown of sphingolipids in *C. elegans*. Sphingolipids are synthesized from a highly conserved pathway. In *C elegans,* it involves the formation of a sphingoid backbone from the combination of serine to C15iso mmBCFA. The addition of FA leads to the formation of ceramide, which is converted to glucosylceramides by the addition of glucose. Glucosylceramides are precursors for the synthesis of complex glycolipids. Synthesis enzymes are highlighted in purple, and degradation enzymes are highlighted in red. Adapted from Watts 2017 and Zhang et al. 2015 [35,96].

1.6.3.2 The role of sphingolipids in *C. elegans*

Sphingolipid metabolism has been shown to play a critical role in *C. elegans*. Interestingly, some of the roles of sphingolipids depend on the FA chain length associated with a specific sphingolipid. The loss of HYL-2, which is required to produce C20-C22, increases sensitivity to anoxia and decreases lifespan. In contrast, the loss of HYL-1, needed to produce C24-C26 ceramides, increases the resistance of the nematode to anoxia and does not affect lifespan. Furthermore, the loss of both HYL-1 and LAGR-1 significantly increases the lifespan in the nematodes [138,139].

The central role of sphingolipids in *C. elegans* has been mainly linked to GlcCer metabolism. Using mutation or RNAi of each of the genes involved in GlcCer synthesis has probed the biological role of GlcCer in the nematode, identifying essential roles for GlcCer in development as depleting glucosylceramides leads to developmental defects and larval arrest [135,140–142]. Specifically, mutations in *cgt-3* lead to embryonic defects and reduced brood size. Nomura *et al*.

(2011) showed the *cgt-3 (tm504)* mutant has abnormal oocytes and eggs that have disrupted membranes and nuclei, accounting for the decreased brood size in this animal. In addition, double mutant *cgt-1;cgt-3* arrest at the L1 stage, are uncoordinated and eventually die. Interestingly, deleting *cgt-2* by mutation or RNAi does not exacerbate early larval arrest phenotype in *cgt-1; cgt-3* double mutant suggests that *cgt-2* is not required for development in the nematode.

The use of *C. elegans* has allowed for the spatial dissection of GlcCer metabolism. For example, the enzymes CGT-1 and CGT-3, are highly expressed in a unique subset cell in *C. elegans*, specifically the pharyngeal intestinal valve (PIV), anterior and posterior intestinal cells, intestinal rectal valve (IRV), and the rectal gland cells (RGCs) [134]. Intriguingly, expressing CGT specifically in this subset of cells can rescue the larval arrest and defects of *cgt-1;cgt-3,* suggesting that the activity of CGT is required in only a small subset of cells [134]. Further studies show improper feeding and deficient cholesterol mobilization contribute to developmental defects and arrest [143]. Although cholesterol is not synthesized *de novo* in *C. elegans*, it is required for growth and larval development, and this study shows that GlcCer are precursors to the synthesis of a novel class of glycosphingolipid known as phosphoethanolamine glucosylceramides (PEGCs), that regulate cholesterol utilization in *C. elegans*. GlcCer deficient animals (*cgt-1;cgt-3*, and *elo-5*) have reduced levels of PEGC, and supplementing the diet with high levels of cholesterol (2.6 mM) can also rescue the larval arrest of *cgt-1;cgt-3* and *elo-5* mutants suggesting that the role of GlcCer may be in the mobilization and regulation of cholesterol. Although there is remarkable homology between sterol regulation in *C. elegans* and mammals, there has not been an established role for PEGCs in mammals [143]. It is possible that PEGCs have not been detected in mammals due to their low abundance or that another molecule acts similarly.

Several studies have examined the phenotypic effects of impaired GlcCer synthesis and have found roles for GlcCer in apical membrane polarity, tubulogenesis, and larval development [111,113,144]. GlcCer has been connected to TOR (Target of Rapamycin) signaling [145]. The TOR complex is a serine/threonine kinase in *C. elegans* that is conserved in mammalian organisms and comprises two main complexes, TORC1 and TORC2 [146]. An unbiased genetic screening in *C. elegans* identified GlcCer as a vital regulator of TORC1 activation. This GlcCer/TORC1 signaling pathway

is proposed to be a metabolic checkpoint in the intestine of the nematodes that coordinates postembryonic growth and development [145].

A recent study identified a role for GlcCer in TOR regulation in a *C. elegans* aging model[137]. In this study, long-lived germline deficient worms (*glp-1*) were shown to exhibit significantly upregulated levels of the sphingolipid synthesis enzyme ELO-3. ELO-3 is an enzyme involved in synthesizing saturated fatty acids with chains longer than twenty carbons that are incorporated into the sphingoid base in *C. elegans* to produce ceramides and GlcCer. Further investigation revealed a specific GlcCer species (C22 GlcCer) as the sphingolipid critical for *glp-1*-mediated lifespan extension. C22 GlcCer modulates lifespan extension by regulating clathrin membrane localization and lysosome homeostasis, resulting in the activation of the transcription factor SKN-1. Activation of SKN-1 leads to the suppression of TOR and the subsequent increase in the lifespan of *glp-1* animals. The contrasting role of GlcCer in TOR activation is intriguing as it suggests that the regulation may depend on the stage of development of the organism and perhaps the type of acyl chain attached to GlcCer. The idea of acyl chain specificity in regulating TOR activation is not surprising, as previous studies show that the acyl chain length of sphingolipids expressed in distinct tissues or cellular compartments can perform unique functions. Thus, it will be interesting to investigate further the detailed role of acyl chain length specificity of GlcCer in TOR regulation.

Finally, a previous study showed the significance of complex glycolipids synthesized from GlcCer by the glycosyltransferases in *C. elegans* (BRE). Loss of BRE enzymes has been observed to correlate with enhanced resistance to *Bacillus* toxin. It is hypothesized that these complex glycolipids serve as cell surface receptors, facilitating the appropriate positioning of the *Bacillus* toxin at the bilayer surface or within the bilayer of intestinal cells [136].

1.7 Membrane lipids can be damaged by lipid peroxidation.

Reactive oxygen species (ROS) generated from internal processes or environmental sources can cause significant damage to tissues and cells by reacting with biomolecules within an organism that constitute these cells and tissues [147]. One of the primary consequences of oxidative stress damage induced by ROS is the lipid peroxidation of membrane phospholipids. Specifically, PUFA within membrane phospholipids is particularly prone to lipid peroxidation (LPO) by ROS. This susceptibility is due to the low bond energies of the carbon-hydrogen (C-H) bond in the methylene between two double bonds (bisallylic hydrogen atoms), making them highly susceptible to attack by reactive radical species [147,148]. Consequently, lipid radicals are generated, which can further attack other lipids and macromolecules. Comparatively, SFA is resistant to LPO, while MUFAs are much less susceptible to lipid peroxidation than PUFA. The propensity of LPO increases as the number of double bonds in a PUFA increases [149,150].

1.7.1 Mechanism of lipid peroxidation

Initiation

Lipid peroxidation begins with the formation of a lipid radical ($L^{\cdot}$), which can arise from the abstraction of hydrogen atoms located in one or more bisallylic positions in a PUFA. This process can occur within an organism by endogenous mechanisms that generate free radicals (R), such as the electron transport chain (ETC) in mitochondria and enzymatic reactions involving cytochrome P450 and NADPH oxidase. In addition, external perturbations such as chemical oxidants or ionization radiation can trigger lipid radical formation. [122,147]

$$L\text{-}H + R \longrightarrow L^{\cdot}$$

Propagation

In the propagation step, molecular oxygen reacts with the lipid radical to generate a peroxy-lipid radical, which serves as the primary chain-carrying species (Step 1). Because the concentration of oxygen varies in various organelles, cells, and tissues, the rate at which these lipid radicals are formed is different within various localizations within an organism. The peroxy-lipid radical generated propagates the damage by abstracting hydrogen atoms from neighboring lipid molecules. Propagation of lipid peroxidation leads to the formation of primary peroxidation products such as hydroperoxide (OOH), hydroxyl (OH), and keto derivatives (Step 2). Further decomposition of hydroperoxide groups leads to the formation of secondary peroxidation products such as carbonyl-based derivatives. Finally, cross-linking reactions of carbonyl groups from oxidized lipids with amino and thiol groups of proteins lead to the formation of tertiary peroxidation products such as phospholipid-protein adducts [122,147].

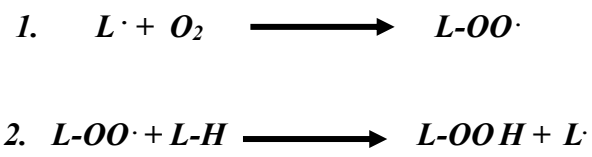

Termination

The termination of LPO occurs by radical-radical reactions, which occur through enzymatic and non-enzymatic pathways. In most organisms, the glutathione peroxidase (GPX) mediates the enzymatic termination of LPO. GPX directly reduces oxidized lipids using its selenocysteine residue and glutathione to convert them into non-radical lipids. The non-enzymatic mechanism for terminating lipid peroxidation involves radical trapping agents (RTA) such as vitamin E (tocopherol) that react with a lipid radical to break the chain of LPO. Finally, under conditions where concentrations of initiating lipid radicals are exceptionally high, they can form radical-radical reactions with one another to produce non-radical lipid products [122,147].

1.7.2 The impact of lipid peroxidation on the membrane and cellular function

The presence of oxidized lipids (oxL) in the membrane severely impacts the biophysical properties of membranes. Specifically, oxidized FA tails within membrane PL are reorientated to protrude into the aqueous environment, forming structures known as lipid whiskers [151,152]. This reorientation makes the membrane bilayer highly hydrated due to increased water permeability and decreases in bilayer thickness, fluidity, and packing [151,152]. Moreover, lipid whiskers can also aggregate and form nanodomains at the surface of the membrane that can be involved in signaling events. Furthermore, these nanodomains can also be recognized by macrophages and trigger immune responses within an organism [153]. Ultimately, the controlled formation of lipid whiskers results in the swelling of cells and eventual rupture, leading to a form of cell death known as Ferroptosis (Figure 1.16) [154,155].

In addition to their impact on the membrane bilayer, oxL products generated from LPO exert other biological effects within an organism. OxL species are chemically reactive and can react with other biomolecules, including proteins and DNA[156,157]. It has been demonstrated that oxL can react with amino residues such as cysteine and lysine in proteins and peptides, leading to significant changes in the conformation and, in some cases, damage to proteins [157]. Moreover, oxL has also been shown to react with nucleic acid, contributing to the mutagenic and carcinogenic effects of nucleic acid damage [158]. In addition, oxL can directly and indirectly influence cellular signaling pathways. OxL has been reported to activate various signaling receptors, including toll-like receptors, G protein-coupled receptors, and nuclear ligand-activated transcription factors [159]. Furthermore, oxidized lipids induce the rapid release of secondary messengers such as Ca^{2+} and cAMP. Finally, oxL influences the expression of several genes involved in many cellular processes, such as inflammation, stress response, lipid metabolism, and cellular proliferation and growth [159–161]. In summary, the presence of oxL not only disrupts the structural integrity of cell membranes but also exerts multifaceted biological effects within organisms.

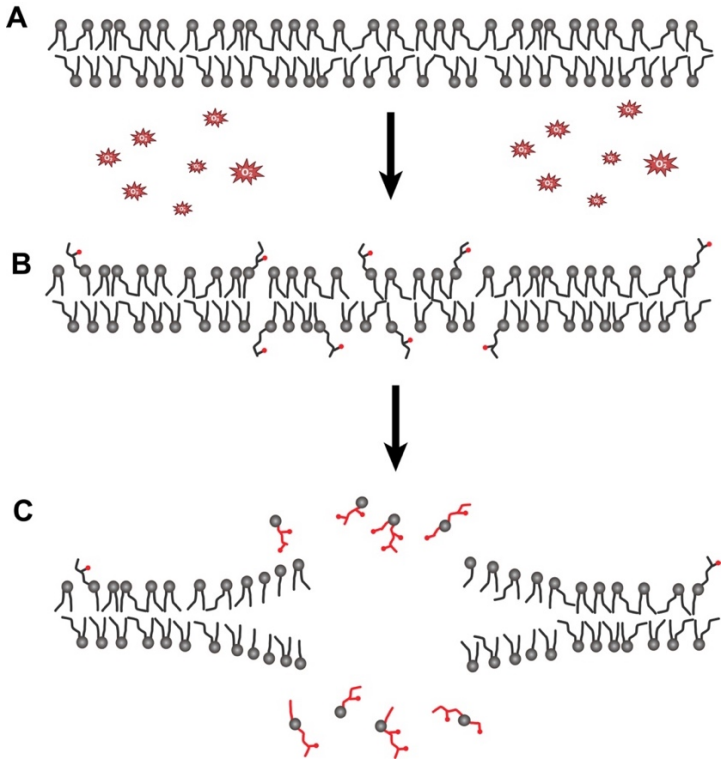

Figure 1.16 Lipid peroxidation of membrane phospholipids.
A) Representation of a typical membrane phospholipid composed of various fatty acids. **B)** Under oxidative stress, membrane phospholipids containing PUFA are vulnerable to attack by oxidants. This oxidative assault results in the generation of oxidized lipids that form whiskers protruding from the surface of the membrane. **C)** Uncontrolled lipid peroxidation eventually leads to the ultimate rupture of the membrane and cell death (Ferroptosis).

1.8 Conclusion

The stability of membrane lipids is essential for the physiological functions of an organism, a fact highlighted by the link between membrane dysregulation and various disease conditions. Therefore, it is critical to continue to probe and understand the regulatory mechanisms required to maintain appropriate membrane composition. Using *C. elegans* as a model coupled with advanced mass spectrometry paves the way for uncovering foundational knowledge in membrane lipid homeostasis. Insights from such studies can be applied to studies in various disease conditions and establish new therapeutic targets. Additionally, alterations in membrane composition are implicated in ineffective therapeutic interventions, and therefore, understanding how membrane composition is modulated can provide new insights that can be applied to improve drug delivery.

CHAPTER 2 - BACKGROUND

This section describes previous studies in our lab and others to uncover the membrane lipid response to glucose stress. I begin by describing earlier work by the Lee lab that identified a link between high glucose and saturated fat accumulation in *C. elegans*. Next, the Pilon lab's work uncovered membrane sensors critical for maintaining membrane homeostasis under glucose stress. Finally, this section ends with a summary of two independently published works (listed below) in our lab that use stable isotope labeling strategies to map the dynamics of membrane lipids under glucose stress.

1. Vieira, A. F. C., **Xatse, M. A.**, Tifeki, H., Diot, C., Walhout, A. J. M., & Olsen, C. P. (2022). Monomethyl branched-chain fatty acids are critical for *Caenorhabditis elegans* survival in elevated glucose conditions. *The Journal of Biological Chemistry*, *298*(2), 101444. https://doi.org/10.1016/j.jbc.2021.101444.
   Contribution- In addition to contributing to writing this article, I conducted independent replicates of the saturated fatty acid supplementation studies for GC/MS analysis and *elo-5* mutants (gk208) lifespan analysis.

2. Vieira, A. F. C., **Xatse, M. A**., Murray, S. Y., & Olsen, C. P. (2023). Oleic Acid Metabolism in Response to Glucose in C. *elegans*. *Metabolites*, *13*(12), 1185. https://doi.org/10.3390/metabo13121185.
   Contribution- I conducted independent replicates of the recovery period and the heat-killed bacteria experiments for this article and contributed to its writing.

2.1 Leveraging glucose stress to study membrane lipid homeostasis

2.1.1 Glucose stress influences lipid metabolism in *C. elegans*

The interconnection of glucose and lipid metabolism has been well-documented [12,18,162]. The classical theory is that glycolytic products from glucose metabolism, such as acetyl CoA, are used to synthesize fatty acids through *de novo* lipogenesis [163,164]. Because SFA is the first product of FA synthesis, glucose is posited to increase the overall SFA pool within the organism. Previous studies in *C. elegans* identified the Sterol regulatory element-binding protein-1 (SREBP) as a critical transcriptional factor that mediates glucose-induced lipotoxicity [85,88]. A high glucose diet leads to the post-transcriptional upregulation of SREBP-1 *C. elegans* homolog SBP-1. Consequently, SBP-1, together with its transcriptional coregulator, the Mediator complex (MDT-15), induces the expression of fatty acid desaturases. These enzymes promote the conversion of saturated fat to unsaturated fat, mitigating the deleterious effects of SFA accumulation induced by glucose stress. Interestingly, genetically inhibiting SBP-1 or MDT-15 exacerbates SFA accumulation and shortens the lifespan of the nematodes under glucose stress. Conversely, overexpressing SBP-1 or MDT-15 confers protection against the detrimental effects of glucose, preventing the shortened lifespan of nematodes on glucose. Therefore, maintaining the flow of unsaturated fat synthesis is critical in nematode response to glucose stress [85,88].

2.1.2 Glucose stress influences membrane composition and requires an adaptive response mediated by membrane sensors

As described earlier, an elevated glucose diet increases the overall pool of SFA that is available in the nematode [88]. A previous study revealed that the nematodes utilize a common pool of fatty acids to maintain the membrane lipids and lipid stores [60]. How does a glucose-mediated increase in the SFA pool impact the membrane lipid composition of the nematode? Recently, the membrane sensor PAQR-2 was identified as a critical transmembrane protein that regulates membrane homeostasis in *C. elegans* [13,14,102,165]. PAQR-2 belongs to the evolutionary conserved Progestin and adipoQ receptors (PAQR) that are localized in the plasma membrane. PAQR-2 was first identified as a critical regulator of membrane fluidity under conditions that promote membrane rigidification,

such as cold and excess SFA in *C. elegans*. PAQR-2 mutants exhibit several phenotypes, such as cold intolerance, withered tail tip, and increased membrane SFA.

Interestingly, a subsequent study revealed that *paqr-2* mutants are intolerant to mild glucose stress (20 mM) and exhibit the same phenotypic defects as conditions that promote membrane rigidification [15]. Further studies show that *paqr-2* animals accumulate excess SFA upon glucose exposure in the membrane and have reduced membrane fluidity as measured by fluorescence recovery after photobleaching (FRAP). The defects of *paqr-2* mutants can be rescued by two classes of mutations. The first class comprises mutations that lead to SBP-1 and MDT-15 overexpression and promote the upregulation of stearyl CoA desaturases (*fat-7*), which converts the excess SFA to UFA [15]. The second class is the mutation in the FLD-1 (membrane fluidity homeostasis-1) gene. FLD-1 is posited to limit the generation of long-chain polyunsaturated fatty acids (LCPUFA)-containing phospholipids or to promote their turnover. Consequently, mutating *fld-1* increases the level of LCPUFA in the membrane, which promotes membrane fluidity and suppresses PAQR-2 defects [166].

To further understand the mechanism by which PAQR-2 mediates membrane response, further studies identified IGLR-2 as an important partner to PAQR-2. IGLR-2 was found to colocalize in the plasma membrane with PARQR-2 based on bifluorescence complementation (BiFC) studies [15]. Therefore, PAQR-2 combines with IGLR-2 in a complex to maintain membrane homeostasis. Mechanistically, the Pilon lab proposed that conditions that reduce membrane fluidity (glucose, cold SFA diet) promote the interaction of IGLR-2 and PAQR-2 that induces a conformational change that displaces the regulatory intracellular domain of PAQR-2, opening the cytoplasm-facing channels for in/out flow of hydrolytic substrates and products that induce a transcriptional response downstream to restore membrane integrity [8,15]. Interestingly, the PAQR-2 and IGLR-2 act cell non-autonomously because expressing PAQR-2 or IGLR-2 in specific tissues such as the intestine or hypodermis rescues membrane fluidity systematically throughout the whole animal [8,15]. Finally, the PAQR-2/IGLR-2 complex is not selective for one particular type of stress but senses a general membrane property, in this case, membrane rigidity. This is because various stresses such as cold, SFA, and glucose that reduce membrane fluidity trigger the same PAQR-2/IGLR-2 response [8,15].

2.2 Mapping the membrane FA dynamics to glucose using ^{13}C-stable isotope labeling strategy

Although an elevated glucose diet requires a compensatory metabolic shift in lipid pathways, the specific adaptive responses of membrane lipids in animals exposed to excess glucose have not been identified. To further understand the mechanistic impact of glucose on membrane FA, we employed our ^{13}C-stable isotope feeding strategy technique and GC/MS to monitor the flux of FA under different concentrations of glucose stress (i.e., 15 mM, 100 mM, and 200 mM). The labeling strategy incorporates a global dietary ^{13}C-stable isotope tracer to monitor the different types of lipids provided to the membrane immediately following glucose supplementation. FA were considered new to the membrane if the molecular weight of intact FA was increased by at least one mass unit (MW + 1, MW + 2, MW + 3, etc.) after correction for the natural abundance of stable isotopes in the environment and the presence of ^{12}C in the labeled OP50 diet. Our investigation unveiled a decline in the incorporation of new SFA. Specifically, we saw a significant decrease in C16:0 at all concentrations and a decrease in C18:0 at 100 mM and 200 mM glucose (Figure 2.1). Furthermore, higher glucose stress (i.e.100 mM and 200 mM) reduced the levels C18:1n9 and C18:2n6 UFA. Despite the potential of a general tracer to probe all the FAs that are present, the extensive fragmentation of highly C20 PUFA (>3 double bonds) by electron impact (EI) source in the mass spectrometer prevents us from monitoring the dynamics of these species. Therefore, the only C20 PUFA we could monitor was the C20:3n6, which was stable at all concentrations relative to the control (Figure 2.1).

Interestingly, we observed an increase in the incorporation of new C17iso into the membrane at 15 mM and 100 mM but not at 200 mM (Figure 2.1). The decrease in the turnover of the SFA was expected as the organism responds to the increase in levels of SFA in the membrane caused by glucose. However, the reduction in new C18:1n9 and C18:2n6 was surprising as the organisms will need to produce MUFA and PUFA to maintain the balance in UFA/SFA levels. The mmBCFAs response to glucose was intriguing, as these FAs have not been associated with glucose stress response. Based on these results, we sought to probe the implications of these responses in the nematode.

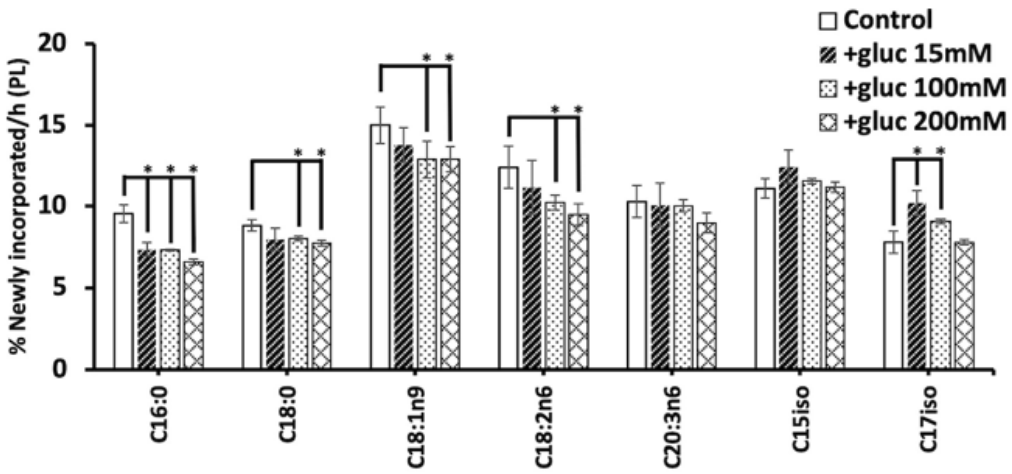

Figure 2.1 Membrane dynamics after exposure to various concentrations of glucose. Synchronized L4 animals were exposed to various concentrations of glucose for 12 hours, followed by 6 h ^{13}C stable isotope feeding. The results show significant changes in the incorporation of new FAs into the membrane after analysis using GC/MS. Results represent the mean ± SEM of at least 9 biological replicates. Statistical significance ($p < 0.05$) was calculated using unpaired t-tests and F-tests to compare variances for each condition compared to the control and is indicated by *

2.3 Oleic acid and Linoleic acid response to glucose stress

2.3.1 Oleic acid and Linoleic acid are funneled to maintain PUFA

To further understand the changes in the flux of oleic acid (C18:1n9) and linoleic acid (C18:2n6), we analyzed the abundance of these FAs using GC/MS. The results unveiled a significant decrease in the abundance of C18:1n9 and C18:2n6 under higher glucose stress conditions (Figure 2.2A). As oleic acid and linoleic acid are precursors for the synthesis of C20 PUFA, we postulated that the decrease in the turnover and abundance of these FA in the higher glucose stress might indicate that they are funneled toward the production of these PUFA. Given that phospholipids containing PUFAs are very susceptible to damage via lipid peroxidation and glucose has previously been shown to cause oxidative stress, we tested this hypothesis by analyzing the composition of the C20 PUFA using GC/MS. Interestingly, the abundance of all C20 PUFA was maintained in all glucose stress concentrations compared to control populations (Figure 2.2 A). These results suggest that the organism funnels C18:1n9 and C18:2n6 towards the production of PUFA to replace those

which is damaged by oxidative stress caused by glucose. Because glucose has been shown to impact lifespan, we sought to determine if the increase in glucose concentration further decreases the longevity of the nematode. To do this, we measured the lifespan under glucose stress for different concentrations, and the results showed that the mean lifespan was decreased under glucose stress as expected, but this effect was not exacerbated by higher glucose concentrations (Figure 2.2B).

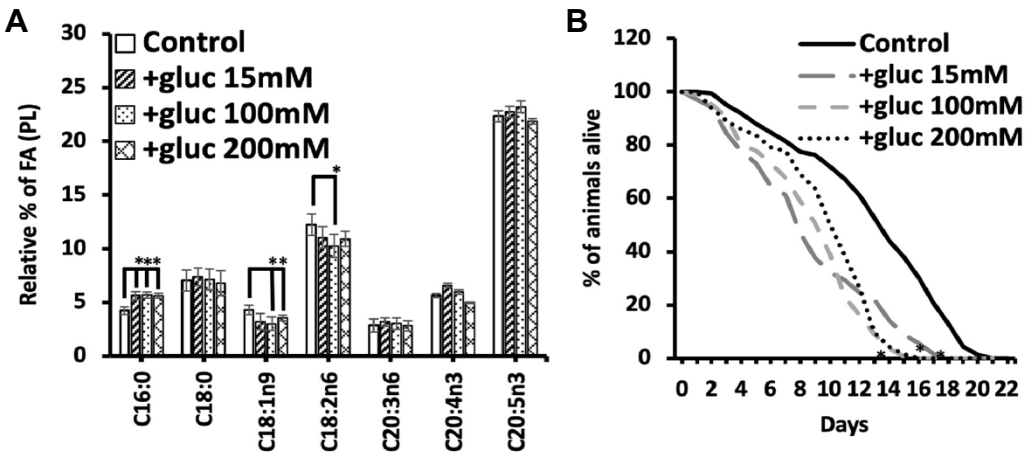

Figure 2.2 The FA composition of animals fed different concentrations of glucose.
A) GC/MS analysis of FA reveal a decrease in the abundance of oleic acid (C18:1n9) and linoleic acid (C18:2n6) and the maintenance of C20 PUFA. **B)** Survival assay shows a significant decrease in lifespan in animals stressed with various concentrations of glucose. Results represent the mean ± SEM of at least 9 biological replicates. Statistical significance ($p < 0.05$) was calculated using unpaired t-tests and F-tests to compare variances for each condition to the control and indicated by *. Survival curves are presented as means of at least three independent replicates with n = 50 nematodes/conditions.

2.3.2 Recovery period drives the shift in Oleic acid and Linoleic acid

The stable isotope labeling protocol necessitates the growth of the animals on an agarose plate containing ^{13}C bacteria. An inevitable consequence is that the animals are off the glucose stress for 6 hours. Consequently, we aimed to probe the impact of this recovery period on the dynamics of C18:1n9 and C18:2n6. To investigate the impact of the recovery, we quantified the abundance of the FAs of animals stressed with 100 mM glucose for 12 hours (+gluc 12 h - no recovery), those subjected to 12 hours followed by a 6-hour recovery period (+gluc 12 h - recovery) and those enduring 18 hours glucose stress (+gluc 18 h - no recovery) (Figure 2.3A). The results show that a recovery period is required for the decrease in the levels of C18:1n9 and C18:2n6 as there was no decrease in the levels in these FAs in +gluc 12 h - no recovery and +gluc 18 h - no recovery (Figure 2.3B). Additionally, we probed the abundance of other FAs in the nematodes. The results revealed an increase in the levels of C16:0 FA in all conditions (Figure 2.3B). Notably, the levels of C16:0 were higher in the treatment group without recovery, with higher levels observed after 18 hours of glucose stress compared to 12 hours of glucose stress (Figure 2.3B). Finally, the levels of all C20 PUFA did not significantly change in all the treatment groups (Figure 2.3C).

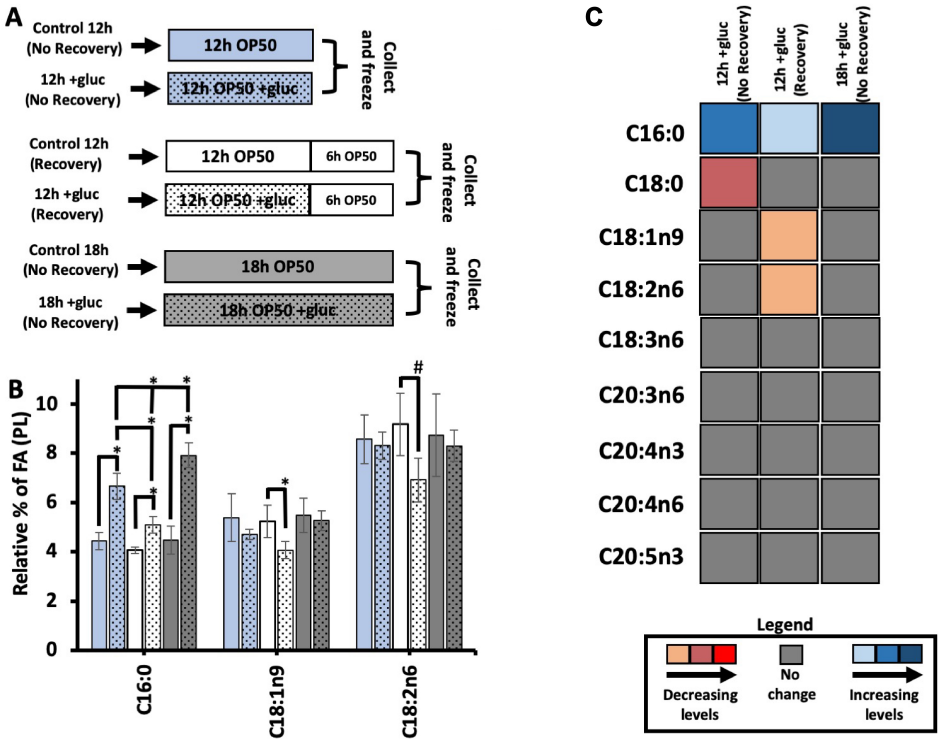

Figure 2.3 Recovery from glucose is required to observe the shift in C18:1n9 and C18:2n6. **A)** Scheme for recovery experiment: For each comparison, the addition of glucose is represented by the inclusion of black dots vs. the control with no dots. **B)** C16:0 SFA showed a significant increase in all glucose-stressed animals relative to its controls, with the 18-h period showing a significantly more accumulation of C16:0. Both C18:1n9 and C18:2n6 maintain stable levels in animals with no recovery but showed a significant decrease in +gluc 12 h (recovery) compared to their respective control. **C)** A heat map shows the alteration in FA levels comparing stressed animals to controls (+gluc/controls). The result represents the mean ± SEM of at least 9 replicates. For statistical significance, $p < 0.05$ is indicated by *, and $p < 0.1$ is indicated by #, calculated using unpaired t-tests and F-tests to compare variances.

2.3.3 Oleic acid and Linoleic dynamics stabilize with longer glucose exposure

To gain a comprehensive understanding of the dynamics of C18:1n9 and C18:2n6, we investigated the impact of varying periods of exposure to glucose on the nematodes. To do so, the animals were stressed with 100 mM glucose for 12 h, 24 h, 48 h, and 72 h with a 6 h recovery period, and the FA composition was measured. Our findings revealed that the levels of C18:1n9 were further decreased in 24 h compared to 12 h. Interestingly, the abundance of C18:1n9 remained stable at 48 hours and 72 hours (Figure 2.4A). Similarly, C18:2n6 significantly decreased in abundance at 24 hours, and there was no significant change at 48 hours. Strikingly, we observed a significant decrease in the abundance of C18:2n6 after 72 hours (Figure 2.4A). In addition to monitoring the abundance, we measured the flux of C18:1n9 and C18:2n6 in all treatment durations using ^{13}C stable isotope feeding strategies. The turnover of C18:1n9 and C18:2n6 remained stable at 24 h, but at 48 h, there was a significant decrease in the turnover of C18:2n6 and not C18:1n9 (Figure 2.4C). Finally, there was a significant increase in the flux of C18:1n9 and C18:2n6 after 72 h (Figure 2.4C). To further probe whether the dynamics of C18:1n9 and C18:2n6 influenced the C20 PUFA, we measured the abundance of C20 PUFA at all treatment durations. There was an increase in C20:4n3 at all treatment duration except 12 h and a decrease in C20:5n3 at 12 h. In addition, C20:5n3 significantly increased at 72 h (Figure 2.4B). Collectively, these results corroborate the upregulation of FAT-7 during glucose exposure, which stabilizes over time, aligning with the hypothesis that C18:1n9 and C18:2n6 are funneled to preserve C20 PUFA.

In addition to monitoring the overall flux of FA, our stable isotope labeling technique can also allow us to define the origin of the FA that is incorporated into the membrane. We utilized this to define the amount of new FAs derived from synthesis. First, we quantified the amount of C16:0 FA derived from synthesis since this FA is the main product of *de novo* synthesis (Figure 2.4D). In doing so, the results show a significant decrease in the synthesis of new C16:0 after 12 h of exposure to glucose but no other time points. The reduction in synthesis further corroborates the need to reduce the amount of SFA accumulated upon glucose stress (Figure 2.4A). We extended this to quantify the overall levels of synthesis in C18:1n9. The results show a significant decrease in the synthesis of C18:1n9 after 12 h of glucose stress (Figure 2.4D). This trend is consistent with

the overall flux results and suggests that the processing of synthesized FA drives these dynamic changes (Figure 2.4D).

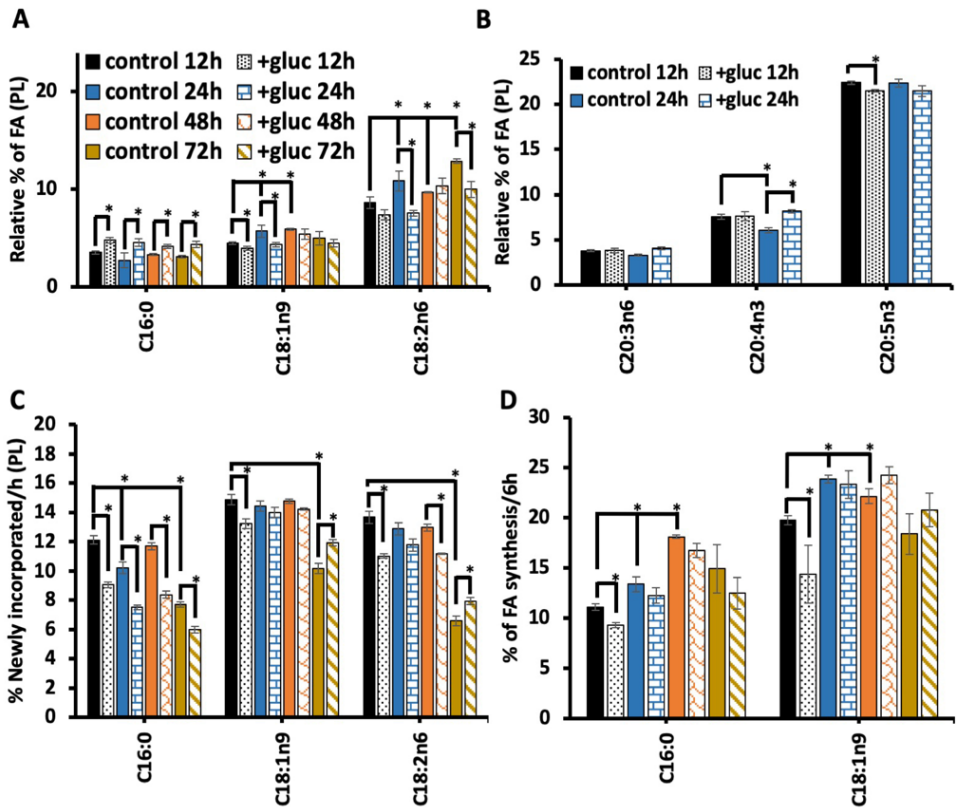

Figure 2.4 Longer stress periods stabilize oleic acid and linoleic acid levels.
A) The relative abundances of C16:0, C18:1n9, and C18:2n6 were found using GC/MS in the following treatment groups: +glu 12 h (black dot), 24 h +gluc (blue horizontal brick), +gluc 48 h (orange hatch) and +gluc 72 h (gold diagonal stripes). The FA abundances were compared to age-matched controls without glucose exposure: 12 h (black bars), 24 h (blue), 48 h (orange), and 72 h (gold). **B)** The relative % of C20:3n6, C20:4n3, and C20:5n3 were assessed in 12 h and 24 h nematodes with and without glucose treatment. **C)** The % of newly incorporated FA was quantified after incorporating dietary stable isotopes in the same treatment groups defined above. **D)** FA synthesis was calculated based on the abundance of isotopomers characteristic of synthesis (i.e., MW 272–284 for C16:0 and MW 301–313 for C18:1n9) after correcting for the natural abundance of isotopes and, correcting via a normalization factor, it accounted for differences in the distribution of isotopes in the diet. The result represents the mean ± SEM of at least 4 replicates. For statistical significance, $p < 0.05$ is indicated by *, and calculated using unpaired t-tests and F-tests to compare variances.

2.4 Monomethyl branched-chain fatty acids (mmBCFAs) response to glucose stress

2.4.1 mmBCFAs are critical for surviving glucose stress

In addition to the canonical saturated FA (SFA) and unsaturated FA (UFA), the membrane lipids of *C. elegans* contain a unique type of FA known as monomethyl branched-chain fatty acids (mmBCFAs). The isotope flux study revealed an increase in the production of mmBCFA (C17iso) at 15 mM and 100 mM glucose stress (Figure 2.5A). The alterations in the flux of C17iso is intriguing, given that these lipids have not been previously associated with a glucose response. To ascertain whether mmBCFA production was required to respond to glucose stress, the mmBCFA production in the nematode was compromised using RNAi. In *C. elegans*, mmBCFAs are synthesized from branched-chain amino acids leucine by fatty acid synthase (FASN-1), and the elongases - ELO-5 and ELO-6 to make C15iso and C17iso (Figure 2.5A). RNAi knockdown of *elo-5,* which reduces the production of C15iso and C17iso, leads to a dramatic shortening of the lifespan of the nematodes under glucose stress (Figure 2.5B). Interestingly, depleting on C17iso alone by *elo-6* RNAi-treatment did not impact the survival of the animals under glucose stress, suggesting that ELO-5 is the primary mmBCFA enzyme responsible for the glucose stress response.

To investigate further whether there is an increase in mmBCFA, we examined the expression of *elo-5* and *elo-6* using qRT-PCR. In doing so, we saw a significant upregulation of *elo-5* and *elo-6* in glucose stress (Figure 2.5C). To further validate the direct influence of mmBCFAs on the response to glucose, we fed nematodes with the bacteria *Bacillus subtilis* (Figure 2.5D). *B. subtilis* consist of ~16 % of iso mmBCFAs, C15iso and C17iso, in its FA composition (Figure 2.5E). Interestingly, supplementing the diet of ELO-5 deficient animals restored their survival on glucose to WT levels (Figure 2.5D). These results underscore the critical role of mmBCFAs in responding to and surviving glucose stress.

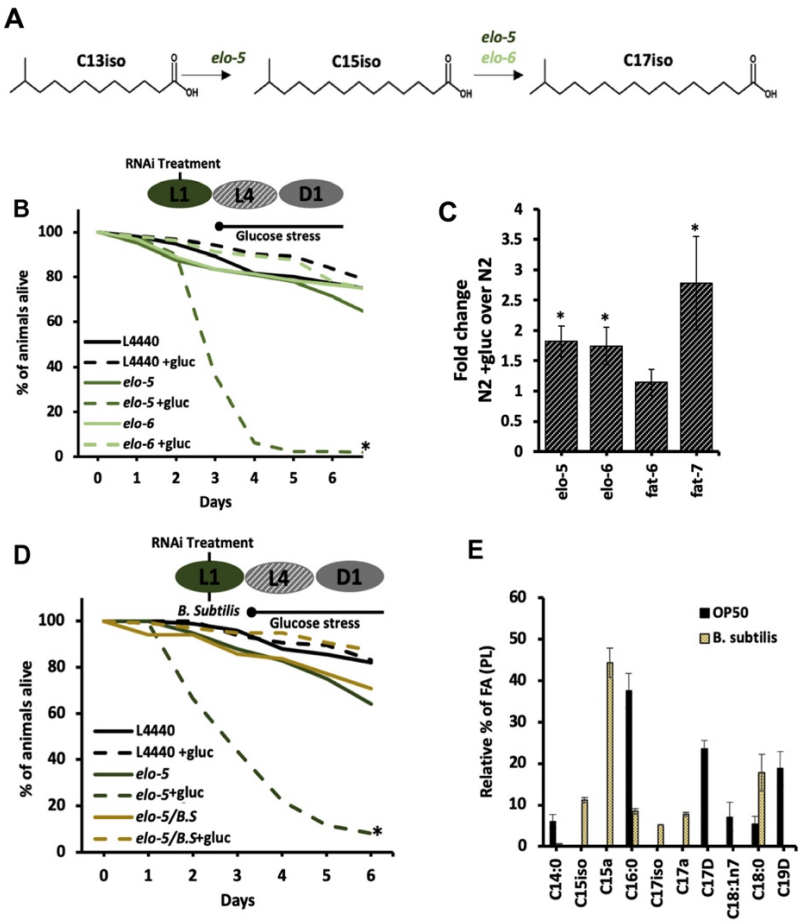

Figure 2.5 mmBCFAs are essential for survival with elevated dietary glucose.
A) The elongases, *elo-5* (dark green) and *elo-6* (light green), produce the two mmBCFAs (C15iso and C17iso) by elongation steps shown here. **B)** Survival assay shows that RNAi knockdown of *elo-5* (dark green) significantly shortened lifespan under glucose stress, while RNAi *elo-6* (light green) does not have any effect. **C)** qRT-PCR was conducted on N2 +gluc and normalized to untreated animals. The expressions of *elo-5*, *elo-6*, and *fat-7* were significantly upregulated. **D)** To confirm the role of mmBCFAs in survival on +gluc plates, L1 animals were fed a bacteria strain rich in mmBCFAs (*B. subtilis*) (yellow). A ratio of 1:1 (RNAi bacteria to *B. subtilis* ratio) was used to ensure sufficient knockdown of *elo-5*. **E)** FAMEs were analyzed by GC/MS to generate an FA profile of the diet. *B. subtilis* (yellow) compared to OP50 (black). There are significant differences, including elevated C15iso and C17iso (mmBCFA) and C15a and C17a (anteiso mmBCFA). Survival curves are presented as means of at least three independent replicates with n = 50 nematodes/conditions.

2.4.2 mmBCFA acts in the PAQR-2 network of response to glucose

The membrane sensor PAQR-2 is well-established as a key player in responding to the impact of glucose on membrane lipids [15]. To investigate whether *elo-5* is also activated as part of the metabolic response to glucose through PAQR-2, we quantified the amount of mmBCFAs in *paqr-2(tm3410)* animals stressed with glucose. Strikingly, the levels of mmBCFAs were significantly decreased in *paqr-2(tm3410)* animals stressed with glucose (Figure 2.6A). Furthermore, when we examined the flux of new fatty acids after the stress, we observed a significant decrease in the turnover of C15iso and C17iso (Figure 2.6B). Notably, analysis of the flux of other FAs reveals a global reduction in the turnover of all species in *paqr-2(tm3410)* animals stressed with glucose. In addition, we monitored the expression of *elo-5* in *paqr-2(tm3410)* mutants under glucose stress (Figure 2.6C). The qRT-PCR analysis revealed that PAQR-2 indeed regulates *elo-5* as the expression *elo-5* is downregulated in *paqr-2(tm3410)* mutant, and this downregulation is further exacerbated with glucose stress (Figure 2.6C). Taken together, these results suggest that PAQR-2 may play a pivotal role in regulating the response of *elo-5* to glucose stress.

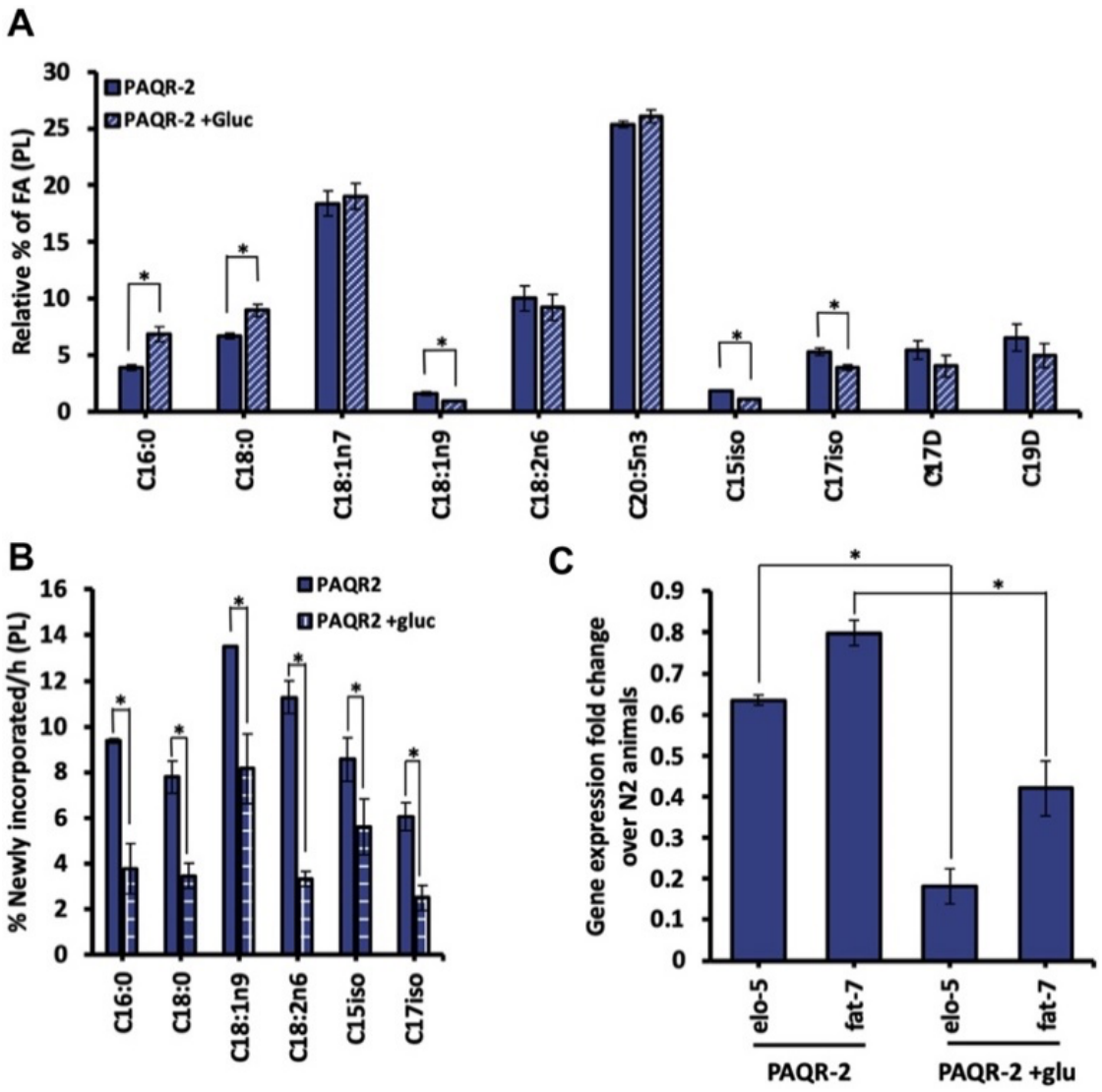

Figure 2.6 PAQR-2 upregulates mmBCFA production under glucose stress.
A) *paqr-2(tm3410)* mutants in the L4 stage (48 h old) were fed OP50 bacteria seeded onto HG plates with (blue stripe) or without 15 mM of glucose (blue) for 12 h. Using GC/MS, the FA composition of PLs was assessed and significant changes were found in C16:0, C18:0, C18:1n9, C15iso, and C17iso as indicated by the *. **B)** a 6 h-period of isotope labeling shows a significant decrease in the amount of newly incorporated FAs (marked by ^{13}C-isotopes) in all species quantified in *paqr-2(tm3410)* animals fed glucose (blue checkered). **C)** quantitative real-time PCR was implemented to quantify the transcript levels of *elo-5* and *fat-7* in *paqr-2(tm3410)* mutants compared with controls. There is a significant reduction in the expression of *elo-5* and *fat-7* compared with N2 controls, as denoted by *. The relative % of FA and the % newly incorporated FA/h represent means ± SEM of at least three independent replicates. Statistical significance ($p < 0.05$) was calculated using an unpaired t-test and F-test to compare variances.

2.4.3 mmBCFAs act in parallel to the fluidity response in glucose stress

The primary response orchestrated by PAQR-2 in response to glucose stress is restoring membrane fluidity caused by the accumulation of excess SFA from glucose stress. The presence of the methyl group at the iso position of mmBCFAs can disrupt the packing of lipids in the membrane and impact membrane fluidity. To investigate whether mmBCFA plays a role in restoring membrane fluidity, the mmBCFA-deficient nematodes were fed 2mM C16:0 SFA (Figure 2.7A). The results reveal that an excess SFA did not shorten the lifespan of either *elo-5* or *elo-6* deficient animals (Figure 2.7A). Additionally, GC/MS analysis confirmed a significant amount of SFA available in the diet of the nematodes and a significant accumulation of the SFA in the nematode (Figure 2.7B). Consequently, the role of mmBCFA is unique to glucose stress response and is independent of the excess SFA caused by glucose stress.

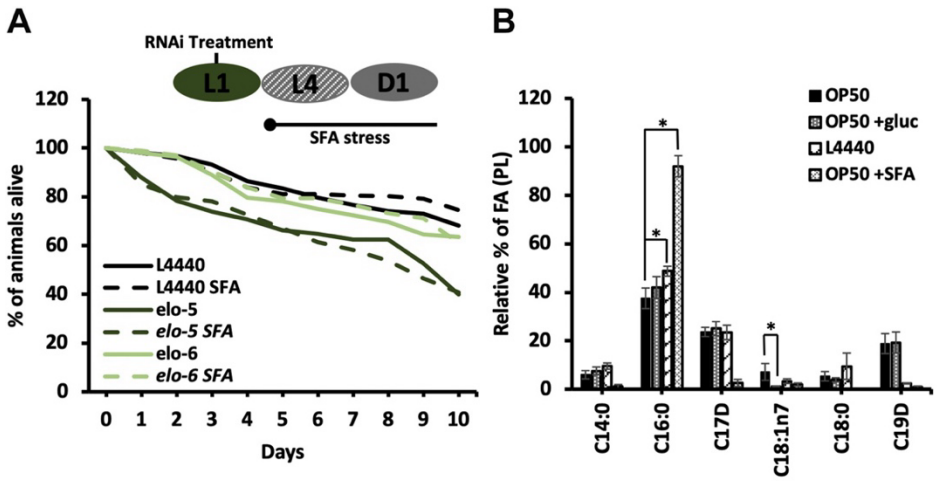

Figure 2.7 mmBCFAs are not required to respond to elevated dietary SFA.
A) Bacteria containing RNAi vectors (L4440, *elo-5*, and *elo-6*) were grown in LB + tetracycline + carbenicillin containing 2 mM of palmitic acid (C16:0), which is labeled as +SFA. Synchronized animals grown under RNAi background were moved to +SFA plates (dashed line) at the end of the L4 stage, and the percentage of animals alive was assessed daily. There was no significant difference in viability with RNAi treatment. **B)** GC/MS was used to assess the FA composition of the supplemented bacteria in comparison to the OP50 (black) and L4440 controls (diagonal bricks). There were slightly higher levels of SFA in the L4440 versus the OP50 control. Significantly higher levels of SFA were measured in the enriched OP50 +SFA (white dotted) as expected.

2.5 Conclusion

In these investigations, we employed a comprehensive approach combining ^{13}C-stable isotope labeling technique, lifespan assays, and time course studies to elucidate the membrane fatty acid response to glucose stress. The response is mediated by the membrane sensor PAQR-2, which activates two distinct downstream pathways. In response to the excess SFA caused by glucose stress, PAQR-2 activates *fat-7,* which upregulates the synthesis of UFAs. This adaptive response requires the funneling of oleic acid (C18:1n9) and linoleic acid (C18:2n6) to maintain the abundance of C20 PUFA. We hypothesized that these C20 PUFA are specifically damaged by elevated oxidative stress caused by glucose stress (Figure 2.8). In Chapter 4 of this dissertation, I probe further to confirm this hypothesis by developing and optimizing targeted mass spectrometry approaches to quantify the extent of damage caused by glucose stress.

Conversely, PAQR-2 activates *elo-5,* which increases the synthesis of mmBCFAs. The role of mmBCFAs is not in restoring the balance in SFA/UFA, but instead, this FA may be involved in other responses, such as signaling via more complex lipids (Figure 2.8). In Chapter 3, I present additional studies to further elucidate the mechanistic role of mmBCFA response to glucose stress. These investigations reveal that mmBCFAs serve a crucial role in producing the complex sphingolipids, glucosylceramides, which are critical for responding to glucose stress.

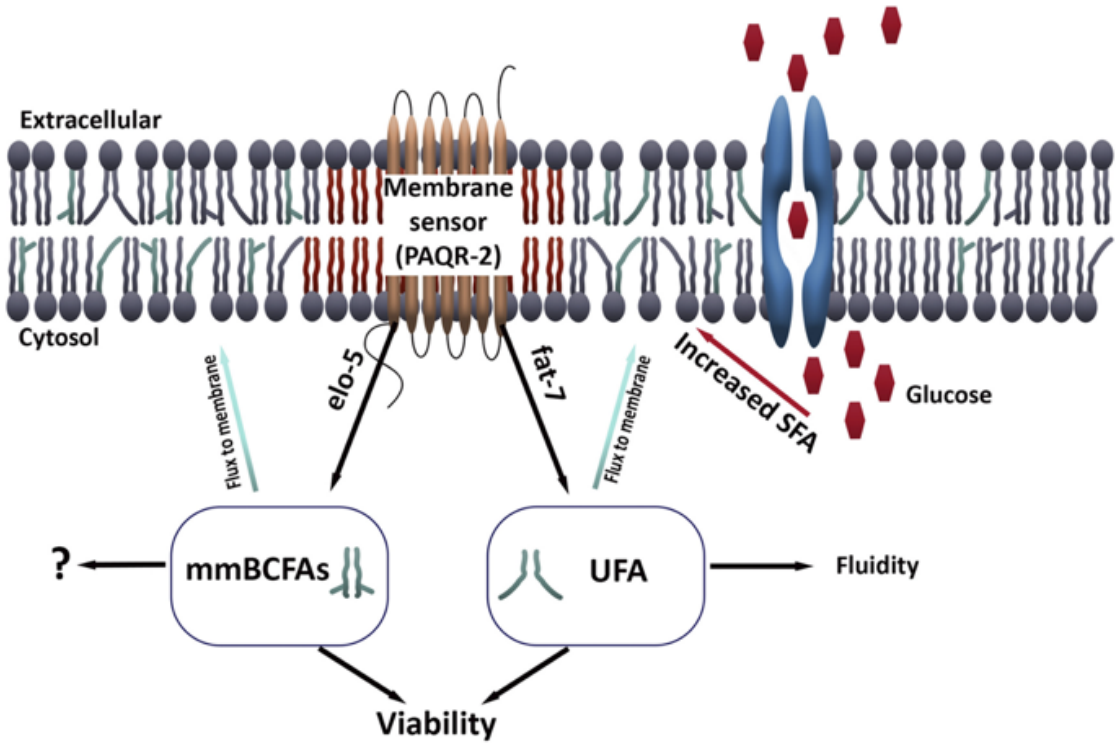

Figure 2.8 Model describing the membrane FA response to glucose stress.
Elevated dietary glucose increases the accumulation of SFA and drives a response coordinated by PAQR-2. Next, PAQR-2 impacts the transcription of *elo-5* and *fat-7* to restore membrane integrity and promote survival under glucose stress. Unlike UFA, the role of mmBCFAs is not to restore overall fluidity; instead, this fatty acid may be involved in signaling.

CHAPTER 3 - TARGETED LIPIDOMICS REVEALS A NOVEL ROLE FOR GLUCOSYLCERAMIDES IN GLUCOSE RESPONSE

Mark A. Xatse, Andre F. C. Vieira, Chloe Byrne, and Carissa Perez Olsen *

Published in Journal of Lipid Research (2023)

Department of Chemistry and Biochemistry, Worcester Polytechnic Institute, Worcester, MA, USA

*Corresponding Author. Email: cpolsen@wpi.edu

Author contributions

The phospholipidomics were done by Mark Xatse and Chloe Byrne. Mark Xatse carried out Sphingolipidomics. Andre F. C. Vieira conducted the *cgt-3* and *cgt-1* lifespan data. Andre Vieira and Mark Xatse generated independent replicates of the *elo-3* lifespan data. Finally, the sphingolipid extract rescue experiment was carried out by Mark Xatse

3.1 Abstract

The addition of excess glucose to the diet drives a coordinated response of lipid metabolism pathways to tune the membrane composition to the altered diet. Here, we have employed targeted lipidomic approaches to quantify the specific changes in the phospholipid and sphingolipid populations that occur in elevated glucose conditions. The lipids within wild-type *Caenorhabditis elegans* are strikingly stable, with no significant changes identified in our global mass spectrometry-based analysis. Previous work has identified ELO-5, an elongase that is critical for the synthesis of monomethyl branched-chain fatty acids (mmBCFAs), as essential for surviving elevated glucose conditions. Therefore, we performed targeted lipidomics on *elo-5* RNAi-fed animals and identified several significant changes in these animals in lipid species that contain mmBCFAs as well as in species that do not contain mmBCFAs. Of particular note, we identified a specific glucosylceramide (GlcCer 17:1;O2/22:0;O) that is also significantly upregulated with glucose in wild-type animals. Furthermore, compromising the production of the glucosylceramide pool with *elo-3* or *cgt-3* RNAi leads to premature death in glucose-fed animals. Taken together, our lipid analysis has expanded the mechanistic understanding of metabolic rewiring with glucose feeding and has identified a new role for the GlcCer 17:1;O2/22:0;O.

3.2 Introduction

Cell membranes are highly organized and dynamic structures made up of hundreds of unique lipids [2,4]. Perturbations, including temperature changes and dietary alterations, can alter membrane composition and require regulation of metabolic pathways to adjust the makeup of the membrane and optimize its function in the new conditions [7,9,103]. Of note, elevated glucose concentrations in the diet of nematodes require an adaptive response coordinated by the membrane sensor, PAQR-2, which is homologous to the mammalian adiponectin receptor. In response to glucose stress and the decreased fluidity associated with high glucose, PAQR-2 activates the desaturase FAT-7, which increases the production of unsaturated fatty acids to restore the fluidity of the membrane [12,15,166]. Recently, a novel role for the elongase, ELO-5, as part of the response of PAQR-2 to glucose was found using stable isotope labeling and mass spectrometry approaches. Specifically,

ELO-5 is required to produce monomethyl branched-chain fatty acids (mmBCFAs), and RNAi of *elo-5* results in a sensitivity to glucose diets [59]. Although the elevated FAT-7 activity results in the production of unsaturated fatty acids to restore membrane fluidity, the impact of ELO-5 is less clear and does not appear to directly impact fluidity [15,59].

Distinct from saturated and unsaturated fatty acids, mmBCFAs have a saturated hydrocarbon chain and a methyl group located in the penultimate carbon, giving these fatty acids a unique shape [106]. In *C. elegans*, the major laboratory diet of *E. coli* (OP50) does not contain mmBCFAs, and thus, they are entirely synthesized de novo via fatty acid synthase, acyl-CoA synthase, and two fatty acid elongase enzymes, ELO-5 and ELO-6 [60]. The mmBCFAs are incorporated into phospholipids [167], and in *C. elegans*, they also serve as precursors for the sphingoid base required to produce sphingolipids (Sphs) [54,55,133]. mmBCFAs production is essential for larval growth and development, and the roles of these fatty acids in adults have recently started to emerge [107,168]. Recently, it was established that mmBCFAs-derived glucosylceramides (GlcCer) are critical in regulating intestinal apical membrane polarity to allow TORC1 activity in response to nutrient signals in the intestine [110,145].

GlcCer are considered Sphs and are intermediates of Sph metabolism. Sphs are a highly diverse group of lipid species that contain a sphingoid backbone made up of a linear hydrocarbon chain attached to an amino and hydroxyl group [42]. The sphingoid base is amide linked to long-chain fatty acids, usually containing 0 or 1 double bond to form ceramides. Ceramides can further be derivatized by the addition of a head group to form more complex Sphs such as sphingomyelin, GlcCer, and other complex glycosphingolipids (GSLs) with higher numbers of sugar residues [40,129]. Ceramides not only are precursors for complex Sphs but also act as a metabolite with roles in stress response, autophagy, apoptosis, and signaling [169–171]. These processes are often mediated by specific chain-length ceramides that are expressed in distinct subcellular compartments that perform unique functions [172,173]. For instance, in *C. elegans*, mmBCFA-derived ceramides are produced by three different ceramide synthases: HYL-1, HYL-2, and LAGR-1. HYL-1 is required to produce ceramides with very long N-linked fatty acids (C24 to C26), HYL-2 is required for ceramides with long N-linked fatty acids (C20-C22), and LAGR-1 has no major effect on ceramide production [132,133].

GlcCer are the precursors to more complex GSLs and are formed by adding a UDP-glucose to an existing ceramide molecule by ceramide glucosyltransferase (CGT) [134]. GSLs impact the structure, localization, and activity of raft-associated proteins and, in doing so, influence cellular activities, including protein-protein interaction and signaling events [174,175]. In fact, recent studies in *C. elegans* suggest that GSL interacts with cholesterol to form lipid rafts that regulate clathrin localization and signaling processes involved in stress response [137]. In *C. elegans*, the production of GlcCer is dependent on ELO-3, a recently characterized elongase that produces the very long-chain saturated fatty acids included in GlcCer. In addition to supplying precursors for GSLs that have been implicated in stress responses, GlcCer have been implicated as important metabolites for aging in *C. elegans* [137]. Because of the crucial roles GSLs play in most organisms, impaired GSL metabolism is linked to many disorders such as cardiovascular diseases, compromised immune response, Gaucher disease, and neurodegeneration [45,176–178]. However, the complexity of these lipid populations has limited the knowledge of how each lipid species impacts cellular function.

C. elegans has become a useful model for studying lipid metabolism using mass spectrometry and genetic approaches [11,32,35]. In addition, the small size of *C. elegans* allows for affordable, stable isotope labeling to monitor lipid dynamics. Our laboratory has developed ^{15}N- and ^{13}C- stable isotope feeding strategies in *C. elegans* combined with mass spectrometry to monitor the dynamics of intact phospholipids and fatty acids, respectively [10,59,60]. Using a combination of approaches, it has been established that mmBCFAs are essential to the nematode's survival with glucose stress. However, it is unknown whether this is through a derived lipid, a structural impact on the membrane, or an unknown alternate mechanism [59]. Here, we use advanced mass spectrometry to profile the changes in the lipids after glucose exposure, which allows a more thorough understanding of how glucose impacts the phospholipids of the membrane with a particular focus on the Sphs, including GlcCer. These lipidomics profiles reveal changes in the ceramide and GlcCer populations following glucose exposure that have been corroborated with glucose survival assays.

3.3 Materials and methods

3.3.1 Strains and RNAi treatment

All experiments were conducted using wild-type N2 nematodes obtained from the *C. elegans* Genetics Center. For RNAi experiments, RNAi bacteria clones from the Ahringer library [L4440 (empty vector), *elo-5, elo-3,* and *cgt-3*] were grown on NGM + Carbenicillin + IPTG plates (NGM+CI) [95].

3.3.2 Nematode growth and elevated glucose feeding protocols

To synchronize the nematodes, gravid adults were exposed to dilute bleach, and the washed eggs were left rotating overnight at 20°C in M9 solution. Approximately 5,000–6,000 synchronized L1 animals were grown at a density of 2,000 worms per 10 cm RNAi treatment plate for 48 h. At L4, nematodes were transferred to NGM+CI plates with (referred to as +gluc plates) or without glucose for an additional 18 h.

The glucose stress was carried out as previously described [59]. Briefly, the glucose plates were made to a final concentration of 100 mM glucose by adding a filtered glucose solution to a cooled autoclaved NGM+CI medium. The glucose plates were seeded with RNAi bacteria for at least four days before plating the worms. RNAi bacteria, along with the control RNAi, were seeded on plates at a density of 0.15 g per 10 cm NGM+CI plate.

3.3.3 Extraction and detection of phospholipids by HPLC-MS/MS

Total lipids were extracted from frozen nematodes via chloroform/methanol (2:1 v/v) solvent system as previously described [10,31]. A 1,2-diundecanoyl-sn-glyerco-3-phosphocholine standard was added for relative quantification later, as described previously (Avanti Polar Lipids). Briefly, total lipid extracts were dried under nitrogen and then dissolved in 200 µl of acetonitrile/2-propanol/water (65:30:5 v/v/v) dilution buffer. Next, 10 µl of resuspended lipids were injected into the HPLC-MS/MS system for the negative ion scanning mode analysis. Lipid samples were separated using an HPLC system (Dionex UHPLC UltiMate 3000) equipped with a C_{18} Hypersil

Gold 2.1 × 50 mm, 1.9 μm column (25002-052130; Thermo Scientific) equipped with a 2.1 mm ID, 5 μm Drop-In guard cartridge (25005-012101; Thermo Scientific). The column was connected to a Dionex UltiMate 3000 RS quaternary pump, a Dionex UltiMate 3000 RS autosampler, and a Q Exactive Orbitrap mass spectrometer from Thermo Scientific coupled with a heated electrospray ionization source.

The HPLC phospholipid separation was carried out with mobile phases A and B consisting of 60:40 water (H_2O): acetonitrile plus 10 mM ammonium formate (NH_4COOH) and 0.1% formic acid and 90:10 isopropyl alcohol (IPA): acetonitrile with 10 mM ammonium formate (NH_4COOH) and 0.1% formic acid, respectively. The gradient method began with 32% B over 0–1.5 min; 32%–45% B from 1.5 to 4 min; 45%–52% B from 4 to 5 min; 52%–58% B from 5 to 8 min; 58%–66% B from 8 to 11 min; 66%–70% B from 11 to 14 min; 70%–75% B from 14 to 18 min; 75%–97% B from 18 to 21 min; 97% B up to 25 min; 97%–32% B from 25 to 26 min; 32% B is maintained until 30 min for column equilibration.

The following parameters were used for the HPLC and MS conditions: column oven temperature was maintained at 50°C, autosampler was set at 10°C with mobile phase flow rate at 300 μl/min, and MS scan range between *m/z* 300 and 1,200. The capillary temperature was set at 325°C, the sheath gas flow rate was set at 45 units, the auxiliary gas flow was set at 10 units, the source voltage was 3.2 kV, and the AGC target was 10^6. The acquisition was carried out with full-scan data-dependent MS2 (ddMS2) mode. For MS1 profiling, scans were run at a resolution of 70k. MS2 analyses were performed using six scan events, where the top five ions were chosen from an initial MS1 scan. For fragmentation, a normalized collision energy of 35 was used. MS1 spectra were collected in profile mode, whereas MS2 spectra were collected in centroid mode.

3.3.4 Extraction and detection of sphingolipids by HPLC-MS/MS

Sphingolipid extractions were conducted based on previous studies [42,55,131]. Briefly, total lipids were extracted from nematodes with 2:1 chloroform: methanol for 1.5 h. Ceramide/sphingoid internal standard mixture II (Avanti Polar Lipids) was added prior to extraction. Extracted lipids were dried under nitrogen, and 50 μl of 1 M KOH in methanol was added. The mixture was

vortexed briefly and incubated at 37°C for 2 h. After incubation, the sample was neutralized with 2–3 µl of glacial acetic acid. After phase separation with 450 µl methanol, 1,000 µl chloroform, and 500 µl of water, the Sph fraction (organic phase) was dried under nitrogen and dissolved in 200 µl of isopropanol/chloroform/methanol (90:5:5, v/v/v).

The Sphs (10 µl injection) were separated and analyzed using the same instrument used for phospholipids with the following modification to the instrument method adapted from a recent study[179]. The mobile phase A consisted of water containing 1% formic acid and 10 mM ammonium formate, while the mobile phase B consisted of 5:2 (v/v) acetonitrile/isopropanol containing 1% formic acid and 10 mM ammonium formate. The gradient method started at 50% mobile phase B, rising to 100% B over 15 min, held at 100% B for 10 min, and the column was then re-equilibrated with 50% B for 8 min before the next injection. The flow rate was 0.150 ml/min. For MS analysis, Sphs were analyzed in the positive mode with the following parameters: the capillary temperature was set at 275°C, the sheath gas flow rate was set at 45 units, the auxiliary gas flow was set at 10 units, the source voltage was 3.2 kV, and the AGC target was 10^6. The acquisition was carried out with full-scan data-dependent MS2 (ddMS2) mode. For MS1 profiling, scans were run at a resolution of 70k. MS2 analyses were performed using five scan events, where the top five ions were chosen from an initial MS1 scan. For fragmentation, a normalized collision energy of 50 was used. MS1 spectra were collected in profile mode, whereas MS2 spectra were collected in centroid mode.

3.3.5 Phospholipid and sphingolipid analysis

Lipid analysis of the LC-MS/MS data was conducted using the software Lipid Data Analyzer (LDA) Version 2.8.1. The LDA utilizes a 3D algorithm relying on the exact mass, predicted isotopic distribution from full scan MS, retention time, and MS/MS spectra for reliable analysis of the lipids [179]. During LDA analysis, a 0.1% relative peak cutoff value was applied to the RAW files in order to focus on the major lipid species. LDA mass lists were generated for phospholipids based on a previous study in our laboratory [10]. A relative quantification was used to compare between samples; however, the lipids were not normalized, so an absolute quantitation was not done.

LDA mass lists for ceramide and GlcCer were created by combining the carbon length of the sphingoid backbone in *C. elegans* (C17iso SPB) [54,131] with *N*-linked fatty acid tail ranging from a chain length of 16–28 with degrees of saturation of 0 and 1, which is common for Sphs [40]. MS2 scans were manually verified on Xcalibur version 4.1.31.9 for the sphingoid base fragment specific for *C. elegans* of ***250.25***.

Statistical analysis for all the studies were performed using GraphPad Prism 9.4.1 software. Multiple *t-tests* (unpaired) corrected by false discovery rate and an adjusted p-value (q) at 5% were used to compare two conditions in the lipidomics data.

3.3.6 Survival analysis

Lifespan was performed with 50 synchronized L4 animals on NGM+CI plates with or without glucose for each replicate. Worms were transferred every day onto fresh plates, and the number of dead animals was confirmed by prodding each animal and recorded daily. For lifespan data, statistical analysis was performed using a log-rank (Cox-Mantel) test.

3.3.7 Sphingolipid supplementation

Sph were extracted from adult WT animals (grown for 66 h post L1) as described above. Ethanol was added to dried Sph at a density of ~50,000 worms per 5 ml of ethanol. The solution was filtered with a 22 µm syringe and stored at -20°C. For lifespan analysis, 50 µl of Sph extract or ethanol was pipetted per 3 cm NGM +CI plates seeded with RNAi bacteria. For large-scale lipidomics analysis, 500 µl of Sph extract or ethanol was pipetted per 10 cm NGM +CI plates.

3.4 Results

3.4.1 Phospholipid populations with glucose exposure

Although it is clear that fatty acid metabolism is perturbed by excess dietary glucose, the specific changes in the phospholipids of the animals have not been defined. Here, we profiled the phospholipids of control RNAi animals in the presence of 100 mM glucose. Populations of nematodes (L4 stage) were grown with (+gluc) and without 100 mM glucose for 18 h, and membrane lipids [i.e., phosphatidylcholine (PC), phosphatidylethanolamine (PE), lysophosphatidylcholine (LPC), lysophosphatidylethanolamine (LPE), plasmanyl ethanolamine (PE O-) and plasmenyl ethanolamine (PE P-)] were analyzed using a Q Exactive mass spectrometer (Thermo Scientific, Waltham, MA). The relative abundance of the lipids was determined using Lipid Data Analyzer software, and the fold change of distinct lipids under glucose stress was compared. The results showed no significant differences in any of the phospholipids in the target list after 18 h of glucose exposure (Figure 3.1A; complete list found as supplemental Table S1). The lack of significant changes in wild-type nematodes fed glucose is not surprising as it has been established that N2 animals can adapt to high-glucose diets [15,59]. In addition, these populations build most of the membrane, and the glucose exposure is relatively short, minimizing the impact of metabolic changes on the entire population due to dilution effects.

We next examined the impact on the phospholipid population when the glucose response is compromised by using an *elo-5* RNAi feeding approach. Here, *elo-5* RNAi was initiated at L1 stage for 48 h, and then the animals were transferred to plates with and without glucose for 18 h. First, to establish a baseline comparison, *elo-5* RNAi and control RNAi-fed animals were compared, and the results reveal that ~58% of the lipids (92/159) were significantly changed with *elo-5* RNAi (Figure 3.1B). Next, *elo-5* RNAi-treated animals were subjected to 18 h of glucose exposure. This glucose treatment led to significant changes (~60% of lipids measured) in the phospholipid composition, indicating that the ability to maintain membrane composition under glucose stress is compromised with the loss of ELO-5 (Figure 3.1C). Because there are a significant number of alterations that occur with *elo-5* RNAi feeding with and without glucose, we compared the species with significant changes and found that only 53 phospholipid species were

altered in both conditions (Figure 3.1D). There are 43 phospholipid species that are significantly impacted when *elo-5* RNAi is combined with glucose treatment, implicating these species in the glucose response. Because ELO-5 is only involved in the production of C15iso and C17iso fatty acids, the impact on this large percentage of membrane lipids implicates ELO-5 or a product of this enzyme in regulating phospholipid metabolism on a larger scale.

To interrogate this further, the MS2 scans of the significantly changed species were used to determine if the lipid contains a mmBCFA in at least one of its tails. In *elo-5* RNAi-fed populations, only 35.8% of the altered species contain a mmBCFA when compared with L4440 controls (Figure 3.1E). In *elo-5* RNAi-fed animals treated with glucose, only 17.7% of the altered species contain a mmBCFA compared with *elo-5* RNAi without glucose (Figure 3.1F). Since most of the changed species do not directly contain a mmBCFA, the role of ELO-5 in glucose response is more wide-reaching than just the production of these fatty acid species for inclusion in phospholipids.

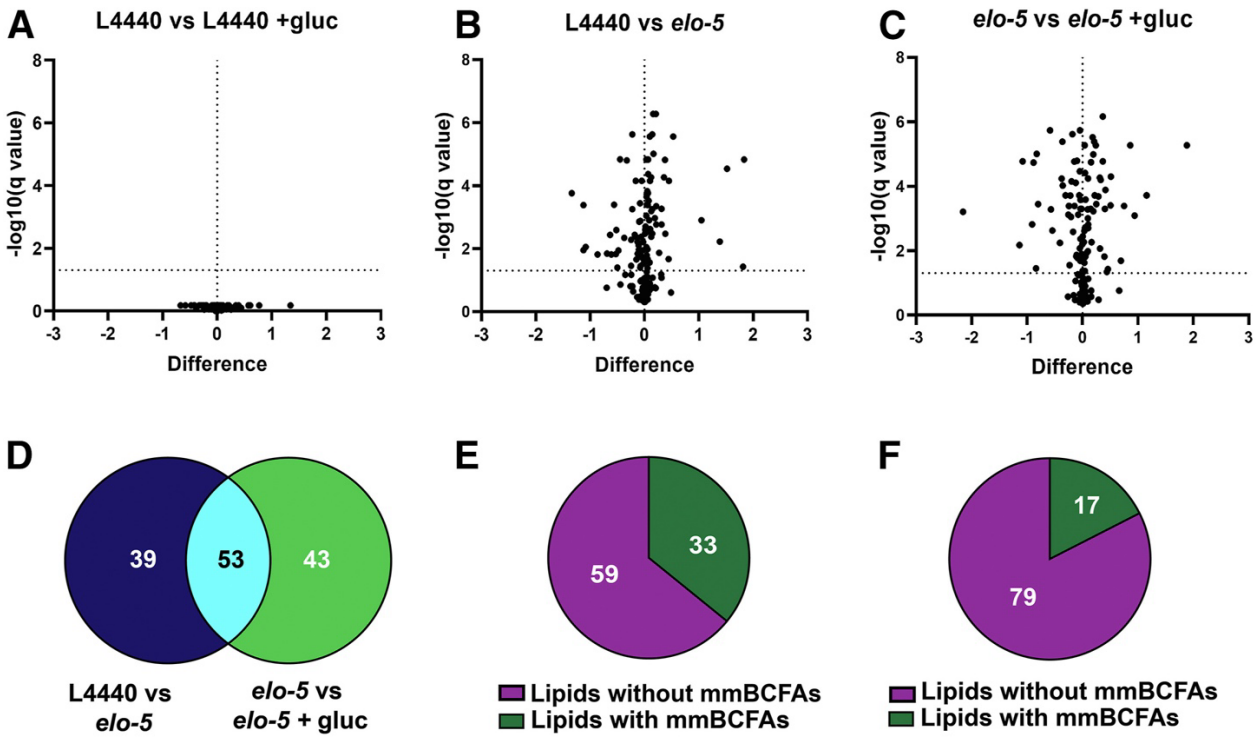

Figure 3.1 Global phospholipidomics were determined after 100 mM glucose exposure. WT animals at L1 stage were fed RNAi (L4440 or *elo-5*) on NGM+CI plates for 48 h, followed by 18 h feeding on NGM+CI plates with or without 100 mM glucose. A total of 159 phospholipids (PL) were characterized, namely, phosphatidylcholines, PC (50); phosphatidylethanolamines, PE (56); lysophosphatidylcholines, LPC (14); lysophosphatidylethanolamine, LPE (20); plasmanyl ethanolamine, PE P- (11); and plasmenyl ethanolamine, PE P- (8). The relative abundance (normalized to total lipids) was quantified, and the volcano plot shows the fold change in the relative abundance of distinct phospholipid species. Each dot above the dashed lines in the volcano plot is significantly changed, with the upper right and upper left panels showing increased and decreased lipid species, respectively. Volcano plot here shows **A)** no significant difference between L4440 worms fed with and without glucose, **B)** significant changes in the PL composition of L4440 compared with *elo-5*-fed worms, and **C)** significant changes between *elo-5*-treated worms with and without glucose. **D)** Venn diagram shows phospholipid species that are common and distinct between species that are significantly changed in L4440 versus *elo-5* compared with *elo-5* versus *elo-5 +gluc*. The results indicate that there are independent changes from each group, with 53 phospholipids common between both groups. **E** and **F** show the distribution of phospholipid species that are significantly changed in (B) and (C), respectively, that have a monomethyl branched-chain fatty acid (mmBCFAs) in at least one of the phospholipid tails as determined by MS2 fragments in the Lipid Data Analyzer software. Data were generated from at least four independent biological replicates; statistical significance was calculated by multiple *t-tests* corrected by false discovery rate, with an adjusted p-value (q) at 5%.

3.4.2 Analysis of phospholipid classes and the associated fatty acid tails

To further investigate the impact of ELO-5 across lipid metabolism pathways, the relative distribution of each phospholipid class was determined. In comparing control and *elo-5* RNAi-fed animals, there was no significant difference between the PC and PE headgroups between L4440 and *elo-5* RNAi (Figure 3.2A). Similarly, there was no change in PC and PE distribution with 100 mM glucose feeding of either control or *elo-5* RNAi (Figure 3.2A, see supplemental Table S2 for complete list). We next probed lipid populations that are less abundant but play critical roles in signaling and stress response, specifically the lysophospholipids and the plasmalogens [31,38]. The abundance of LPE is significantly lower in *elo-5* RNAi compared to controls (1.24 ± 0.13% vs. 2.13 ± 0.22%). The reduction in the LPC and LPE population in the *elo-5* RNAi-treated animals is largely from the depletion of lysophospholipids containing an mmBCFA tail, suggesting that the pool of precursors for mmBCFA-containing fatty acids is severely limited (supplemental Table S1 for full list). The abundance of the LPC and LPE was not altered by glucose exposure in control RNAi and *elo-5* RNAi populations, suggesting that this reduction in LPE is due to a lack of ELO-5 activity in building the membrane lipids but not in response to short-term glucose stress (Figure 3.2B). In analyzing the plasmalogens, we observed an increase in both PE O- and PE P- abundances in *elo-5* RNAi-treated animals from 3.68 ± 0.50% to 5.79 ± 0.67% and from 4.50 ± 0.53% to 6.46 ± 0.46%, respectively (Figure 3.2B). Despite the elevated PE O- and PE P- levels in untreated *elo-5* RNAi animals, again, the glucose exposure does not lead to an additional increase in the *elo-5* RNAi animals, suggesting that these animals have a compromised lipid pool and that plasmalogens are not an induced response to glucose.

The types of fatty acids in each pool have a dramatic impact on lipid metabolism and membrane function [4,18]. We analyzed the overall degree of saturation within the PC and PE classes as these glycerophospholipids comprise ~88% of the total phospholipid population. First, the PC species were sorted in bins by the number of total double bonds within the animal to define the overall level of saturation in the phosphatidylcholine lipids in the control RNAi and the *elo-5* RNAi-fed animals without glucose (Figure 3.2C). In animals fed *elo*-5 RNAi, there are alterations in the distribution of unsaturated lipids with a significant increase in PC lipids with 2–3 and 6–7 double

bonds and a significant decrease in PC lipids with 4–5 and ≥8 double bonds. Importantly, there is a significant decrease in the 0–1 double bond bin between control RNAi and *elo-5* RNAi that includes mmBCFAs (Figure 3.2C). The addition of glucose did not alter the level of unsaturation of the majority of PC lipids in control and *elo-5* RNAi worms except for a small but statistically significant increase in the 0–1 double bond bin (Figure 3.2C). In analyzing the level of unsaturation in the PE population, there were fewer alterations between control RNAi and *elo-5* RNAi than in the PC; however, we did observe a significant decrease in the 0–1 double bond bin, consistent with mmBCFA loss, and a decrease in 4–5 double bonds. In addition, there was a significant increase in the level of PE lipids with 2–3 double bonds and 6–7 double bonds (Figure 3.2D). The addition of glucose did not impact the level of saturation of control animals, but interestingly, the addition of glucose significantly increased the levels of lipids with 2–3 double bonds and significantly decreased lipids with ≥4 double bonds in *elo-5* RNAi-treated worms (Figure 3.2D). Overall, the phospholipidomics analysis indicates that the most significant differences in *elo-5* RNAi-treated animals are due to the loss of the enzyme, but there is a significant role for *elo-5* in the alterations of PE lipids in animals treated with glucose.

The biophysical properties of phospholipids are also impacted by the chain length of the associated fatty acid tails [22,180]. Therefore, we performed a similar analysis, but binning based on chain length (i.e., ≤32, 33–34, 35–36, etc., carbons in both fatty acid chains). Like the double bond analysis, there are multiple significant changes between control RNAi and *elo-5* RNAi-fed animals in the PC (Figure 3.2E) and the PE classes (Figure 3.2F), specifically decreases in ≤32 and 33–34 carbons. Interestingly, these decreases are offset in each lipid class differently, with an increase in 37–38 for PC and in 35–36, 37–38, and 39–40 for PE, indicating that the regulation is not occurring in the fatty acid pool but in phospholipid metabolism pathways. The addition of glucose shows no impact on the chain length in control animals; however, there are several significant changes in *elo-5*-treated animals fed high-glucose diets. Here, the chain length changes are similar in both PC (Figure 3.2E) and PE (Figure 3.2F): elevated ≤32, 33–34, and 35–36 bins and decreased 37–38 and 39–40 bins. These changes cannot be explained by the reduced capacity to produce mmBCFA and further support that ELO-5 plays roles in regulating metabolism, perhaps through impacting signaling lipids.

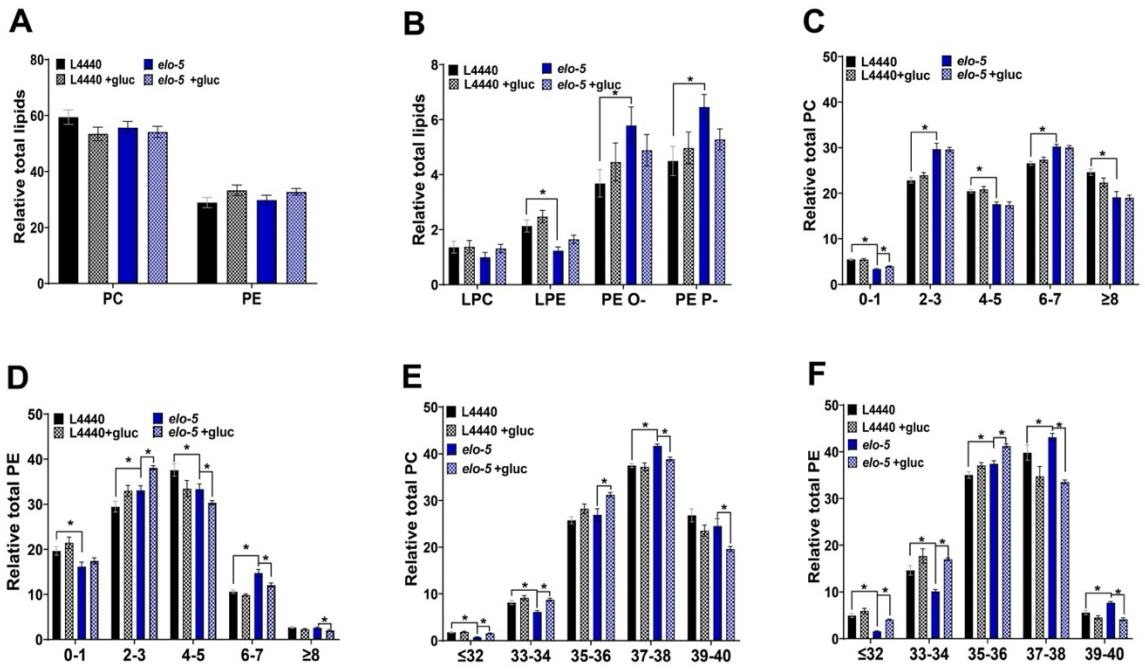

Figure 3.2 Glucose feeding impacts fatty acid saturation and length in phospholipids. **A)** The relative distribution of the major PL class, PC and PE, for L4440 (black), L4440 +gluc (black and checkered), *elo-5* (blue), and *elo-5* +gluc (blue and checkered) was generated by targeted lipidomic analysis. **B)** The distribution of the less abundant lipid classes, LPC, LPE, PE O- and PE P-, was generated for the same populations of animals. The results show a significant decrease in the LPE population and a significant increase in the plasmalogen (PE O- and PE P-) species in L4440 compared with *elo-5* RNAi. Glucose stress did not significantly impact the distribution of each lipid class. **C)** PC phospholipids were binned by the total number of double bonds associated with their fatty acids for each treatment group. Glucose stress did not greatly alter the distribution of double bonds apart from a significant increase in PC species with 0–1 double bonds in *elo-5* glucose-stressed animals. **D)** Similarly, the double bond distribution of PE lipids was quantified. Glucose stress did not alter the PE double bond distribution in control animals but led to a significant increase in PE species with 2–3 double bonds and a significant decrease in species with 4 or more double bonds in *elo-5* animals stressed with glucose. **E)** PC lipids were binned according to the total number of carbons in the fatty acid tails. Glucose did not impact the chain length of control animals but led to a significant increase in shorter-chain lipids (less than 36) and a decrease in longer chains. (36 carbon or more). **F)** Similarly, PE lipids binned according to chain length show a significant decrease in lipids with shorter chain length (less than 36 carbons) and a significant increase in lipids with longer carbon chains (36 or more) in *elo-5* RNAi worms compared with controls (L4440). Contrastingly, the presence of glucose showed a significant increase in lipids with relatively shorter carbon chains (36 carbons or less) and a significant decrease in lipids with longer carbon chains (more than 36 carbons) in *elo-5* worms stressed with 100 mM glucose while controls remained unchanged. Data were generated from at least four independent biological replicates. Statistical significance was calculated by multiple *t-tests* corrected by false discovery rate, with an adjusted p-value (q) at 5%.

3.4.3 Glycolipid populations respond to glucose diets

The GlcCer population is of particular interest in *elo-5*-treated animals as the mmBCFA population provides precursors for their synthesis. In particular, GlcCer 17:1;O2/22:0;O is a critical metabolite that is responsible for regulating postembryonic growth and development but has not been implicated in response to glucose [145]. The Lipid Maps nomenclature for Sphs is GlcCer XX/YY;O where GlcCer represents the headgroup, XX represents the sphingoid base, YY represents the *N*-linked FA, and O represents the hydroxyl group attached to the *N*-linked FA [101]. Because all the GlcCer species examined here contain a d17iso sphingoid backbone, we will report the associated fatty acid chain only for readability. For example, GlcCer 17:1;O2/22:0;O will be referred to as 22:0;O GlcCer. The synthesis of 22:0;O GlcCer requires ELO-5 to produce the mmBCFA backbone and ELO-3 to produce saturated very-long-chain fatty acids, which are both further processed before ultimately being joined to glucose by a CGT to produce 22:0;O GlcCer (Figure 3.3) [137,145]. In order to determine if the 22:0;O GlcCer has a role in glucose response, we first established an assay by HPLC-MS/MS to quantify the abundance of this species based on a method previously developed [55,131]. Although our method does not distinguish between the isomeric hexosylceramides (HexCer), GlcCer, and galactosylceramides (GalCer), there are no data available currently about the presence of GalCer in *C. elegans*. The HexCer measured in *C. elegans* in previous studies is GlcCer [55,134,137,145], and for the rest of the paper, we assume that the HexCer measured here is GlcCer. Animals treated with *elo-3* RNAi were included as a control as ELO-3 is required to produce 22:0;O GlcCer, and indeed, the abundance of this lipid was significantly reduced from 34.12 ± 0.40% in control

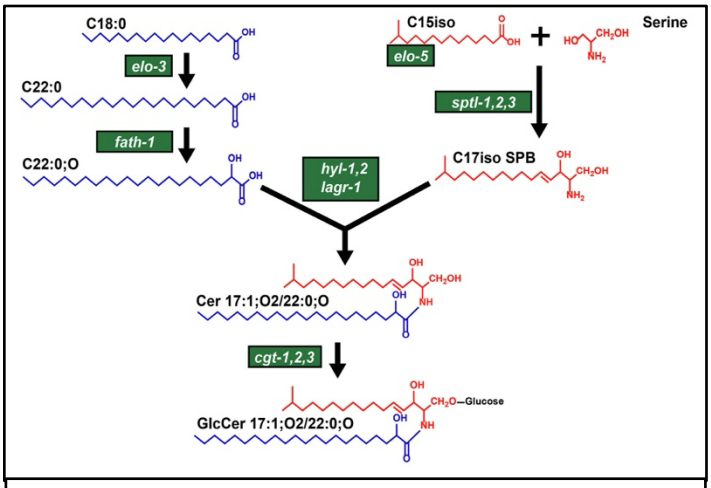

Figure 3.3 Biosynthesis pathway for GlcCer 17:1;O2/22:0;O.

Glucosylceramides (GlcCer) are synthesized from C15iso and saturated fatty acid (C18:0) through a series of steps catalyzed by various enzymes (highlighted in green) (adapted from Zhu *et al.*, 2013 [145]

animals to 26.07 ± 1.59% with *elo-3*RNAi validating the methodology (Figure 3.4A, supplemental Table S3). Similarly, *elo-5* RNAi led to a strongly reduced 22:0;O GlcCer to 11.69 ± 0.47% (Figure 3.4A).

C. elegans has three CGTs, *cgt-1,2,3*. We focused on the impact of *cgt-3* RNAi because CGT-3 protein was previously shown to have the highest CGT activity compared with *cgt-1* and *cgt-2* [135] and has also been recently shown to be important for stress response [137]. Interestingly, there was no significant reduction in 22:0;O GlcCer with *cgt-3* RNAi; however, we observed death in the *cgt-3* RNAi, suggesting the RNAi was effective (Figure 3.4A). We hypothesized that this lack of reduction may result from the relatively short-term RNAi exposure. To test this, we extended the RNAi period to 3 days, at which point we observed significant death among the *cgt-3* RNAi-treated animals. In these longer-term *cgt-3* RNAi-treated animals, we were able to quantify significantly reduced 22:0;O GlcCer but not to the same extent as with *elo-5* and *elo-3* RNAi, which we hypothesize is a result of the death of the animals with the most reduced levels (Figure 3.4B, supplemental Table S4). Because of the power of HPLC-MS/MS, the levels of 22:0;O Cer, the immediate precursor to 22:0;O GlcCer, were also quantified. The same trends were observed in this population with significantly reduced 22:0;O Cer in *elo-5, elo-3*, and long-term *cgt-3* RNAi treatment (Figure 3.4 C, D).

Once the assays were validated, the abundance of 22:0;O GlcCer was quantified after 100 mM glucose exposure, and there was a significant increase from 34.12 ± 0.40% to 36.96 ± 0.48% in control animals Figure 3.4A. There was no increase in 22:0;O GlcCer in *elo-3, elo-5*, or long-term *cgt-3* RNAi treatment, indicating that this elevation with glucose treatment is due to increased synthesis of 22:0;O GlcCer and not reduced consumption or degradation (Figure 3.4A, B). Interestingly, glucose exposure did not lead to an increase in the production of 22:0;O GlcCer with long-term glucose treatment in control populations, implicating the increased production as a short-term impact that is modulated with time. Similarly, there is no change in the 22:0;O Cer pool in controls treated with glucose (Figure 3.4C), suggesting that there is an immediate role for CGT in funneling precursors to 22:0;O GlcCer production.

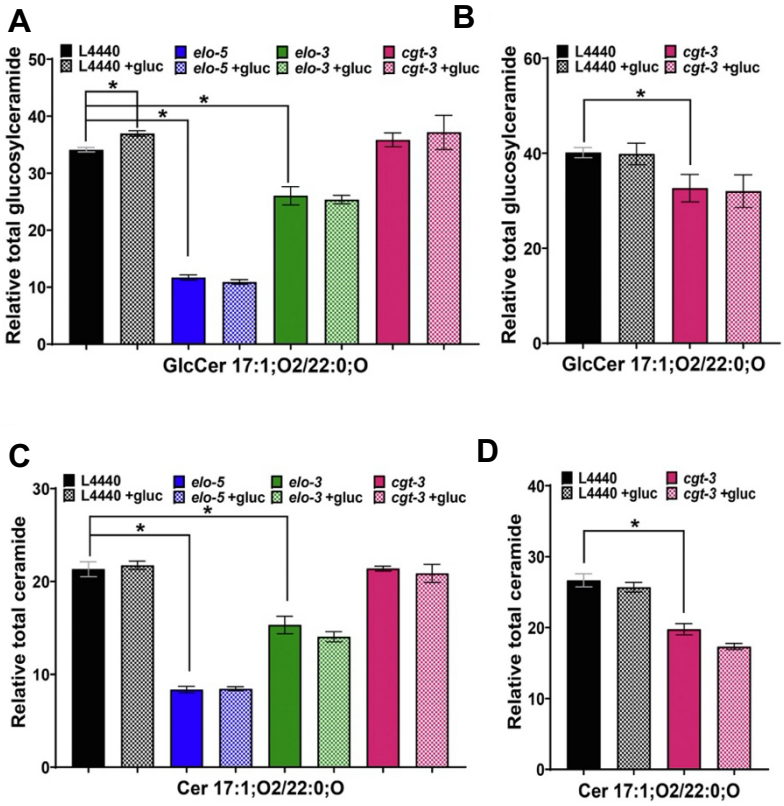

Figure 3.4 The level of GlcCer 17:1;O2/22:0;O and Cer 17:1;O2/22:0;O under different backgrounds in glucose stress.
A) WT animals at L1 stage were fed RNAi (L4440, *elo-5, elo-3,* and *cgt-3)* on NGM+CI plates for 48 h followed by 18 h feeding on NGM+CI plates with or without 100 mM glucose. Following alkaline hydrolysis of phospholipids, the ceramide and glucosylceramide levels were measured using HPLC-MS/MS. The level of GlcCer 17:1;O2/22:0;O is significantly increased in control animals exposed to 100 mM glucose. *elo-5* and *elo-3* RNAi-fed animals have lower levels of GlcCer 17:1;O2/22:0;O, and exposure to glucose does not further increase the levels of this sphingolipid. Surprisingly, *cgt-3* did not alter the levels of GlcCer 17:1;O2/22:0;O. **B)** Longer *cgt-3* RNAi treatment (3 days after L4 stage) led to a significant decrease in the level of GlcCer 17:1;O2/22:0;O. **C)** In analyzing the ceramide precursor for GlcCer 17:1;O2/22:0;O- Cer 17:1;O2/22:0;O, *elo-5* and *elo-3* have significantly lower levels compared with control animals, while *cgt-3* levels are not impacted. Glucose stress did not impact the level of Cer 17:1;O2/22:0;O in any of the treatment conditions. **D)** Longer *cgt-3* RNAi treatment led to a significant decrease in the level of Cer 17:1;O2/22:0;O. Data were generated from at least three to five independent biological replicates. Statistical significance was calculated by multiple *t-tests* corrected by false discovery rate, with an adjusted p-value (q) at 5%. For the purposes of clarity, the statistical comparison shown in the graphs are between controls and RNAi backgrounds and the change in abundance of each background upon glucose exposure for GlcCer 17:1;O2/22:0;O and Cer 17:1;O2/22:0;O.

3.4.4 Ceramide and Glucosylceramide pools change with high glucose diets

Although 22:0;O GlcCer has been implicated in other phenotypes of mmBCFA deficiency, there are many other GlcCer and ceramide species within the nematode. We next quantified the effects of glucose exposure on all the major GlcCer in the nematode along with ceramide species that are precursors to those GlcCer (Figure 3.5A, B) (see supplemental Table S3 for full list). First, we examined lipid species that changed with glucose exposure in L4440 RNAi animals and found that the majority of ceramides and GlcCer are stable, except there was a slight significant decrease in 23:0 Cer and a significant increase in 22:1 GlcCer. Overall, this suggests that the response to glucose in the diet alters Sph metabolism to keep the levels of most individual species relatively stable (Figure 3.5A, B, supplemental Table S3).

We next interrogated how these lipid populations are impacted without the ability to synthesize new Sph molecules. Because *elo-5* RNAi had the greatest impact on the 22:0;O GlcCer pool, we first compared the Sph profiles in *elo-5* RNAi-fed animals that were also subjected to high-glucose diets. There were significant alterations in ceramides with species that have shorter (≤23 carbons) FA attached to the sphingoid backbone; specifically, 21:0 Cer, 21:0;O Cer, and 23:0 Cer increased significantly by ∼144%, 93%, and 67%, respectively (Figure 3.5C). Interestingly, this trend was observed for the odd-chain FA but not the even-chain FA. Conversely, there were decreases in several species that have longer chains (≥24), namely, 24:0;O Cer, 24:1 Cer, 26:0;O Cer, and 26:1 Cer, which decreased significantly by ∼21%, 23%, 28%, and 28%, respectively (Figure 3.5C). In the GlcCer pool, there were significant changes in 6 of 10 species with trends similar to the ceramide pool. Specifically, species with shorter (≥23) and odd FA attached to the sphingoid backbone including 21:0;O GlcCer and 23:0;O GlcCer are significantly increased by ∼69% and 27%, respectively (Fig. 4D). GlcCer species with longer (≤24) and even FA sphingoid backbone, namely, 24:0;O GlcCer, 24:1 GlcCer, and 26:0;O GlcCer, were significantly decreased, by ∼26%, 20%, and 31%, respectively (Figure 3.5D). Because ELO-5 is not directly responsible for the synthesis of the long-chain FA associated with these ceramides, the significant perturbation of the ceramide pool further implicated ELO-5 in broader regulation of Sphs following glucose stress.

We next examined the impact of compromising ELO-3, which is directly important in synthesizing the long-chain FA found in the ceramide and GlcCer populations. Interestingly, we found that *elo-3* RNAi does not have any major effect on the Cer and GlcCer pools under glucose stress (Figure 3.5E, F), with the only significant change observed being a decrease in 25:0 Cer (supplemental Table S3). The more minimal effect on the Sph pool may be due to compensatory pathways or a milder decrease in enzyme levels by the *elo-3* RNAi clone. Regardless, the impact of glucose stress on ceramide and GlcCer is more severe in *elo-5*-fed RNAi animals compared with control and *elo-3*-fed animals. The specificity of ELO-5 in impacting the overall Sph pool, even when ELO-5 is not directly implicated in synthesizing components, strongly suggests that ELO-5 is responsible for producing a specific species that orchestrates a shift in the composition of the Sph pool. We predict that this species is 22:0;O GlcCer, which is the most depleted in *elo-5* RNAi-fed animals.

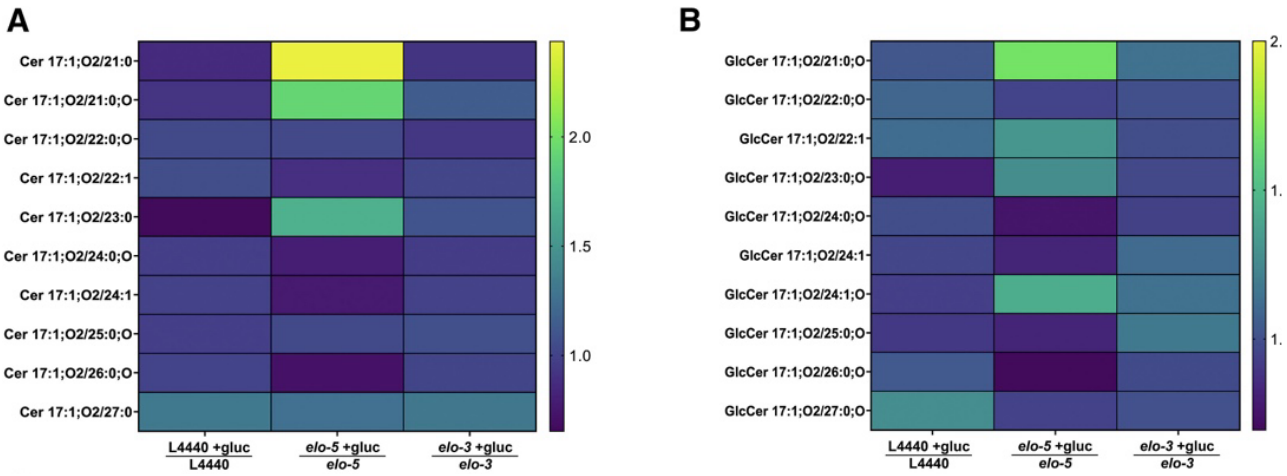

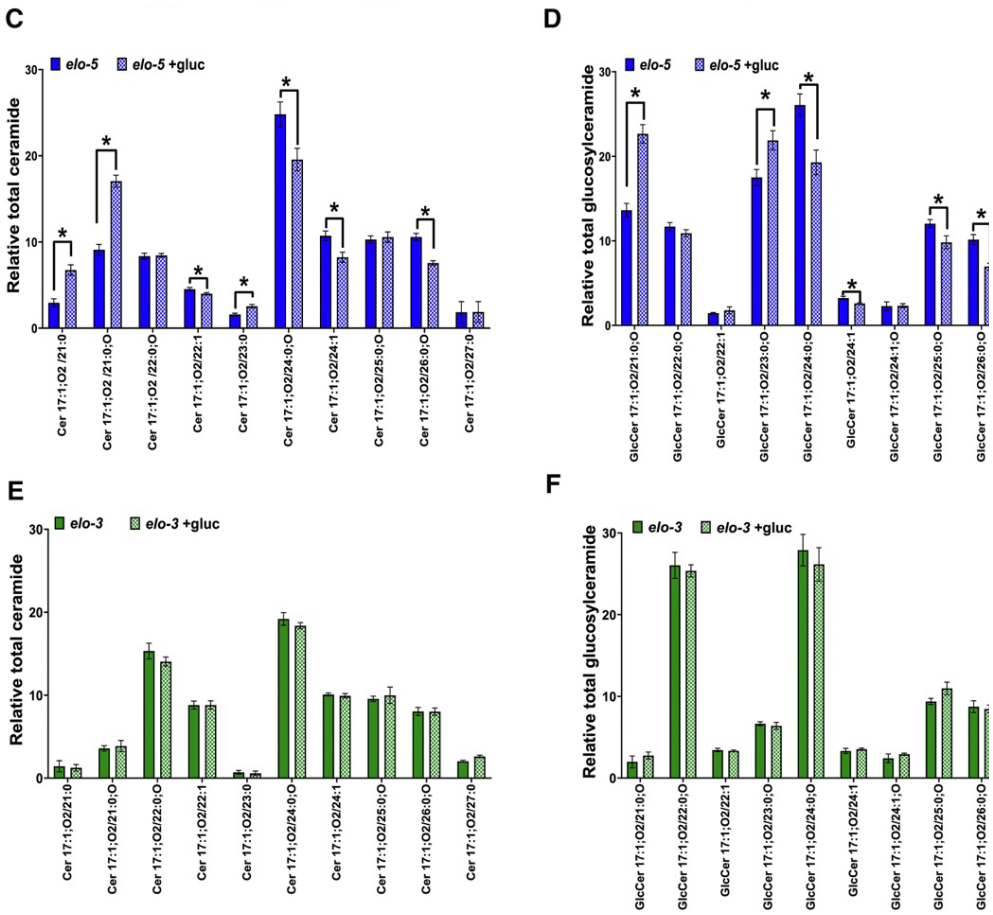

Figure 3.5 Sphingolipid profile shifts after 100 mM glucose exposure.
The other sphingolipid populations in animals treated in the conditions described in Fig 3.4 were measured. The heatmap shows the fold change after glucose stress (mean of RNAi-treated worm/mean of glucose stress RNAi) for **A)** the ceramides that are precursors to GlcCer **B)** and all the glucosylceramides measured detected in *C. elegans* under different RNAi backgrounds (see full target list in supplemental Table S3). The results show a unique response for each RNAi-treated worm group under glucose conditions, with *elo-5* animals having significant shifts with glucose treatments. Specifically, in *elo-5* animals fed with glucose compared with *elo-5* animals **C)** ceramides with odd-chain FAs (21:0 Cer, 21:0;O Cer, 23:0 Cer) were significantly increased, while species with even-chain fatty acids (22:1 Cer, 24:0;O Cer, 24:1 Cer, 26:0;O Cer, 26:1) were significantly decreased. **D)** This trend was consistent in the GlcCer pool with a significant increase in shorter and odd-chain GlcCer (21:0;O GlcCer, 23:0;O GlcCer) and a significant decrease in even-chain GlcCers (24:0;O GlcCer, 24:1, and GlcCer, 26:0;O). Interestingly, there were no significant changes in the **E)** ceramides species shown here and **F)** glucosylceramide species in *elo-3* compared with *elo-3* animals stressed with 100 mM glucose. Data were generated from at least three to five independent biological replicates. Statistical significance was calculated by multiple *t-tests* corrected by false discovery rate, with an adjusted p-value (q) at 5%.

3.4.5 Sphingolipid synthesis is critical for survival in elevated glucose conditions

Because of the altered 22:0;O GlcCer levels observed in the *elo-3* RNAi animals, we examined whether *elo-3* RNAi also caused glucose sensitivity. Synchronized L1 animals were fed control or *elo-3* RNAi, and after 48 h, L4 stage animals were transferred to RNAi plates with or without 100 mM glucose. The results show that *elo-3* RNAi significantly decreased the median lifespan of WT animals under glucose stress from approximately 11 days to 8 days (Figure 3.6A). Because the majority of the Sph pool is stable with *elo-3* RNAi except for 22:0;O GlcCer, this result suggests that this lipid has a specific effect on glucose survival. We cannot distinguish whether the *elo-3* RNAi animals survive better than *elo-5* RNAi animals because of the reduced impact on 22:0;O GlcCer levels or because of the alterations in the other Sph pools that are only seen with *elo-5* RNAi.

Next, to further confirm the need for 22:0;O GlcCer in glucose response, we examined the survival of nematodes under glucose stress in the absence of the CGT. As previously described, we focused on *cgt-3* RNAi based on its established role in stress response. Interestingly, *cgt-3* RNAi dramatically shortened the lifespan of the animals under glucose stress, with a maximum lifespan of 3 days (Figure 3.6B). This dramatic decrease in lifespan was more severe than the shortened lifespan observed previously in *elo-5* RNAi animals [59]. We next wanted to determine if this sensitivity was unique to CGT-3, so we monitored glucose stress survival with cgt-1 RNAi as well. There was no significant effect on the survival of the *cgt-1* RNAi-fed animals under glucose stress (supplemental Fig. S1A). Furthermore, the combination of *cgt-3* and *cgt-1* RNAi (1:1 ratio) did not exacerbate the *cgt-3* lifespan decrease (supplemental Fig. S1A). This result suggests a critical role of GlcCer production in the survival of glucose stress.

Because the sensitivity of *cgt-3* RNAi-fed animals strongly suggests a role for GlcCer in adapting to elevated glucose conditions, we next fed animals a combination of *cgt-3* and *elo-5* RNAi and quantified survival with glucose treatment. The combined *cgt-3/elo-5* RNAi treatment did not increase the rate of death in the glucose-treated nematodes, suggesting that these genes function in the same pathway in response to glucose (supplemental Fig. S1B). It is important to note that

the *cgt-3* RNAi treatment leads to very rapid death, with all animals dying within 4 days; therefore, it is possible that additive effects with the *elo-5* RNAi would not be detectable.

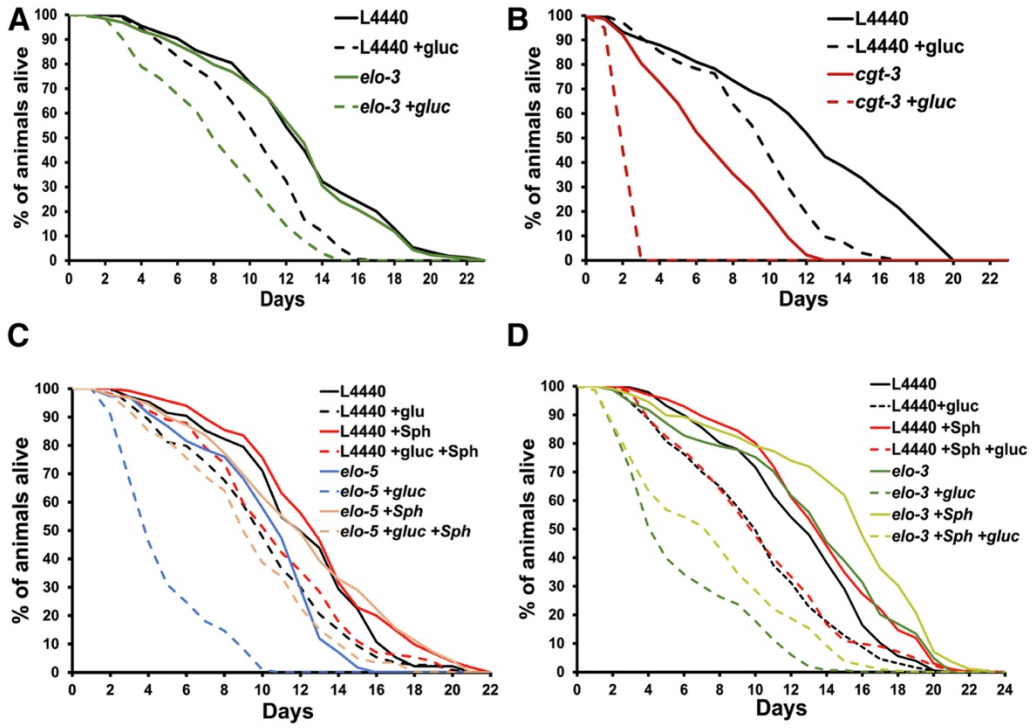

Figure 3.6 *elo-3* and *cgt-3* RNAi decrease the survival of the nematodes under glucose stress. **A)** RNAi knockdown of *elo-3* (green) and control (black) in N2 worms was initiated from the L1 stage. After 48 h (L4 stage), the animals were transferred to NGM+CI plates with (dashed line) or without (solid line) 100 mM glucose (+gluc). The loss of ELO-3 significantly shortened the mean (± SD) lifespan of WT animals under glucose stress from 9.6 ± 1.5 days to 7.5 ± 1.6 days. **B)** *cgt-3* (red) RNAi knockdown animals had a dramatic decrease in lifespan under glucose stress with a maximum lifespan at 3 days. **C)** To further interrogate whether *elo-5* sensitivity to glucose was through the production of GlcCer, *elo-5* RNAi animals were supplemented with sphingolipids (Sph) purified from WT animals (light red) or ethanol control (blue). RNAi was initiated ~12 h after L1 to prevent the smaller size and shorter lifespan observed when *elo-5* RNAi is initiated at L1 [59]. Supplementing *elo-5* RNAi with purified sphingolipid restored the mean lifespan from 5.0 ± 0.5 days to 9.6 ± 0.8 days. **D)** Similarly, *elo-3* RNAi animals were supplemented with sphingolipid extract. The addition of the supplement partially rescued the survival of *elo-3* animals from a mean lifespan of 6.0 ± 1.4 days to 7.6 ± 2.0 days. The survival curves are presented as means of at least three to five independent replicates with 50 worms per condition for each replicate. The statistical analysis of the survival curve was performed using the Log-rank (Mantel-Cox) test.

Next, to confirm that the *elo-5* RNAi acts through the GlcCer pathway and not through an alternative mmBCFA function, we sought to rescue the *elo-5* RNAi-treated animals with GlcCer. To do so, we purified Sphs that contain the Cers and GlcCer from wild-type nematodes (the composition of the Cer and GlcCer is found in supplemental Table S5 and supplemental Fig. S1C, D). The purified Sphs were fed to *elo-5* RNAi-treated animals in the presence and absence of glucose (Figure 3.6C). The addition of WT Sph to RNAi control animals (mean lifespan of 12.5 ± 1.6 days) did not significantly impact the lifespan of control animals (mean lifespan of 12.1 ± 0.5 days). However, the addition of WT Sph to the *elo-5* RNAi animals restores the lifespan of these animals (mean lifespan, 12.1 ± 1.4 days) to wild-type levels (Figure 3.6C). The impact of WT Sph on *elo-5* animals' survival in the presence of glucose is even more dramatic, with a mean lifespan increased to 9.6 ± 0.8 days from 5.0 ± 0.5 days (Figure 3.6C). Taken together, these lifespan curves implicated GlcCer production as the primary critical role for ELO-5 in the nematode, particularly in response to glucose. Similarly, we supplemented *elo-3* RNAi animals with the Sph extract and monitored their survival under glucose stress. Here, the Sph was able to partially rescue the shortened lifespan of *elo-3* RNAi animals under glucose stress from 6.0 ± 1.4 days to 7.6 ± 2.0 days (Figure 3.6C). Interestingly, the Sph supplement extended the mean lifespan of control *elo*-3 animals from 12.5 ± 2.1 days to 14.3 ± 1.9 days, suggesting that the *elo-3* RNAi background enhances the impact of Sph supplementation (Figure 3.6D).

It is possible that the Sph supplementation rescues the animal's ability to survive on glucose stress because the Sph pool contains mmBCFA. One of the challenges of metabolic studies is that we cannot discount the possibility that the mmBCFA supplementation and not intact GlcCer supplementation is responsible for the rescue. In fact, lipid absorption in the gut would necessitate GlcCer to be broken down before absorption can occur. To understand the supplementation, we analyzed the GlcCer pool from the Sph-supplemented animals by HPLC-MS/MS. There are no significant changes in the GlcCer with Sph supplementation in control nematodes; however, there are many changes in the *elo-5* RNAi animals fed the supplement (Figure 3.7A). Most importantly, there is a significant increase in 22:0;O GlcCer from 10.35 ± 0.19% to 22.77 ± 1.61% in *elo-5* RNAi upon supplementation. There are also significant increases in 22:1 GlcCer (1.19 ± 0.04% to 2.84 ± 0.18%), 24:0;O GlcCer (23.97 ± 1.33% to 30.87 ± 1.87%), and 24:1 GlcCer (2.32 ±

0.47% to 3.42 ± 0.21%). Importantly, there are also GlcCer species that are decreased significantly upon supplementation including 21:0;O GlcCer (14.78 ± 0.55% to 5.78 ± 0.80%), 23:0;O GlcCer (21.51 ± 0.58% to 11.66 ± 1.09%), and 25:0;O GlcCer (11.86 ± 0.48% to 10.14 ± 0.42%). Again, there is distinct regulation of odd-chain versus even-chain GlcCer species. The remaining GlcCer species were stable regardless of supplementation (see supplemental Table S6 for full list). Although we cannot determine if there is an increase in GlcCer production or absorption, it is clear that the GlcCer pool is much more similar to WT Sph levels following supplementation (Figure 3.7A). Even though the rescue was less pronounced in *elo-3* RNAi-fed animals, we profiled the GlcCer in those animals as well (Figure 3.7B). In doing so, we found no significant changes with WT Sph exposure; however, it is important to note that the *elo-3* animals have a much more similar GlcCer profile to WT animals, to begin with (see supplemental Table S7 for full list). We believe that ELO-5 plays a more prominent role in regulating the GlcCer pool upon glucose exposure. Taken together with the small-scale recovery from glucose sensitivity, the lipidomic profiling supports the conclusion that the mmBCFA synthesis via ELO-5 is critical to produce certain GlcCer species, specifically 22:0;O GlcCer.

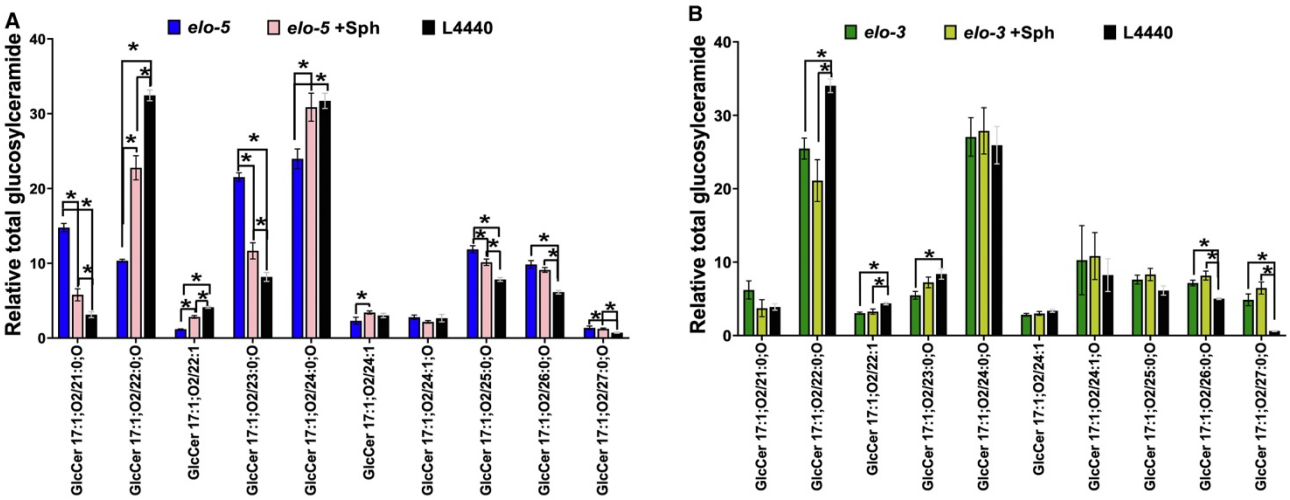

Figure 3.7 Glucosylceramide profile of *elo-5* and *elo-3* animals supplemented with sphingolipids.

A) Synchronized L1 animals were treated with L4440 or *elo-5* RNAi for 48 h and then transferred to NGM +CI plates supplemented with 500 µl sphingolipid (Sph) extract or ethanol control for 18 h. The sphingolipids were extracted and analyzed, and the results show a significant increase of 22;0;O GlcCer in *elo-5* +Sph compared with *elo-5* from 10.34 ± 0.19% to 22.77 ±1.61%. In addition, there were other significant changes in multiple species, and some species were stable. **B)** Similarly, the glucosylceramide profile of *elo-3* animals supplemented with Sph extract was analyzed. Surprisingly, there was no significant difference between *elo-3* controls and *elo-3* animals supplemented with Sph extract (see supplemental Table S7 for full list). Data were generated from three independent biological replicates. Statistical significance was calculated by multiple *t-tests* corrected by false discovery rate, with an adjusted p-value (q) at 5%.

3.5 Discussion

In this study, we have established 22:0;O GlcCer as a critical mediator of the response to glucose in *C. elegans.* The monomethyl branched-chain fatty acids and this derived GlcCer have been previously implicated in postembryonic development and foraging in *C. elegans* [110,145]. Here, we define a new role for this Sph in participating in the nematode's response to high-glucose diets. In doing so, ELO-5, ELO-3, and CGT-3, all enzymes involved in 22:0;O GlcCer production, have been established as participants in the system of metabolic pathways that are critical for surviving high-glucose diets. The response network to glucose stress in *C. elegans* has been developing over the last decade, and our work here expands the knowledge of how this response acts mechanistically.

One of the striking features of these glucose-response targeted lipidomic datasets is the lack of significant changes in wild-type animals. In fact, we found no significant changes in animals fed 100 mM glucose in our initial global comparison, highlighting the rewiring of metabolic pathways with glucose. This maintenance of overall phospholipid composition is somewhat unexpected as a few changes in fatty acid composition have been documented [59,88]. We hypothesize that the existence of so many individual phospholipid species dilutes the impact of the fatty acid changes on any given lipid. The adjustment in metabolic pathways can be observed by compromising the genes in pathways required for the response, including the membrane sensor, PAQR-2. PAQR-2 has been established as a critical mediator of the transcriptional changes that occur with glucose exposure, including increased expression of desaturases and elongases required to produce unsaturated fatty acids and monomethyl branched-chain fatty acids [15,59]. Here, we have found that the role of mmBCFAs in this response is in providing the precursors for GlcCer synthesis; thus, the PAQR-2 sensor may be connected to Sph metabolism. This is of particular interest as GlcCer is a mediator of TOR activity in other conditions [145], although further studies would be needed to confirm the role of TOR in glucose response.

This study revealed interesting membrane remodeling seen in *elo-5* RNAi-fed animals under glucose. In general, the results show that *elo-5*-fed RNAi worms under glucose stress had relatively fewer double bonds and an overall shorter chain length. This shift is characteristic of an

adaptation of the membrane to a phospholipid composition that is resistant to oxidative stress, as highly polyunsaturated fatty acids are most susceptible to damage by reactive oxygen species [121,181]. We hypothesize that GlcCer production helps promote a response to the high level of glucose, and therefore, the absence of ELO-5 would increase the oxidative burden in the cell. The higher oxidative load would then promote a shift in membrane composition that would be protective against the higher levels of oxidative species seen in high-glucose diets [182,183]. Although it has been hypothesized that glucose supplementation results in excess saturated fatty acid in the membrane [12,15], we believe that the extra glucose may be increasing the oxidative load in the animal, and this shift lends support to that model.

RNAi of CGT led to a perturbation in GlcCer populations and a dramatically shortened lifespan on glucose. We were intrigued by the fact that *cgt-3* RNAi needed a longer timeframe to see significant decreases in Sph populations while compromised survival happens readily. In fact, the longer RNAi period required for the lipidomic analysis results in a significant death of the treated animals, with only 80 ± 3.1% of animals remaining at the time of collection. The rapid rate of death in *cgt-3* RNAi suggests an additional role for CGT-3 that may be independent of the Sph regulation. We believe that this rapid death may be explained by the accumulation of a toxic intermediate, which will be the subject of future studies. In addition, it is possible that the role of GlcCer in glucose response may be required only in a specific subset of cells within the intestine. In support of this tissue specificity, studies in the nematode have found that mutations in any of the three CGT genes can be rescued by expression in a small subset of intestinal cells [134]. Many lipid signaling pathways have been found to work in a cell nonautonomous manner, and it is likely that the GlcCer response to glucose follows that pattern.

One of the major challenges of metabolic studies is proving causality between a single lipid species and the phenotype of interest. The interconnected nature of metabolic pathways makes it impossible to cleanly test how that species of interest works, as compromising its levels and rescue studies will impact other intermediates of the pathway and have a ripple effect on the metabolism of the animals. For example, here we identify 22:0;O GlcCer as a potential specific regulator of glucose response, and we can compromise the production of that species with *elo-5* RNAi. However, in doing so, we also perturb many additional Sph pools. Other genes within the synthesis

pathway can be used to corroborate the role of 22:0;O GlcCer, but it is also important to note that perturbations at different enzymes lead to unique Sph profiles. Finally, 22:0;O GlcCer is not commercially available, but we can supplement WT Sph to look for rescue. The process of lipid absorption, where lipase activity removes the fatty acid tails before absorption into cells, may impact the Sph pool. Although the options for direct testing are limited, we believe that the results presented here, viewed in total, provide a strong argument that 22:0;O GlcCer is largely responsible for the glucose response.

Our study here highlights the power of mass spectrometry in the genetic organism *C. elegans.* Stable isotope labeling originally identified mmBCFA as implicated in the response to glucose. In fact, this role was only observed using stable isotopes as the populations of these fatty acids are not significantly altered in wild-type nematodes [59]. The stability of lipid populations is a common trend in wild-type worms; however, by combining stable isotope and genetic approaches, it is clear that multiple pathways are required to maintain the membrane populations under these stressed conditions. In fact, the reduction or elimination of these pathways, including ELO-5 and CGT-3, led to reduced survival under high-glucose diets. Overall, the utilization of mass spectrometry methods combined with genetic tools has identified a novel and specific role for a particular GlcCer in membrane adaptation.

3.6 Supplemental data

The supplementary figures contained in this article can be found at https://www.sciencedirect.com/science/article/pii/S0022227523000676?via%3Dihub#fig1

3.7 Acknowledgments

The authors would like to thank the *Caenorhabditis elegans* Genetics Center (CGC) at the University of Minnesota for the *C. elegans* strains. They would also like to thank all the members of the Olsen lab for their comments and suggestions on the manuscript.

CHAPTER 4 – BUILDING OXIDIZED LIPID PROFILES FOLLOWING STRESS IN *C. ELEGANS*

Mark A. Xatse, Paige Silvia, Alvan Okechwuku, Peter Allen, and Carissa Perez Olsen *

Department of Chemistry and Biochemistry, Worcester Polytechnic Institute, Worcester, MA, USA

*Corresponding Author. Email: cpolsen@wpi.edu

Author contributions

Mark Xatse oversaw all experiments and analysis for this paper, including method development. Mark Xatse, Alvan Okechukwu, and Peter Allen conducted the initial experiment for LPPtiger predictions for TBHP experiments and the glucose study. Paige Silvia and Mark Xatse carried out the MDA assay for TBHP treatment. Finally, Mark Xatse conducted the quantitative oxidized lipid profiles for glucose stress and paraformaldehyde-killed bacteria experiments.

4.1 Abstract

The oxidative modification of membrane lipids through lipid peroxidation induces profound alterations in membrane structure, which are intricately linked to biological events such as inflammation, aging, and cell death. Identifying these oxidized lipids of biological relevance is challenging due to their low abundance as well as the vast diversity of lipids within organisms, which amplifies the number of potential oxidized lipid derivatives. Furthermore, the unique chemical properties and extensive mass range of these oxidized lipids make it analytically challenging to detect oxidized lipids within biological samples. This study employed the innovative computational bioinformatic tool, LPPtiger, to predict oxidized lipids in *C. elegans*. Through the combination of the predictive power of the LPPtiger software and advanced mass spectrometry, we have identified and quantified oxidized lipids in *C. elegans* under basal and stress conditions. Our results show the presence of both oxidized phosphatidylcholines (oxPC) and phosphatidylethanolamine (oxPE) in the nematode, with oxPC being the most abundant oxidized lipid present under basal conditions. Under TBHP-induced stress and glucose stress conditions, we see a significant increase in the overall oxPE. Notably, while certain oxPE are commonly associated with both stress forms, we also see a distinct oxidized lipid profile for each type of stress. Together, our data unveils distinctive sample-specific oxidized lipid profiles corresponding to each stress scenario, providing valuable insights into the nuanced responses of the organism to diverse environmental challenges.

4.2 Introduction

Cell membranes are highly organized and dynamic structures that are essential for cellular life[2,4]. Comprised predominantly of lipids, with phospholipids being the most prevalent, membranes undergo various enzymatic and non-enzymatic modifications that profoundly influence their properties [122,153]. The most common damage to lipids is caused by lipid peroxidation, which results in the oxidative modification of acyl chains in phospholipids [147,153]. The oxidative modification increases the polarity of the acyl chain and leads to the formation of "whiskers" where the acyl chain reorients such that it protrudes outside into the aqueous extracellular environment instead of being embedded inside the membrane bilayer [151,152]. The presence of whiskers on the surface of cells has been shown to be recognized by cell surface-associated receptors and induces signaling processes [159,184]. Additionally, oxidized lipids (oxL) have been shown to influence several cellular processes, such as apoptosis, inflammation, and immunity [160,184]. Unrestrained oxidation of phospholipids can increase these whiskers, which can significantly increase the formation of pores in the membrane, leading to the rupturing of the plasma membrane and a type of cell death known as ferroptosis [154,155,185,186]. Ferroptosis and lipid peroxidation have been linked to the development and progression of several disease conditions such as diabetes, cardiovascular disease [161,187], cancer [188,189], and neurological disorders [147,190].

Canonical phospholipids are amphipathic molecules made up of a hydrophobic tail composed of two fatty acyl chains linked to the *sn*-1 and *sn*-2 positions of a glycerol backbone and a hydrophilic head group consisting of a phosphate group linked to the *sn-3* position of the glycerol via a phosphodiester bond [1,2,22]. The headgroup can vary, forming phosphatidylcholines (PC) and phosphatidylethanolamine (PE), the two predominant phospholipid classes in most organisms [4,11]. Much of the diversity in membrane lipids stems from the type of fatty acids (FA) attached to the glycerol backbone. The FA can be saturated (SFA) with no double bond, monounsaturated (MUFA) with one double bond, or polyunsaturated (PUFA) with two or more double bonds [3,7,35]. Phospholipids containing PUFA are very susceptible to damage via lipid peroxidation[153,191]. This is because free radicals easily remove hydrogen atoms from the carbon in between double bonds due to the weak C-H bond at this position in PUFA. The removal of hydrogen can occur randomly

and in different positions along the acyl chain, forming a primary lipid radical (initiation step). This lipid radical, when unchecked, can undergo several modifications and initiate a chain reaction where it attacks and oxidatively damages other lipids and biomolecules (propagation). The reaction can be terminated non-enzymatically, through antioxidants, or enzymatically by cellular mechanisms such as glutathione peroxidase [122,147,155,159]. Notably, the susceptibility to lipid peroxidation increases as the number of double bonds in a FA increases because of the increase in the number of *bis*-allylic hydrogen, which are targets for lipid peroxidation[121,191]. For instance, linoleic acid (C18:2n6), which has two double bonds, is ~ 62 times more likely to be oxidized compared to oleic acid (C18:1n9) with one double bond [147,150,191]. Strikingly, arachidonic acid (C20:4n3), which has four double bonds, and eicosapentaenoic acid (C20:5n3), which has five double bonds, are ~201 and ~249 times more likely to be oxidized compared to oleic acid [147,150,191].

The oxidation of a single phospholipid species can generate several distinct oxL products [192,193]. In organisms with high membrane lipid diversity, this process significantly amplifies the potential number of oxL that can be generated. The low abundance of each oxidation product makes it analytically challenging to detect oxidized phospholipids present [194,195]. Additionally, the diverse oxL products formed have various chemical properties over a wide mass range. Therefore, the classical ways to quantify lipid peroxidation *in vivo* is by measuring end products of lipid peroxidation such as malondialdehyde (MDA), 4-hydroxynonenal (4-HNE), and 4-hydroxyhexenal (4-HHE) using spectroscopic techniques and mass spectrometry [193,196–198]. Although these are a good proxy for identifying the presence of lipid peroxidation, they cannot provide information on the full spectrum of oxL present in an organism that is required to understand the activities of oxL *in vivo* further. Recent advances in high-resolution mass spectrometry offer the opportunity to directly measure these diverse oxL [199,200]. In addition, coupling mass spectrometry to liquid chromatography allows for the separation of isobaric and isomeric oxL species [48,193]. To further help the identification of oxL, a novel computational bioinformatic tool called LPPtiger has been developed to predict the oxidized lipid in a biological sample. LPPtiger utilizes three algorithms to predict oxL, generate spectra libraries, and identify oxidized lipids. This tool offers a tremendous advantage by identifying novel and sample-specific oxL [192,201,202]. LPPtiger was recently used to identify and quantify oxL in blood plasma samples

obtained from lean and obese individuals with or without type 2 diabetes. Interestingly, the study revealed a unique oxL profile where lean individuals had oxL enriched with C18 acyl chains while obese and diabetic individuals had oxL profiles enriched with C20 acyl chains. This study demonstrated a unique remodeling of the oxL profile upon the development of obesity and its complications [201].

A primary challenge of studying oxL is identifying a suitable model organism that can be used to study their functional activity *in vivo*. The rapid and cost-effective cultivation of *Caenorhabditis elegans* (*C. elegans)* under standard laboratory conditions makes it an excellent model organism for probing oxL in a living system. Additionally, the membrane lipids of *C. elegans* have been well characterized, making it suitable for identifying and quantifying potential oxL [10,31,100]. The genetic flexibility of *C. elegans,* including mutants and RNA interference (RNAi) libraries, can allow precise targeting of biosynthetic pathways involved in lipid peroxidation, leading to a comprehensive understanding of the biological activities oxL [35,95,203]. Furthermore, the diet of the nematode can be manipulated by adding oxidants, allowing the study of lipid peroxidation *in vivo* [11,89,182]. In fact, lipid peroxidation has been implicated in many biological processes in the nematode, including ferroptosis-induced germ cell death, aging, and glucose stress. These studies generally use fluorescence techniques or MDA analysis to assess the level of lipid peroxidation [128,182,204]. Although these are useful indicators of lipid peroxidation, they do not provide information about the kinds of oxL that drive these responses. Advancing our ability to detect and quantify these oxL may provide a more comprehensive mechanistic insight into the role of lipid peroxidation in these critical processes.

In this study, we employed the innovative computational bioinformatic tool LPPtiger to predict oxidized lipids in *C. elegans*. By combining the predictive capabilities of LPPtiger with advanced mass spectrometry techniques, we successfully identified and quantified oxL in *C. elegans* under both tert-butyl hydroperoxide (TBHP) and glucose stress conditions. Our data unveiled distinctive sample-specific oxL profiles corresponding to each stress scenario, offering valuable insights into the organism's nuanced responses to diverse insults.

4.3 Methods

4.3.1 *In vitro* oxidation for lipid standard

In vitro oxidation of standard was carried out based on previously established methods [192,200,205]. Briefly, 65 µL of 10 mg/mL lipid standard PC 16:0/18:2 (Avanti polar) was diluted with 300 µL chloroform. The mixture was dried down under a stream of nitrogen. To generate lipid vesicles, ammonium bicarbonate 143 µL (3 mmol/L) was added, followed by sonication for 15 minutes. After, 125 µL of the lipid vesicle was pipetted into a new vial and 50 µL of copper sulfate (0.75 mmol/L), 50 µL sodium ascorbate (1.5 mmol/L), and 275 µL of water to make a final lipid concentration of 1.5 mM. The liposome was incubated at 37 ^{o}C for 24 hours and 72 hours. After *in vitro* oxidation of the lipid standard, 20 µL of the sample was dried under nitrogen and resuspended in 200 µL acetonitrile/2-propanol/water (65:30:5 v/v/v) to make a final solution of 0.15 mM of lipid.

4.3.2 Worm growth and maintenance

All experiments were conducted using wild-type N2 worms obtained from the *C. elegans* Genetics Center (CGC, University of Minnesota). All worms strained were maintained at 20 ^{o}C for the duration of the experiment.

4.3.3 Tert-butyl hydroperoxide (TBHP) stress to induce lipid peroxidation

TBHP stress was carried out using published protocols with modifications described here [32,128]. TBHP plates were made by adding concentrated TBHP to cooled HG media to a final concentration of 15 mM. Approximately 4000–5000 day 1 adult animals (66 hours after plating L1s) were transferred to HG supplemented with or without 15 mM TBHP for 2 hours at 20 ^{o}C. The animals were then collected by washing twice with M9, snap-frozen, and stored at - 80 ^{o}C until analysis.

4.3.4 Malondialdehyde (MDA) assay

Control and TBHP-stressed worms were resuspended in RIPA buffer (150 mM NaCl, 1% NP40, 0.5% sodium deoxycholate, 0.1% SDS, 50 mM Tris) supplemented with Pierce Protease Inhibitor (Thermo Scientific) and incubated on ice for 15 minutes. The worm samples were then lysed and homogenized using a QIAshredder spin column and centrifuged at maximum speed in a microcentrifuge for 2 minutes. This was repeated three times to ensure thorough lysis. The samples were finally centrifuged at maximum speed at 4 ^{o}C, and the supernatant was used for the MDA assay. MDA was measured using the Cayman Chemical thiobarbituric acid reactive substances assay (TBARS) (TCA method) assay kit following the manufacturer's instruction. The MDA concentration was measured fluorometrically at an excitation wavelength of 530 nm and emission wavelength of 550 nm using a NIVO plate reader (Perkin Elmer) along with appropriate standard curves using pure MDA standard. MDA levels were normalized using protein content measured using a Pierce BCA assay kit. Statistical analysis was performed with unpaired t-tests and F-tests to compare variances where statistically significant results had a $p<0.05$.

4.3.5 Glucose stress assay

The glucose stress was carried out as previously described [59,61,100]. Briefly, the glucose plates were made to a final concentration of 100 mM glucose by adding a filtered glucose solution to a cooled autoclaved NGM+CI medium. RNAi bacteria clones from the Ahringer library L4440 (empty vector) and *elo-5* RNAi were grown overnight in an LB media containing carbenicillin and tetracycline. The overnight cultures were resuspended at a 0.15 g/ml density to ensure sufficient bacterial lawn. These were then seeded onto the glucose and control plates four days before stress.

Synchronized L1s were grown for 48 hours on each RNAi background. The L4 animals were then transferred to seeded glucose or control plates for 18 hours at a density of 2500 worms/plates. After the stress period, the nematodes were snap-frozen and stored at - 80 ^{o}C until analysis.

4.3.6 Paraformaldehyde (PFA) killed bacteria experiment

OP50 cultures grown overnight were spiked with 32% paraformaldehyde at a final concentration of 0.5% based on a previous study [206]. The PFA-treated bacteria was shaken at 37 ºC at 200 rpm in a shaker for 1 hour. The PFA-killed and living bacteria were resuspended at a density of 0.15 g/ml and seeded onto HG plates supplemented with or without 100 mM glucose. Similar to the stress scheme outlined, the plates were seeded four days prior to stressing with L4 animals.

4.3.7 LPPtiger prediction and identification of oxidized lipid species

A lipid list containing pure lipid standard (PC16:0/18:2) or the most abundant PUFA containing PE and PC phospholipid (≥ 1.5%) was used for *in silico* prediction in the LPPtiger software (Supplement Table 1 and 2). The list of modifications was hydroperoxy, hydroxy, epoxy, and keto and truncated products. The prediction was performed considering a maximum modification of 2 sites on a phospholipid. Lipid samples from *in vitro* oxidation of pure standard or purified from *in vivo* studies carried out in the nematodes were run on a data-dependent acquisition (DDA), and the results from this analysis, together with the prediction, were run on LPPtiger software again to detect the lipid species that were present. For TBHP stress, the initial prediction was generated from comprehensive preliminary studies conducted by rotating day 1 animals with 15 mM TBHP solution for 1 hour (Supplement Table 3). The glucose stress list was generated using previously acquired data-dependent acquisition (Supplement Table 4) [100]. The predicted oxidized lipid list generated from LPPtiger was used for targeted Parallel Reaction Monitoring (PRM) for quantification [192,201].

4.3.8 Lipid extraction for intact phospholipids and oxidized lipids

Total lipids were extracted from worm samples using 4 ml of chloroform: methanol (2:1) spiked with 0.01% BHT and the internal standard 1,2-diundecanoyl-sn-glycero-3-phosphocholine (Avanti Polar Lipids) for 1.5 hours. Worm carcasses and water-insoluble molecules were then separated from the lipids by adding ~800 µL of 0.9 % NaCl. The separated lipids were then dried down under

a stream of nitrogen and resuspended in 200 µL of acetonitrile/ 2-propanol/water (65:30:5) for analysis [10,100].

4.3.9 Chromatographic separation of intact phospholipids and oxidized lipids

The lipid samples were separated using a Dionex UHPLC system, which was equipped with a C18 Hypersil Gold 2.1 × 50 mm, 1.9 µm reverse-phase column (Thermo Scientific, Waltham, MA) based on a previous study. A volume of 10 µL of the sample was injected, and the lipids were separated on a reverse-phase column at a flow rate of 300 µL/min. The separation was achieved using a gradient elution method with mobile phase A (60:40, water: acetonitrile, containing 10 mM ammonium formate and 0.1% formic acid) and mobile phase B (90:10, isopropyl alcohol: acetonitrile, containing 10 mM ammonium formate and 0.1% formic acid). The gradient elution schedule was as follows: 32% B from 0 to 1.5 min, 45% B at 4 min, 52% B at 5 min, 58% B at 8 min, 66% B at 11 min, % B at 14 min, 75% B at 18 min, 97% B from 18 to 25 min, and finally 32% B from 25 to 30 min for column equilibration [100].

4.3.10 Mass Spectrometry acquisition for intact phospholipids

Phospholipids separated by chromatography were then analyzed by Full MS data-dependent acquisition using a Q Exactive mass spectrometer (Thermo Scientific, Waltham, MA) as previously published. The phospholipids were acquired in the negative ion mode at a scan range of m/z 300-1,200 at a resolution of 70000. The HESI capillary temperature was maintained at 325°C, the sheath gas flow rate was set at 45 units, the auxiliary gas flow was set at 10 units, the source voltage was 3.2 kV, and the AGC target was 10^6. MS2 analyses comprised six scan events, where the top five ions were chosen from an initial MS1 scan for fragmentation at a normalized collision energy of 35. MS1 spectra were collected in profile mode, while MS2 spectra were collected in centroid mode [100].

Lipid data analyzer software (v. 2.8.3) from the Thallinger Lab (Graz University of Technology, Graz, Austria) was used to quantify the area of each phospholipid based on the mass list from a recent study [207].

4.3.11 Mass Spectrometry acquisition and quantification of oxidized lipids

Oxidized lipid species were acquired with a Parallel Reaction Monitoring (PRM) acquisition in the negative ion mode using an inclusion list containing a predicted oxidized list. MS/MS spectra were acquired at the resolution of 70, 000, AGC target 10^6 counts, maximum injection time of 100 ms, and isolation window of 2.0 m/z.

Oxidized lipid species were quantified using Skyline.ms v. 22.2.0.527 (MacCoss Lab, University of Washington, Seattle, USA) using a transition list containing precursor oxL list [208]. For each precursor, the oxFA or FA fragment was used for quantification. The peaks were manually verified and corrected. The raw areas were exported and normalized with the abundance of the total phospholipid.

4.4 Results

4.4.1 Establishing a workflow to quantify oxL using *in vitro* oxidation of PC 16:0/18:2

The oxidation of a fatty acid from an unmodified lipid depends on several factors, including the number, type, and position of the double bonds of the fatty acid within the complex lipid [122,205]. Considering these factors leads to several possible oxidized lipids (oxL) in a specific lipidome. To probe our ability to identify possible oxL in *C. elegans*, we used the newly developed open software LPPtiger 2 [192,201] to predict the possible oxL in a pure lipid standard PC (16:0_18:2). The LPPtiger 2 software predicted a total of 17 (16 unique m/z) possible oxL products from the oxidation of the PC (16:0_18:2) (see list in Supplemental Table 1.1). The lipid standard was oxidized *in vitro* for 1 day and 3 days using copper sulfate and sodium ascorbate as previously described[201,202,205] (Figure 4.1A), and the oxidized standard was run alongside the pure standard using a Full MS data-dependent acquisition (DDA) mode analysis on a Q Exactive mass spectrometer (Thermo Scientific, Waltham, MA). The results from this acquisition and the predicted oxidized lipid list were then run on the LPPtiger to identify the oxidized lipid species that were present. The LPPtiger prediction confirmed the presence of 15 (14 unique m/z) out of the 17 predicted oxL products (Supplement Table 1.2). The generated list was used as an inclusion list for parallel reaction monitoring acquisition (PRM) for 0.15 mM pure standard and oxidized lipid standard (1-day and 3-days oxidized).

Further quantification of the oxL was carried out using Skyline.ms (22.2.0.527). Skyline is an open-source software tool used to quantify proteins, small molecules, and metabolites such as oxL [208]. Skyline analysis only confirmed the presence of 12 (11 unique m/z) oxL due to the low abundance of other predicted oxL (Supplement Table 1.3). The results from the quantification showed a significant accumulation of oxL species in 1-day and 3-day oxidized samples compared to the pure standard, which contained mainly the unmodified PC lipid (~99 % of the total pool of lipids) (Supplement Table 1.4). Here, we used the lipid map nomenclature AB (XX_YY<Z>) for oxL where AB represents the head group, XX represents the FA chain, and YY represents oxidized

FA with modification <Z>. For 1-day oxL, the abundance of the unmodified lipids (PC 16:0_18:2) was reduced to 52.56 ± 3.24 % of the total lipids (Figure 1B). The oxL species that was most increased after in vitro oxidation for 1-day was the hydroperoxide-modified lipid, PC (16:0_18:2<OOH>), which accounted for 28.71 ± 0.80 % of the total lipid pool. For 3-day oxL species, there was a further decrease in the abundance of the unmodified species to 19.03 ± 6.52 % (Figure 1B). Similar to the 1-day oxL, the most increased oxidized lipid was the hydroperoxide-modified lipid species PC (16:0_18:2<OOH>), which accounted for 19.39 ± 2.87 % of the total lipid pool. In addition, there was also a significant accumulation of oxL with more than one modification attached to the oxL. Specifically, PC (16:0_18:2<OH, oxo>) accounted for 16.04 ± 3.30 % in 3-day oxidized samples compared to 1.68 ± 0.33 % in the 1-day oxidized lipid (Figure 4.1B). This trend was consistent for other oxL species as well, where there was a significant accumulation of oxL in 1-day oxidized lipids compared to 3-day oxidized lipids.

In summary, we established a workflow to measure the oxL from *in vitro* oxidation. Using reverse phase chromatographic separation allowed us to define the elution order of oxL compared to the standard (Figure 4.1). Intact phospholipids eluted later than the modified oxL, as previously reported[193]. The retention time decreased as the number of modifications on the oxL increased [201]. Furthermore, we demonstrated that a more extended period of oxidation led to an increase in the accumulation of oxidized lipid products.

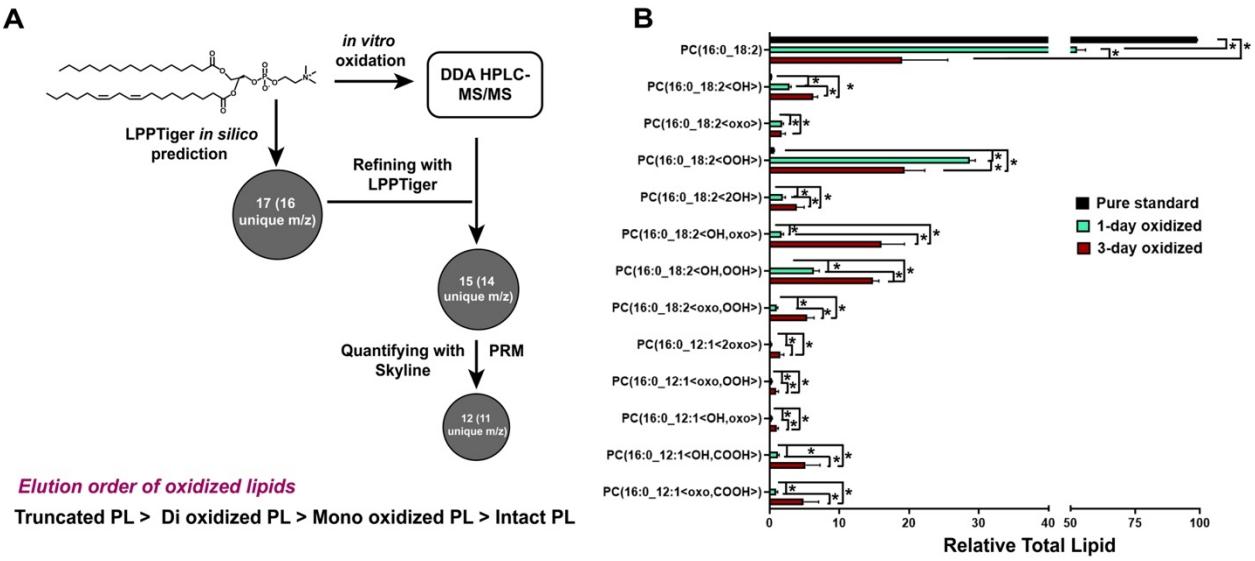

Figure 4.1 Workflow for quantifying oxidized lipids from *in vitro* oxidation of PC16:0_18:2 standard.

A) A total of 17 (16 unique m/z) theoretical oxidized lipids (oxL) was predicted using the LPPtiger software. Next, to determine which oxidized lipids were present, we oxidized pure lipid standard *in vitro* using copper sulfate and sodium ascorbate for 1 day and 3 days. The oxL were run on a data-dependent acquisition, and the results from this analysis, together with the prediction, were run on LPPtiger software again to detect the lipid species that were present. A total of 15 (14 unique m/z) was detected, and further quantification using Skyline showed only 12 (11 unique m/z) oxL. Using a C18 reverse phase column for HPLC separation prior to mass spectrometry analysis allowed us to define the elution order for oxL. The oxL eluted earlier than the intact PL. The retention was shorter as the number of modified groups increased in an oxL. **B)** The relative amount of each lipid was calculated, and the results show a significant accumulation of oxL in 1-day oxidized (green) and 3-oxidized lipids (red) compared to pure standard (black). The relative abundance of pure standard decreased to ~52 % and 19 % in 1-day oxidized and 3-day oxidized lipids, respectively. In 1-day oxidized lipids, oxidized lipids mainly accumulated possess a single modification with PC16:0_18:2 <OOH> accounting for 28.71 ± 0.80 % of the total lipids. 3-day oxidized lipid accumulated lipid with one and two modifications and truncated oxidized lipids. Data was generated from 3 independent replicates. Statistical significance was calculated by multiple t-tests with an adjusted p-value (corrected by FDR) at 5 %.

4.4.2 Adapting LPPtiger to quantify oxidized lipids *in vivo* in *C. elegans.*

Once the workflow was established for the pure standard, we sought to adapt the prediction to detect oxidized lipids products *in vivo* using *C. elegans* grown under standard laboratory conditions. To do so, a lipid list was generated that contains the most abundant PUFA species for PE (13 species with 10 unique m/z) and PC (19 species with 16 unique m/z) lipids which are the most abundant lipid class in *C. elegans* based on a previous lipidomics analysis[61,100] (Supplement Table 2.1). Theoretical oxidized lipid prediction based on this list generated 936 possible oxidized lipid species, with 346 (159 unique m/z) and 590 (321 unique m/z) being oxPE and oxPC species, respectively. Next, using Full MS DDA acquired from analyzing day 1 WT animals, we used the LPPtiger software to refine and detect the oxL species present in WT animals. In doing so, we were able to detect a total of 33 (26 unique m/z) oxL with oxPE and oxPC accounting for 10 (6 unique m/z) and 23 (20 unique m/z) respectively (Figure 4.2A) (Supplement Table 2.3). The refined list was used as an inclusion list for PRM acquisition. For accurate quantification, oxL must be detected based on their m/z, fragmentation pattern, and MS/MS pattern [153,193]. Because of the low abundance of oxL, achieving detailed MS/MS structural identification is not always possible. Furthermore, the limited availability of pure oxL standards specific to a biological sample makes it challenging to accurately map the retention time of different oxL species in a sample-specific manner. To further validate the targets after the PRM acquisition, we used a few decision rules to detect and eliminate false positives. First, we used the oxFA of the oxL species for quantification on Skyline. In doing so, we were able to quantify three oxL, namely PC (18:2_18:2<OH>), PC (18:1_18:2<OH>), PE (18:1_18:2<OH>). We used the FA fragment to quantify species where the oxFA fragment was absent. To further validate whether these were truly oxidized lipids, we compared the retention time behavior with that of the non-oxidized PL precursor. Because we used a reverse phase column for HPLC separation prior to mass spectrometry analysis, oxL, which are more polar than their corresponding intact PL, will elute first [193,201]. We were able to accurately quantify 9 more oxL with a unique m/z which were annotated based on the LIPID maps nomenclature for oxL quantified with the FA fragment (Supplement Table 2.4).

Using these decision rules, we could accurately quantify a total of 12 oxL, representing ~ 40 % of the predicted pool within WT animals (Supplement Table 2.4). The oxPC was the majority of the oxL, accounting for ~91 % of the total pool of oxL (Figure 2B, Supplement Table 2.5). This is not surprising as most of the PUFA are accumulated in PC species (~ 60 % of total FA) compared to PE (~30 % of total FA) in *C. elegans* [35,61,100]. The oxPC consisted of species with one, two, or three modifications and truncated oxL species. The oxL PC (18:1_20:5<2O>) accounted for ~50 % of the pool of oxL (Figure 4.2B), and the truncated ox PC (16:0_15:2<3O>) accounted for ~23 % (Figure 4.2C). For the oxPE pool, the most abundant oxL was the PE (18:1_18:2<OH>), which represented over ~51% of the total PE pool (Figure 4.2D).

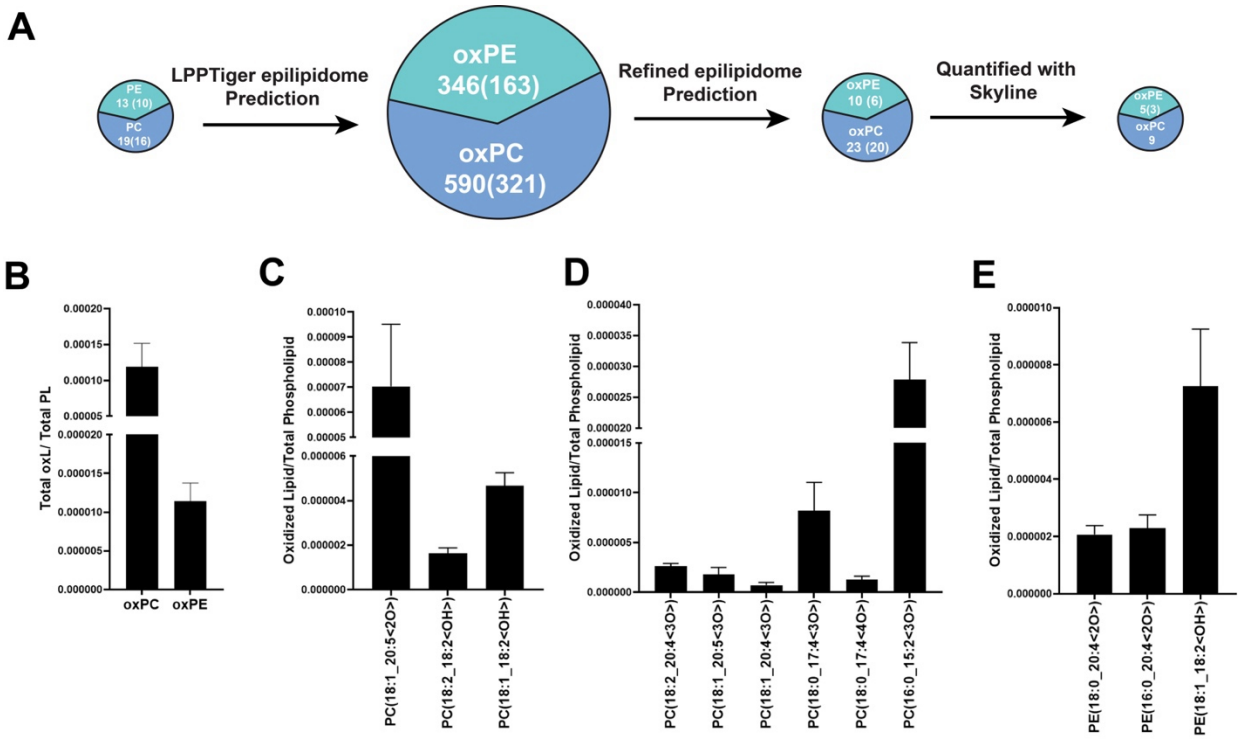

Figure 4.2 Basal oxL profile of WT animals.
A) To identify the baseline oxL composition of WT animals, we selected the most abundant PUFA in WT animals (> 1.5% total PC or PE). The list was used in the LPPtiger software to generate the possible theoretical oxidized lipids based on the worms' lipidome. In total, we identified 346 (163 unique m/z) potential oxPE and 590 (321 unique m/z) potential oxPC. Lipids were extracted from day 1 animals and analyzed using a Full MS DDA. LPPtiger was used to refine and identify oxL species in WT animals. In doing so, we identified 10 (6 unique m/z) oxPE and 23 (20 unique m/z) oxPC species. Based on retention time mapping, we were able to quantify a total of 12 oxL (3

oxPE and 9 oxPC) on Skyline. **B)** The overall abundance of oxL showed a significant accumulation of oxPC lipid species (~91%) compared with oxPE (9%). **C)** The distribution of oxPC with one and two modifications within the oxL **D)** The distribution of oxPC with three modifications and truncated oxPC species **E)** The overall distribution of oxPE present within WT animals is shown. These oxPE have either only one or two modifications present. Data was generated from at least 4 biological replicates.

4.4.3 Tert-butyl hydroperoxide (TBHP) stress induces the accumulation of oxidized lipids in *C. elegans*

Once the assay was established for WT animals in normal growth conditions, we sought to detect oxidized lipids products *in vivo* in *C. elegans* under oxidative stress. To induce the accumulation of oxidized lipids, day 1 adult worms were transferred to a 15 mM TBHP-supplemented plate for 2 hours. TBHP is a strong oxidant shown previously to induce lipid peroxidation in the nematodes, as assessed by the accumulation of malondialdehyde (MDA) in the nematodes upon stress. We measured the levels of MDA in nematodes treated with 15 mM TBHP and saw a 2.5X increase in MDA levels compared to control (Figure 4.3A). Next, oxL lipids were quantified using the predicted list from LPPtiger described in the methods. In doing so, we identified and quantified ten oxL, which included 7 oxPE and 3 oxPC (Figure 4.3B, Supplement Table 3.2). During the TBHP exposure, we noticed that the bacteria lawn on the TBHP plates was very thin compared to the control plates. Thus, to disentangle between the perturbations by TBHP stress and the possibility of starvation, day 1 adult worms were transferred to plates without any bacteria (starved) alongside the control and TBHP-stress plates. We quantified the abundance of the predicted pooled oxidized lipids using PRM acquisition, and the results show that TBHP stress did not significantly change the overall abundance of oxPC compared to control worms. Interestingly, we saw a significant increase in the abundance of oxPE by ~10 in TBHP-stressed animals compared to the control (Figure 4.3B). This result shows that the extent of damage caused by TBHP stress is higher in PE phospholipids compared to PC lipids. Furthermore, we confirmed that the changes in TBHP stress were not due to starvation, as the oxL profile in TBHP-stressed worms was not seen in the starved animals. Interestingly, we saw an accumulation of unique oxL in TBHP-

stressed animals that were not present in the control population, namely, PC (20:5_20:5<OH>), PE (18:0_20:5<OH>), and PE (18:0_20:4<OH>) (Figure 4.3C).

To further probe the changes after TBHP stress, we quantified the fold change in individual oxL and identified species significantly altered in TBHP-stressed animals compared to control (Figure 4.3D, Supplement Table 3.3). The most changed oxL species was PE (17:0_20:5<O>), which increased by ~15X in TBHP-stressed animals compared to controls. In addition, other oxPE species that were significantly changed were PE (18:1_20:5<O>), PE (17:0_20:4<2O>), PE (18:0_20:4<3O>), and PE (18:0_20:5<3O>) that increased by ~13X, ~2.5X ~4X, and ~9X respectively (Figure 3E). For oxPC, there was a significant increase in PC (18:1_20:5<O>) and PC (18:1_20:4<3O>) by 3X and 5X, respectively (Figure 3E).

Finally, although there were no changes in the overall abundance of oxL in starved animals, we noticed a significant change in the abundance of two oxL in starved animals. Specifically, PC (18:1_18:2<OH>) was significantly decreased in starved animals compared to the control population and TBHP-stressed animals. Furthermore, PE (17:0_20:4<2O>), which was significantly increased in TBHP-stressed animals, was also elevated in starved animals by ~ 2.5X compared to control (Figure 4.3E). Collectively, these results show, for the first time, a unique oxL profile for worms after oxidative stress.

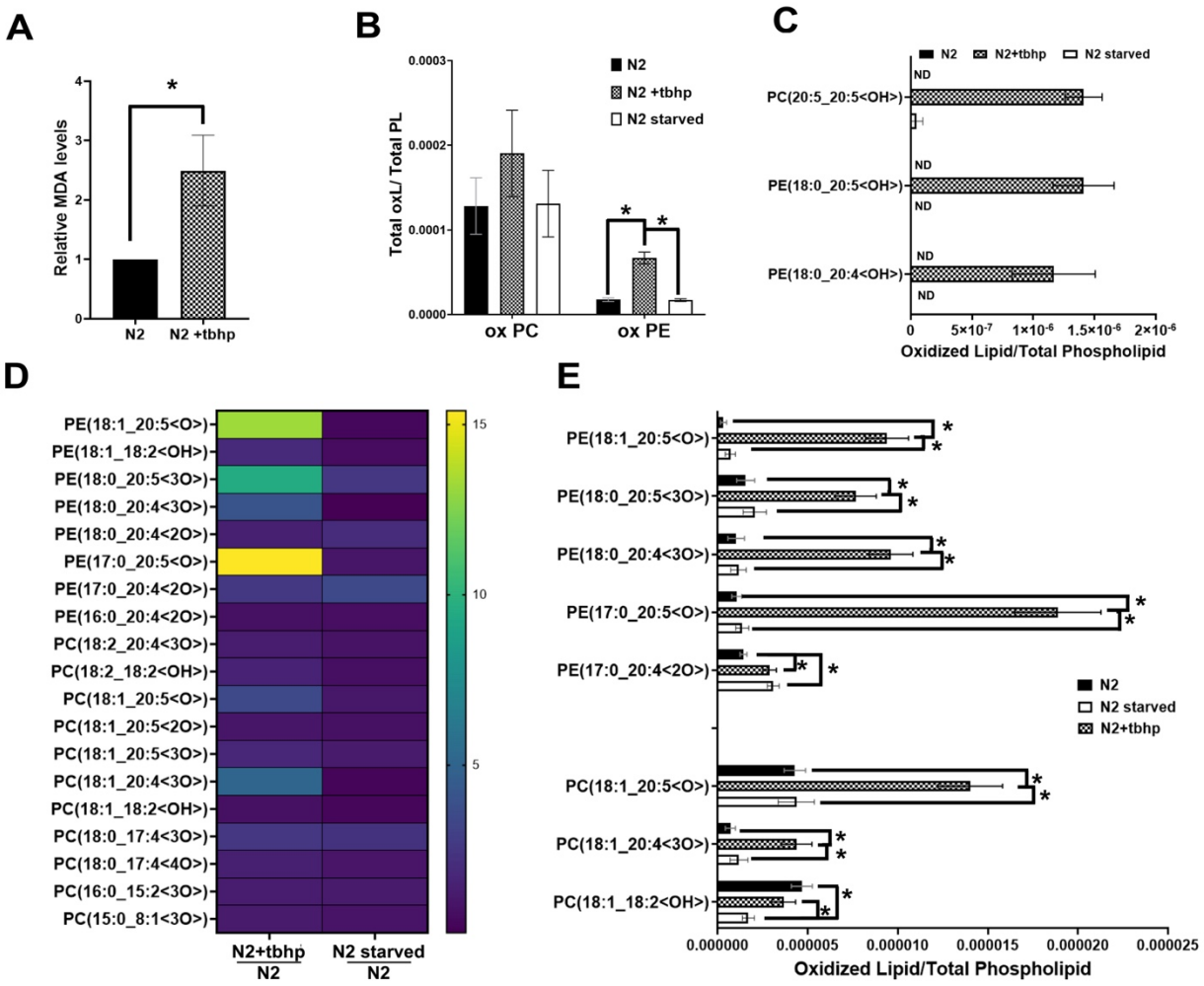

Figure 4.3 Oxidized lipid profile of WT exposed to 15 mM TBHP stress.
A) The level of malondialdehyde (MDA) is increased in WT animals exposed to 15 mM TBHP stress for 2 hours. MDA levels were normalized to total protein content, and the data represents three independent trials. **B)** We implemented our workflow to detect oxL in WT animals exposed to 15 mM TBHP stress for 2 hours. After manually refining the prediction as described previously, we identified and quantified ten new oxL species that accumulate upon TBHP stress. These new species were made up of 7 oxPE and 3 oxPC species. The total oxL in each class was quantified, and the results show a significantly increased oxPE in WT animals (black) compared to WT animals exposed to 15 mM TBHP (black checkered). Because of the thin bacteria lawn on the TBHP-stress plate, we analyzed animals that were starved for the same duration of time during the stress to delineate whether the changes were not induced by starvation. In doing so, we saw that the significant shift in oxPE was only present in TBHP-stressed animals and not in starved animals (white). C) Three hydroxylated oxL that were uniquely accumulated in TBHP-stressed animals, namely PC (20:5_20:5<OH>), PE (18:0_20:5<OH>) and PE (18:0_20:4<OH>) and not detected in either control or starved animals. **D)** The heat map shows the fold change in all the pooled oxL quantified in TBHP-stressed animals and starved animals relative to WT control populations. **E)**

The oxL species that are significantly increased in TBHP-stressed animals are shown here and contain either at 20:5 or 20:4 FA with one, two, or three modifications. Data was generated from at least 4 independent replicates. Statistical significance was calculated by multiple t-tests with an adjusted p-value (corrected by FDR) at 5 %.

4.4.4 Phospholipid double bond distribution in TBHP-stressed and starved animals

Because the TBHP stress led to the accumulation of oxL in animals, we wanted to probe whether these effects translated to the intact phospholipid. Since these lipids are a substrate for lipid peroxidation caused by TBHP stress, we expected to see a decrease in the species with a higher number of double bonds. To do this, we binned PCs and PEs by the total double bonds present within the FA tails, i.e., 0-1, 2-3, 4-5, 6-7, and 8 or more (Supplement Table 3.4). In PC lipids, there was a significant decrease in PL with 2-3 double bonds from 27.68 ±1.98 % to 23.05 ± 1.95 % in TBHP-stressed animals compared to controls (Figure 3A). In addition, there was a significant increase in phospholipid with 8 or more DB in TBHP-stressed animals (25.96 ± 1.37 %) compared to control animals (20.71 ± 1.98 %) (Figure 4.4A). Interestingly, the changes that were observed in the PC DB distribution in TBHP-stressed animals were similar to starved animals as there was also a significant decrease in PL with 2-3 DB (20.72 ± 1.42 %) and an increase in phospholipid with 8 or more double bonds (26.87 ± 1.11 %) (Figure 4.4A).

Similarly, we binned the PE phospholipids according to the total PL within the FA tails (Supplement Table 3.4). In comparing TBHP-stressed animals to controls, we saw a significant decrease in PL with 0-1 and 2-3 DB from 23.63 ± 4.01 % to 20.49 ± 2.09 % and 37.94 ± 1.69 to 33.60 ± 1.61 % respectively (Figure 4.4B). Furthermore, there was an increase in PL with 4-5 (28.74 ± 3.66 % to 34.23 ± 1.64 %) and 6-7 DB (7.70 ± 0.74 % to 9.34 ± 1.41 %) in TBHP-stressed compared to control animals (Figure 4.4B). Strikingly, there was a significant decrease in PL with 2-3 DB and an increase in PL with 4-5 DB in starved animals. Although not significant, the trends in the distribution of the other DB bins for starved animals were similar to those of TBHP-stressed animals and not the control population. Collectively, the PL distribution of the TBHP-stressed

animals suggests that these changes may reflect alterations induced by both the TBHP stress and starvation.

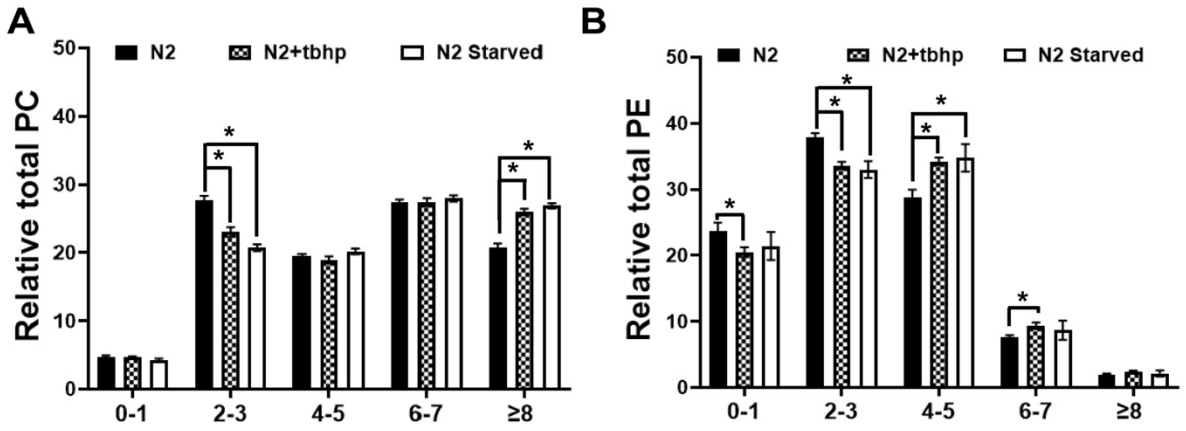

Figure 4.4 Phospholipid (PC and PE) double bond distribution of TBHP-stressed animals. **A)** Analysis of the double bond distribution of intact PC phospholipids shows a significant decrease in PL with 2-3 double bonds and a significant increase in PL with 8 or more DB in starved and TBHP-stressed animals compared to controls. **B)** Similarly, in PE, there was a significant decrease in the PL with 2-3 double bonds and an increase in species with 4-5 double bonds. Furthermore, there was a significant decrease in lipid species with 0-1 double bonds and a significant increase in PL with 6-7 double in TBHP-treated animals compared to controls. Similar trends were observed in starved animals but were not statistically significant. Data was generated from at least 4 independent replicates. Statistical significance was calculated by multiple t-tests with an adjusted p-value (corrected by FDR) at 5 %.

4.4.5 Glucose stress induces the accumulation of oxL in the nematodes

Elevated glucose in the diet of nematodes has previously been shown to lead to changes in lipid metabolism pathways that lead to the accumulation of saturated fat (SFA), which activates the membrane sensor PAQR-2 (Progestin and AdipoQ receptors). PAQR-2 is a transmembrane protein that responds by upregulating the synthesis of unsaturated fatty acid (UFA) by activating stearyl CoA desaturase (FAT-7). The exact mechanism of how the accumulation of SFA occurs is unclear as the nematodes do not increase the synthesis of fat or receive excess SFA from bacteria processing glucose based on previous studies [61]. Using ^{13}C-stable isotope labeling techniques, we show that PUFAs are preferentially maintained during glucose stress. Specifically, the precursors of PUFA are funneled towards the production and maintenance of longer, more unsaturated C20 PUFAs. Therefore, we hypothesized that glucose causes oxidative stress, and PUFA are preferentially synthesized to correctly replace oxidatively damaged PUFAs to prevent membrane dysregulation. To test this hypothesis, we sought to quantify the oxL species present during glucose stress in WT animals and in a glucose-sensitive background using *elo-5* RNAi. We previously showed that a loss of ELO-5 leads to a remodeling of membrane lipids towards a membrane composition that would be protective against oxidative stress [100]. We used the LPPtiger software to identify new oxL in our pooled experiments of worms stressed with glucose (Supplement Table 4.1). We were able to refine and accurately quantify five oxPC upon glucose stress (PC (18:1_20:5<oxo>), (PC (18:1_20:5<O>), PC (18:1_20:4<2O>), and PC (18:1_20:4<2OH>) based on the decision rules outlined earlier (Supplemental Table 4.2).

We quantified the overall abundance of oxL with this new pool of oxL and WT oxidized lipids described earlier. In doing so, we identified a significant increase in the levels of oxPE by ~ 3X in WT animals stressed with glucose (L4440 +gluc) compared to the control population (L4440) (Figure 4.5A). We also compared *elo-5* RNAi animals stressed with glucose (*elo-5* +gluc) with *elo-5* RNAi animals and saw a significant increase in oxPE. Notably, the fold increase in oxPE for *elo-5* RNAi upon glucose stress was lower (2X) than in control animals stressed with glucose (3X). Furthermore, there were no changes in the overall level of the oxPC population (Figure 4.5A).

Next, we probed the individual lipids and identified a few oxL species that altered upon glucose stress in L4440 +gluc vs L4440 control animals, as shown in Figure 4.5B. Specifically, there was an accumulation of PE (16:0_20:4<2O>) and PE (18:0_20:4<2O>), in L4440 +gluc compared to L4440 controls by ~6X and 2.5X respectively (Figure 4.5C). We also applied the oxL generated from TBHP-induced stress and were able to detect and quantify two oxPE (PE (17:0_20:4<2O>) and PE (18:1_20:5<O>) that were also significantly changed upon glucose stress. Specifically, the oxL PE (17:0_20:4<2O>) and PE (18:1_20:5<O>) were increased by ~3X and 4X respectively (Figure 4.5C). Although the overall pool of oxPC did not change, we also probed the individual oxPC species and noticed changes in some species. The oxPC species PC (18:1_20:5<O>) and PC (18:1_20:5<oxo>) were both increased in L4440 +gluc compared to L4440 controls by ~ 2X (Figure 4.5C). Furthermore, we observed a few oxPE that were changed in *elo-5* animals stressed with glucose (*elo-5* +gluc) compared with control (*elo-5*). Specifically, PE (16:0_20:4<2O>) and PE (18:0_20:4<2O>) increased by 6X and 1.5 X respectively in *elo-5* animals stressed with glucose (Figure 4.5D). Similarly, we also observed that PC (18:1_20:5<O>) and PC (18:1_20:5<oxo>) were also doubled in *elo-5* +gluc compared to *elo-5*. Collectively, our results confirm that glucose causes oxidative stress and unveil, for the first time, a unique oxL profile induced by this metabolic challenge.

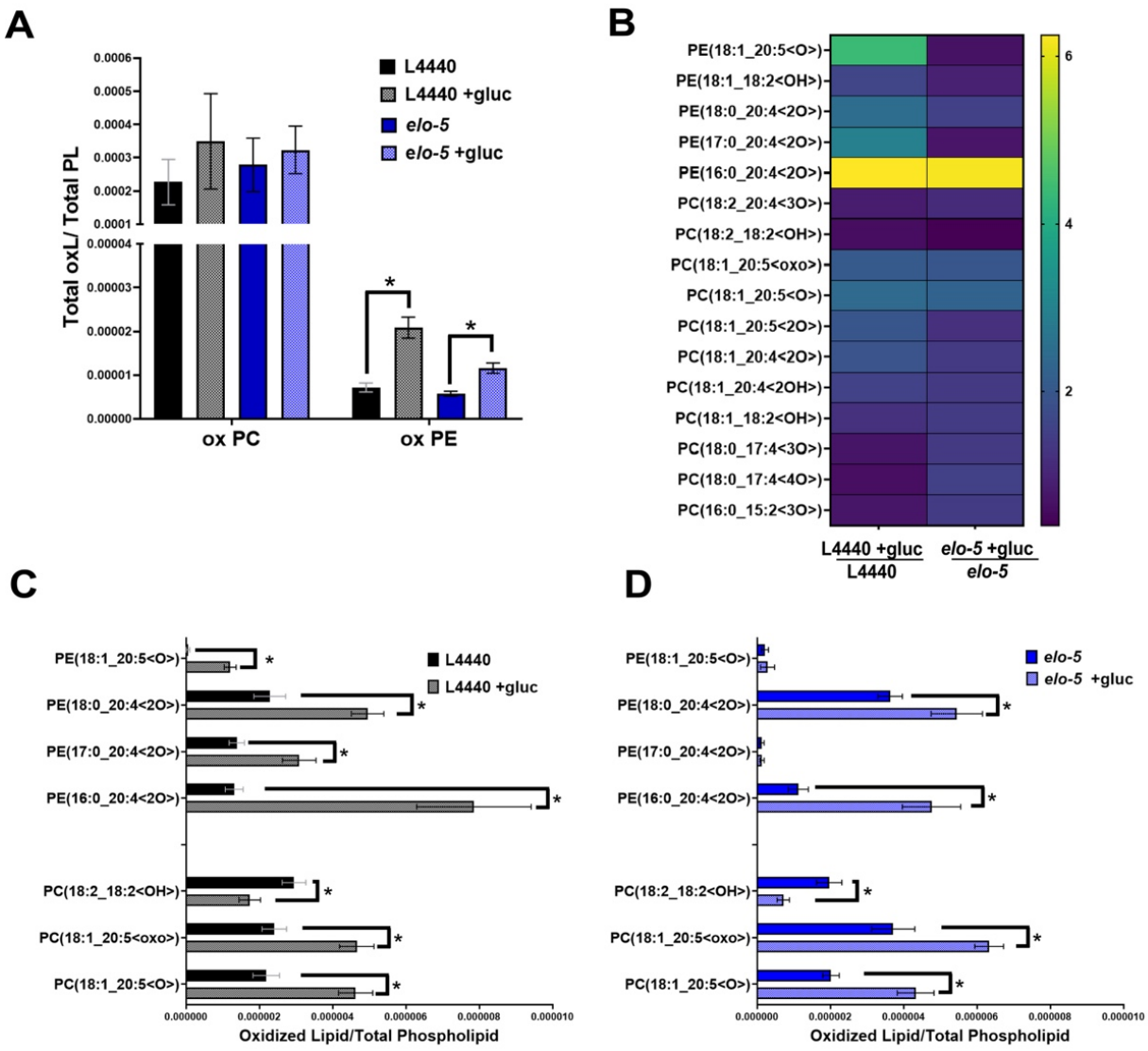

Figure 4.5 Oxidized lipid profile of animals stressed with 100 mM glucose.
In glucose-stressed animals, we identified and quantified five new oxPC in addition to the native oxL of WT animals. PC (18:1_20:5<oxo>), PC (18:1_20:5<O>), PC (18:1_20:4<2O>), and PC (18:1_20:4<2OH>). We also included two oxPE from the TBHP-induced oxL pool, which also increased under glucose stress. Specifically, PE (17:0_20:4<2O>), PE (18:1_20:5<O>). **A)** The total of oxL in each class was quantified, and the results show a significant increase in oxPE in WT animals (black) compared to WT animals exposed to 100 mM glucose (black dotted). Similar trends in oxPE levels were also noted in *elo-5* animals stressed with glucose (blue dotted) compared to control *elo-5* (blue). **B)** The heat map shows the fold change in all the pooled oxL quantified in glucose-stressed animals under various backgrounds relative to their respective control populations. **C)** The oxL species significantly changed in L4440+gluc compared to the L4440 control background. **D)** The oxL species significantly changed in *elo-5*+gluc compared to

the *elo-5* RNAi background. The oxL changed more in control animals stressed with glucose (L4440 +gluc) than *elo-5* stressed with glucose (*elo-5* + gluc). In fact, in some cases, the oxL species are missing in *elo-5* animals, or the levels are very small compared to WT animals. Data was generated from at least 3 independent replicates. Statistical significance was calculated by multiple t-tests with an adjusted p-value (corrected by FDR) at 5 %.

4.4.6 Bacteria processing glucose contributes to the accumulation of oxL in the nematodes

Our glucose stress experiment required that the bacteria be seeded to the glucose plates four days prior to stress. It has been shown that bacteria processing glucose can increase the levels of oxidative stress to the nematode [209]. Because of the prolonged exposure of the bacteria to glucose on the plate, we wanted to ascertain the impact of bacteria processing glucose will have on the accumulation of oxL. To disentangle the role of bacteria processing glucose during stress, we utilized paraformaldehyde (PFA) to kill the bacteria. PFA has been suggested to kill bacteria by permeating cells and making them inviable without disrupting structures, including the plasma membrane [206]. Additionally, our recent application of heat to kill the bacteria, induced a significant shift in the lipid composition, particularly increasing the levels of C16:0 FA [61]. Therefore, to test the impact of killing bacteria, we stressed nematodes with glucose and control plates seeded with living and PFA-killed bacteria. We analyzed the FA composition of the PFA-killed bacteria compared to control populations and surprisingly saw a significant change in the FA composition. Specifically, the most notable change was an increase in the MUFA C18:1n7 and C16:1n7 and a decrease in C19D FA (Figure 4.6A).

The total oxL in each class was quantified, and the results showed a significant increase in the levels of oxPE in glucose-stressed animals fed with living bacteria. Interestingly, in control animals fed with PFA-killed bacteria, there was a trend towards an increase in oxPE in glucose stress conditions; however, this was not significant. In *elo-5* deficient animals fed with PFA-killed bacteria, there was no change in the levels of oxPE under glucose stress (Figure 4.6B). As observed previously, there was no difference in the levels of oxPC lipids. The oxL species PE (16:0_20:4<2O>) was increased in control animals stressed with glucose on living bacteria by ~ 5X; however, in animals on PFA killed bacteria, this oxL was only significantly increased ~2X

(Figure 4.6C). Similarly, in *elo-5* animals stressed with glucose on living bacteria, PE (16:0_20:4<2O>) increased by 5X, while on PFA-killed bacteria, there was no significant increase in the level of this oxL. Next, PE (18:0_20:4<2O>), which was significantly increased in control and *elo-5* glucose-stressed animals fed living bacteria, was not increased in glucose stress animals fed with PFA-killed bacteria (Figure 4.6C and 4.6D). Finally, PE (17:0_20:4<2O>), which is significantly increased in L4440 +gluc populations compared to control, was also increased significantly in glucose-stress animals fed with PFA-killed bacteria (Figure 4.6D). These results suggest that bacteria processing glucose may partly contribute to the damage caused by glucose stress. However, fully delineating this effect is complicated due to the alterations in bacterial lipid composition following PFA treatment.

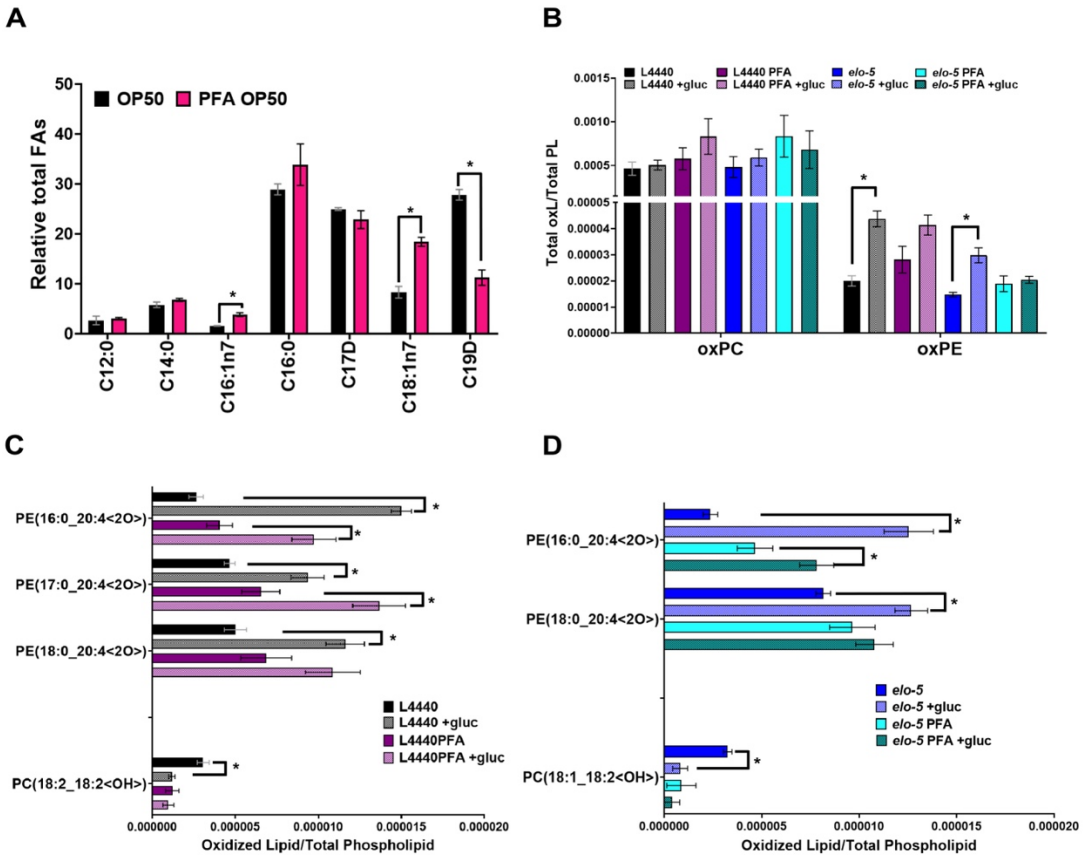

Figure 4.6 Impact of bacteria processing glucose on the oxL profile of the nematode.
To disentangle the impact of bacteria metabolizing glucose on the effects of glucose stress, we fed nematodes with living bacteria and dead bacteria killed with 0.5% PFA. The living bacteria and PFA-killed bacteria were resuspended at a density of 0.15 g/mL. The bacteria were seeded on control HG plates and HG plates supplemented with 100 mM glucose for four days prior to stress. **A)** The relative % of FA in bacteria was assessed using GC/MS. Comparing the PFA-killed bacteria to living bacteria showed a significant increase in C16:1n7 and C18:1n7 and a significant decrease in C19D. We also observed a trend toward an increase in C16:0 in PFA-killed bacteria. Data was generated from 3 independent replicates. **B)** The total oxL in each class was quantified, and the results show a significant increase in oxPE in WT animals (black) compared to WT animals exposed to 100 mM glucose (black dotted). Interestingly, control animals fed PFA-killed bacteria show a trend towards an increase in oxPE, but this was not significant. Similar trends were observed in *elo-5* animals as feeding these animals with living bacteria increased the oxPE, while PFA-killed bacteria did not increase the level of oxPE species in *elo-5* animals. **C)** The oxL species significantly changed in stress conditions compared to the control background. PE (18:0_20:4<2O>) was significantly increased in glucose stress conditions with living bacteria and not in PFA-killed bacteria. **D)** Similar trends were observed in *elo-5* RNAi animals, as there was a significant decrease in oxL species in glucose animals treated with PFA-killed bacteria. Data was generated from at least 4 independent replicates. Statistical significance was calculated by multiple t-tests with an adjusted p-value (corrected by FDR) at 5 %.

4.5 Discussion

In this study, we described the oxL composition of nematodes *in vivo* using the novel bioinformatic software LPPtiger and advanced mass spectrometry. The inherent challenges posed by the low abundance and extensive chemical diversity of oxL have historically hindered their comprehensive analysis. LPPtiger provides a platform to define sample-specific oxL profiles by using the lipid composition of the organism to predict oxL that may be present. However, our initial predictions of the oxL utilized a Full MS data-dependent acquisition data, which may limit our coverage of other lowly abundant oxidized lipids. Recently, an optimized mass spectrometry setting has been outlined to increase coverage to detect lowly abundant species by using a semi-targeted data-dependent acquisition (stDDA) for the initial prediction step. The stDDA leverages the *in silico* predicted oxidized lipids as an inclusion list in the mass spectrometry method to improve the coverage of oxL that can be detected [201,202]. We intend to adopt this approach to optimize our mass spectrometry parameters in subsequent experiments to increase the amount of oxidized lipids present. Furthermore, we plan to expand our oxL pool by conducting experiments with other perturbations to induce oxidative stress in the nematode. Despite this limitation, we were able to present results that show oxL species in the nematode under both basal conditions and stress induced by tert-butyl hydroperoxide (TBHP) and glucose. The results unveil a distinctive sample-specific oxidized lipid profile corresponding to each stress scenario, providing valuable insights into the nuanced responses of the organism to diverse environmental challenges.

We were able to define the basal oxL profile of the nematodes using the approach described. In the natural oxL profile, we saw a significant amount of oxPC species compared to oxPE. This was unsurprising as PC lipid species contain more PUFA than the PE population in the nematodes [35,61,100]. The spectrum of oxL ranged from species with just one modification to species with more than one modification and truncated species. The presence of oxL has been shown to interact with proteins and other biomolecules [151,156]. In fact, it has been shown that oxL species interact with scavenger receptors and toll-like receptors to induce signaling pathways *in vivo* [159,160,184]. Therefore, the presence of these basal oxL in the nematode suggests their potential involvement in

mediating signaling events and underscores the importance of further elucidating the functional roles of oxL in biological processes.

Despite the high levels of oxPC compared to oxPE under basal conditions, we were intrigued to notice an overall increase in the abundance of oxPE when nematodes were subjected to TBHP-induced stress. A few studies have reported selective oxidation of PE over PC [186,210–212]. This selectivity is attributed to the availability of intact PL substrates positioned within specific cellular compartments where they may be exposed to varying degrees of oxidative damage [210,213]. PEs are particularly enriched in the inner leaflet of the plasma membrane and the mitochondria, regions prone to heightened oxidative conditions [5,26,155]. Therefore, our results suggest that the increase in oxPE may be occurring in these specific cellular compartments. This selectivity is further underscored by the differential responses observed in individual oxL species. Specifically, PE (18:1_20:5<O>) is increased by ~13X while the PC with the same modification PC (18:1_20:5<O>) is only increased by 3X. To further understand whether the changes in the oxL may be reflected in non-oxidized PLs, we looked at the abundance of the direct substrate to the oxL that was generated (Supplement Figure 1). Interestingly, analyzing the phospholipid composition shows that the direct substrates for these oxL were mostly unchanged under stress. For those that were altered, the trends were similar to that of starved worms, suggesting changes may not be driven by oxidative stress alone but by starvation as well. While the precise mechanism underlying this lack of correlation remains elusive, we posit that it further bolsters the notion of oxidation occurring within specific domains of subcellular compartments. Given our comprehensive lipidomics approach focusing on whole animals, the presence of non-oxidized lipid species from various tissues and cells may potentially dilute changes occurring specifically within subcellular compartments. Future subcellular lipidomic studies may shed light on this intricate mechanism. The lack of correlation between the direct substrate and its oxL product was also observed in the recent study,[201] highlighting a complex interplay of factors governing lipid peroxidation.

Previous studies have shown that glucose causes oxidative stress in the nematodes [182,183,209]. We recently corroborated this using ^{13}C stable isotope labeling strategies, which showed that PUFA may be preferentially maintained in the nematode in glucose stress conditions. This maintenance

requires funneling C18:1n9 and C18:2n6 to produce longer, more unsaturated C20 PUFAs[61]. Here, we found that glucose stress leads to an accumulation of oxL, particularly oxPE species. However, the extent of increase in oxPE was not as pronounced as observed under TBHP-induced stress, suggesting that glucose induces a milder oxidative stress compared to TBHP. Interestingly, specific individual oxPE species that were increased under TBHP stress, namely PC (18:1_20:5<O>), PE (18:1_20:5<O>), and PE (17:0_20:4<2O>), were changed under glucose stress conditions as well, suggesting these species may be a general indicator of oxidative stress. Furthermore, we saw a significant increase in the level of PE (16:0_20:4<2O>) and PE (18:0_20:4<2O>), which was not increased in TBHP stress which suggests this may be a glucose-driven accumulation of oxL. This demonstrates that the accumulation of oxL depends on the type of stress an organism encounters. Additionally, we measured the oxL profile of glucose-sensitive animals *elo-5*. The enzyme ELO-5 produces mmBCFA and is critical for surviving glucose stress. Surprisingly, we found that the accumulation of oxL was reduced in *elo-5* animals under glucose stress compared to controls. This phenomenon may be attributed to the remodeling of membrane lipid composition resulting from the loss of mmBCFA, affecting the pool of substrates available for oxidation. Notably, the oxL PE (17:0_20:4<2O>) contains a mmBCFA and was lowly abundant in *elo-5* deficient animals. Phospholipid analysis also shows that the levels of non-oxidized PL substrate for this oxL, PE 37:4, is significantly reduced (Supplement Figure 2). Furthermore, we previously showed that loss of *elo-5* leads to the accumulation of plasmalogens [100]. Plasmalogen has been suggested to play a protective role in oxidative stress by acting as a sacrificial antioxidant [31–34]. Therefore, the remodeling of membrane PL may confer a protective effect on *elo-5* animals against glucose-induced oxidative stress.

Previous research suggests that oxidative stress induced by glucose stress may be attributed to the processing of glucose by bacteria in the diet [209]. In this study, the bacteria were killed by heat treatment, which we recently showed significantly altered the membrane composition of the bacteria by increasing the overall levels of C16:0 SFA [61]. Given that an increase in C16:0 is a hallmark of glucose-induced membrane stress, this method of killing the bacteria precludes a clear understanding of the metabolic effects of bacteria in glucose stress. To address this, we used paraformaldehyde in this study to kill the bacteria, which has been suggested to kill bacteria while

maintaining the internal structure of the cells, such as the cell membrane intact [206]. Although we did not see an accumulation of C16:0 in bacteria after PFA treatment, we still observed alterations in the lipid composition of PFA-killed bacteria—specifically, an increase in MUFA (C18:1n7 and C16:1n7) and a decrease in C19D. When the oxL profile was assessed in animals fed with PFA-killed bacteria, we noticed a marginal reduction in the overall levels of oxL present in glucose-stressed animals. This result suggests that bacteria metabolizing glucose stress may partly contribute to the accumulation of oxL. However, because of the significant alteration in the dietary composition of PFA-killed bacteria, it is challenging to fully elucidate the role of bacteria metabolism in the glucose-induced response. It will be important to investigate other methods that will inhibit bacteria growth without significantly altering their membrane composition to precisely delineate the role of bacteria processing glucose in the stress response.

In summary, we identified and quantified oxL in the nematode under different stress scenarios, unveiling crucial insights into the organism's adaptive responses. Further investigation is warranted into the functional consequences of oxL accumulation and their impact on cellular pathways. Such investigations will contribute to a comprehensive understanding of lipid peroxidation and stress adaptation mechanisms in *C. elegans*.

4.6 Acknowledgments

The authors would like to thank the *Caenorhabditis elegans* Genetics Center (CGC) at the University of Minnesota for the *C. elegans* strains. They would also like to thank Diana DiTullio and Liliana McDonald of the Olsen lab for their contributions to this work.

CHAPTER 5 - CONCLUSION AND FUTURE DIRECTIONS

5.1 Overall conclusion

Maintaining appropriate membrane lipid composition is critical for cellular function and the overall physiological health of an organism. Despite this, the regulatory mechanisms maintaining membrane composition have yet to be fully elucidated. This thesis has contributed to a deeper understanding of membrane lipid homeostasis by unveiling active response mechanisms that ensure optimum membrane composition under stress conditions. Through the application of targeted mass spectrometry, isotope labeling strategies, lifespan assays, and other biochemical methods, this research has uncovered response mechanisms to glucose-induced stress in *C. elegans*. Our findings reveal novel membrane regulatory mechanisms critical for maintaining membrane homeostasis under glucose stress, as described in chapters 3 and 4 and illustrated in the model (Figure 5.1).

Glucose stress induces oxidative stress in the nematode, damaging membrane PUFAs and the subsequent accumulation of oxidized phospholipids, notably oxPE. The specific accumulation of oxPE suggests a subcellular or tissue-specific oxidative stress induced by glucose stress. Given that PUFA are more susceptible to oxidation, we hypothesize that the consequence of this is the loss of PUFA and an accumulation of SFA, which are less impacted by oxidative stress. In response, the membrane sensor PAQR-2 is activated, which induces the expression of *fat-7* and *elo-5*. FAT-7 promotes the synthesis of MUFA and PUFA, which are crucial for maintaining optimum membrane fluidity. In addition, the increased synthesis of PUFA is also required to actively replace membrane PUFA damaged by glucose-induced oxidative stress. Furthermore, PAQR-2 also activates *elo-5* to promote the production of mmBCFAs, which are funneled towards the production of glucosylceramides. The generation of glucosylceramides is speculated to mediate signaling events, potentially through the TORC complex. This intricate response network is required for optimum function and survival under glucose stress.

This work has provided foundational knowledge that has deepened the understanding of membrane biology. Given the broad implications of membrane composition in various disease conditions, the findings from this research could be instrumental in future research that seeks to understand how membrane dysregulation contributes to disease pathologies. Further exploration of these regulatory mechanisms could lead to significant pharmaceutical developments, including identifying novel therapeutic targets for many diseases

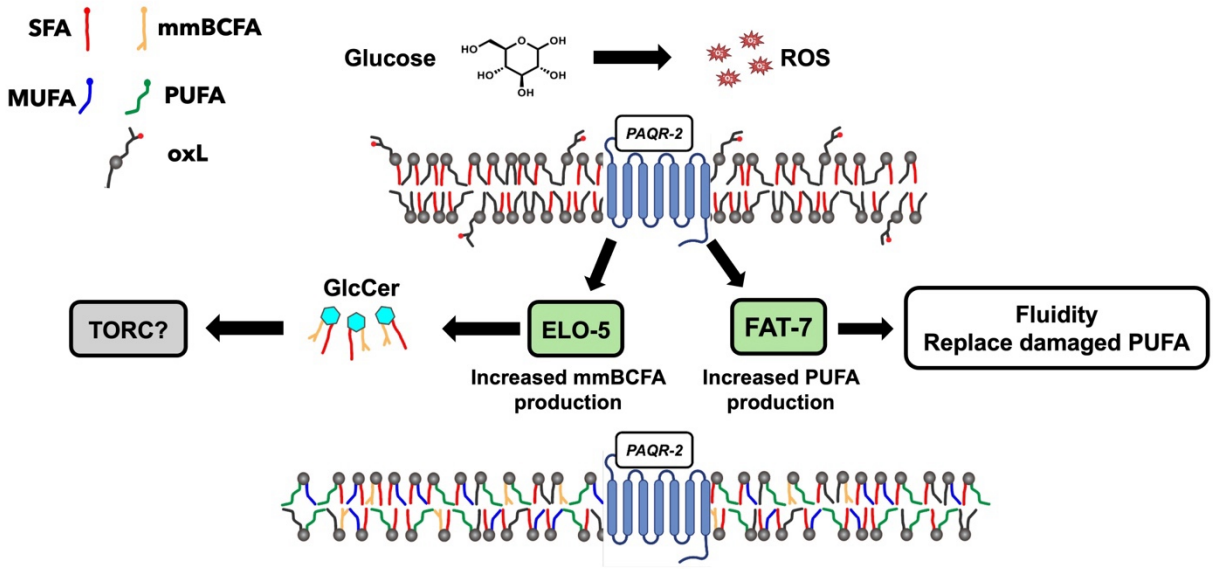

Figure 5.1 Model summarizing the membrane lipid response to glucose stress from this thesis.
Elevated dietary glucose causes oxidative stress, which promotes the formation of oxidized lipids and accumulation of SFA, driving a response coordinated by PAQR-2. PAQR-2 activates *elo-5* and *fat-7* to restore membrane integrity and promote survival under glucose stress. FAT-7 facilitates the synthesis of MUFA and PUFA, which are imperative for maintaining optimal membrane fluidity and replenishing damaged PUFAs. In addition, ELO-5 promotes the production of glucosylceramides (GlcCer), which we hypothesize mediates signaling pathways, potentially via the TORC complex, for the nematodes to respond and survive glucose stress.

5.1.1 Conclusion- Chapter 3

This chapter significantly advanced our understanding of glucosylceramide (GlcCer) metabolism within *C. elegans*. One of the significant challenges of metabolic studies is establishing a causal link between an individual lipid species and the phenotype of interest due to the interconnected nature of metabolic pathways. Nevertheless, through targeted mass spectrometry and lifespan assays, we uncovered a novel role for GlcCer in response to an elevated glucose diet, expanding on the role of GlcCer in the nematode. Specifically, we established GlcCer 17:1;O2/22:0;O as a critical metabolite responsible for the glucose response. In WT animals, exposure to glucose significantly increases the levels of GlcCer 17:1;O2/22:0;O. Compromising the production of this GlcCer using *elo-5* and *elo-3* RNAi leads to a significant shortening of the lifespan of the nematodes. To further corroborate that the shortened lifespan of animals with ELO-5 knockdown was due to compromised GlcCer production, we supplemented *elo-5* RNAi with sphingolipid extract from WT animals. Interestingly, supplementing *elo-5* RNAi-treated animals with WT sphingolipid extract not only restored their reduced lifespan under glucose stress but also shifted GlcCer levels in *elo-5* RNAi towards WT GlcCer levels, including a significant surge in the levels of the GlcCer 17:1;O2/22:0;O. The successful rescue with the lipid supplementation is striking, underscoring the potential of lipid supplements to ameliorate specific phenotypic defects. This finding may have broader implications, bolstering the feasibility of lipid supplementation as a viable therapeutic strategy in conditions characterized by the depletion of specific lipid species.

Furthermore, we found that compromising CGT-3, which catalyzes the addition of glucose to ceramide to form GlcCer via RNAi, dramatically reduces the lifespan of animals on glucose. Surprisingly, the levels of GlcCer 17:1;O2/22:0;O were not significantly impacted by compromising *cgt-3*. Given that CGT-3 is essential in only a select group of intestinal cells, it is plausible that its influence on GlcCer levels is localized, not systemic, suggesting that GlcCer-mediated signaling in these cells may be a key driver of the organism's overall glucose response. Collectively, our lipidomic and survival analyses have shed light on the intricate metabolic reprogramming that nematodes undergo in response to glucose stress, highlighting an indispensable role of GlcCer in this response.

5.1.2 Conclusion- Chapter 4

Phospholipids, particularly those containing polyunsaturated fatty acids (PUFA), can be damaged via lipid peroxidation, significantly altering the membrane properties. The alterations induced by this damage can compromise membrane integrity and impact many critical biological events, such as signaling, inflammation, and cell death [153,156,186,201]. The quantification of these oxidized lipids has been challenging due to their low abundance and high number of potential oxidized lipids that can be derived based on the lipidome within a specific biological organism. In this chapter, we utilized the LPPtiger software and mass spectrometry to elucidate the oxidized lipid profile of *C. elegans* under basal and stress conditions. Our findings reveal the presence of oxPC and oxPE species, with oxPC being the most predominant species. The overall presence of oxL in wild-type animals suggests these are not only formed under stress conditions but are generated under basal conditions as well, indicating specific biological roles of oxL in the nematode under normal conditions. Under stress conditions induced by TBHP or glucose, there is a significant accumulation of oxPE. This finding suggests that oxidative stress induced by these perturbations may occur in specific cellular components such as mitochondria and inner membrane leaflets where PE lipids are enriched.

Furthermore, we uncovered that although each stress scenario leads to the accumulation of oxPE, distinct oxPE are associated with each stressor, indicating that the oxidative stress caused by each perturbation imprints a unique oxidized lipid profile within the organism. Collectively, these findings show the nuanced response to various perturbations in the nematode, unveiling crucial insights into the organism's adaptive responses. Further research into the functional implications of oxL accumulation and its influence on cellular pathways will deepen our understanding of the role of lipid peroxidation in stress response and adaptation in *C. elegans*.

5.2 Future directions

5.2.1 Chapter 3- Future directions

Our studies have established that the GlcCer-mediated glucose response is essential for survival in the nematode. The roles of GlcCer in *C. elegans* have been unfolding over the years, and this work has expanded on the role of this lipid class. Building on findings from this study, further research can broaden our understanding of the biological role of GlcCer metabolism in the nematode.

5.2.1.1 Deciphering the mechanistic role of CGT-3 in glucose stress

In our study, we reveal a dramatic shortening of the lifespan of CGT-3 animals in glucose stress. Because these are expressed in limited cells [134], it suggested that the role of GlcCer in the intestine may mediate signaling events required for glucose response. Therefore, further studies will be necessary to identify downstream signaling targets of CGT-3 deficient animals under glucose stress. The major signaling complex TORC has been associated with GlcCer metabolism [110,137,145]. It will be interesting to investigate whether the role of CGT-3 in glucose response is through the activation of the TORC complex. In addition, identifying other novel downstream signaling targets of CGT-3 could provide valuable insights. An approach that can be used to identify these downstream targets is through genetic screening to identify mutations that enhance the survival of CGT-3 deficient animals under glucose stress. This can be done by mutagenizing CGT-3 deficient animals using ethyl methane sulfonate (EMS). Suppressor candidates can be identified by their ability to survive glucose stress. The findings from this investigation will further enhance our understanding of the interconnection between GlcCer metabolism and TORC signaling, as well as identify new signaling targets that are mediated by GlcCer.

5.2.1.2 Explore other perturbations that influence GlcCer metabolism in *C. elegans*

To broaden our understanding of GlcCer metabolism in the nematode, it will be interesting to investigate these populations using other stressors. Further research should extend to other dietary metabolites to assess whether this GlcCer-mediated response is specific to glucose or other metabolites. Other candidates that can be screened are intermediate metabolites from glucose metabolisms such as dihydroxyacetone phosphate (DHAP), which is known to shorten lifespan significantly [88]. Consequently, exploring whether DHAP and other glycolytic intermediates influence GlcCer metabolism may shed light on the broader implications of GlcCer-mediated responses.

5.2.1.3 Assess GlcCer-mediated glucose response in mammalian models

Considering the conservation of GlcCer synthesis and degradation pathways from *C. elegans* to mammals, it is compelling to explore if the glucose stress response is similarly conserved. Investigating the viability of mammalian cells with GlcCer knockdown under high glucose conditions could shed light on the evolutional conservation of this stress response mechanism.

5.2.2 Chapter 4- Future directions

In this study, we developed targeted mass spectrometry methods to quantify oxidized lipids, allowing us to uncover the effects of glucose stress on nematodes. This approach provided new insights into how glucose supplementation impacts these organisms. Future research should apply this methodology to different conditions to further expand our understanding of the biological role of oxidized lipids.

5.2.2.1 Identify oxidized lipid species in aging worms

One of the hallmarks of aging is the accumulation of reactive oxygen species due to the decline in cellular homeostasis in aging [214]. One of the consequences of the imbalance between the generation of oxidants and antioxidant systems that eliminate them is the damage of membrane PUFA via lipid peroxidation [16,152]. Therefore, it will be beneficial to adapt this workflow to identify novel oxidized lipids associated with the nematode's aging process. Additionally, aging compromises the ability to respond appropriately to stress [214–217]. Unpublished data from our lab have observed reduced PUFA levels in animals stressed with glucose over aging. It will be imperative to expand and investigate whether unique oxidized lipids are associated with the decline of stress response in aging. Identifying these unique oxidized lipids could provide valuable insights into the molecular mechanisms underpinning aging and aging-related decline in stress response.

5.2.2.2 Investigate other oxidized lipids associated with lipid peroxidation-mediated stress response in *C. elegans*

In this chapter, we demonstrated that the accumulation of oxidized lipids exhibits specificity for different types of stress encountered by the nematode. Lipid peroxidation is associated with biological processes, including germ cell defects, drug-induced toxicity, and ferroptosis cell death in *C. elegans* [128,218,219]. Extending this workflow to detect oxidized lipid profiles under these diverse stress conditions will deepen the understanding of how unique oxidized lipids modulate the biological responses of the nematode.

REFERENCES

1. Ingólfsson, H. I. *et al.* Lipid Organization of the Plasma Membrane. *J Am Chem Soc* **136**, 14554–14559 (2014).
2. Van Meer, G., Voelker, D. R. & Feigenson, G. W. Membrane lipids: where they are. *Nat Rev Mol Cell Biol* **101**, 1–4 (2009).
3. Antonny, B., Vanni, S., Shindou, H. & Ferreira, T. From zero to six double bonds: phospholipid unsaturation and organelle function. *Trends Cell Biol* **25**, 427–436 (2015).
4. Holthuis, J. C. M. & Menon, A. K. Lipid landscapes and pipelines in membrane homeostasis. *Nature* **510**, 48–57 (2014).
5. Meer, G. Van, Anton, I. P. M., Meer, G. Van & Kroon, A. I. P. M. De. Lipid map of the mammalian cell Lipid Map of the Mammalian Cell. *cell science* **2011**, 5–8 (2011).
6. Ernst, R., Ballweg, S. & Levental, I. Cellular mechanisms of physicochemical membrane homeostasis. *Curr Opin Cell Biol* **53**, 44–51 (2018).
7. Ernst, R., Ejsing, C. S. & Antonny, B. Homeoviscous Adaptation and the Regulation of Membrane Lipids. *J Mol Biol* **428**, 4776–4791 (2016).
8. de Mendoza, D. & Pilon, M. Control of membrane lipid homeostasis by lipid-bilayer associated sensors: A mechanism conserved from bacteria to humans. *Prog Lipid Res* **76**, (2019).
9. Levental, K. R. *et al.* Lipidomic and biophysical homeostasis of mammalian membranes counteracts dietary lipid perturbations to maintain cellular fitness. *Nature Communications 2020 11:1* **11**, 1–13 (2020).
10. Dancy, B. C. R., Chen, S. W., Drechsler, R., Gafken, P. R. & Olsen, C. P. 13C- and 15N-labeling strategies combined with mass spectrometry comprehensively quantify phospholipid dynamics in C. elegans. *PLoS One* **10**, 1–23 (2015).
11. Sultana, N. & Olsen, C. P. Using stable isotope tracers to monitor membrane dynamics in C. elegans. *Chem Phys Lipids* **233**, 104990 (2020).
12. Pilon, M. Revisiting the membrane-centric view of diabetes. *Lipids Health Dis* **15**, 1–6 (2016).
13. Svensk, E. *et al.* PAQR-2 Regulates Fatty Acid Desaturation during Cold Adaptation in C. elegans. *PLoS Genet* **9**, (2013).
14. Devkota, R. *et al.* The adiponectin receptor AdipoR2 and its Caenorhabditis elegans homolog PAQR-2 prevent membrane rigidification by exogenous saturated fatty acids. *PLoS Genet* **13**, 1–19 (2017).
15. Svensk, E. *et al.* Caenorhabditis elegans PAQR-2 and IGLR-2 Protect against Glucose Toxicity by Modulating Membrane Lipid Composition. *PLoS Genet* **12**, 1–24 (2016).
16. Almeida, I., Magalhães, S. & Nunes, A. Lipids: biomarkers of healthy aging. *Biogerontology* **22**, 273–295 (2021).
17. Gille, B., Galuska, C. E., Fuchs, B. & Peleg, S. Recent Advances in Studying Age-Associated Lipids Alterations and Dietary Interventions in Mammals. *Frontiers in Aging* **0**, 63 (2021).

18. Gianfrancesco, M. A., Paquot, N., Piette, J. & Legrand-Poels, S. Lipid bilayer stress in obesity-linked inflammatory and metabolic disorders. *Biochem Pharmacol* **153**, 168–183 (2018).
19. Fanning, S., Selkoe, D. & Dettmer, U. Parkinson's disease: proteinopathy or lipidopathy? *NPJ Parkinsons Dis* **6**, 1–9 (2020).
20. Bandu, R., Mok, H. J. & Kim, K. P. Phospholipids as cancer biomarkers: Mass spectrometry-based analysis. *Mass Spectrom Rev* **37**, 107–138 (2018).
21. Fecchio, C., Palazzi, L. & Polverino de Laureto, P. α-Synuclein and polyunsaturated fatty acids: Molecular basis of the interaction and implication in neurodegeneration. *Molecules* **23**, (2018).
22. Klose, C., Surma, M. A. & Simons, K. Organellar lipidomics — background and perspectives. *Curr Opin Cell Biol* **25**, 406–413 (2013).
23. Stefan, C. J. *et al.* Membrane dynamics and organelle biogenesis — lipid pipelines and vesicular carriers. 1–24 (2017) doi:10.1186/s12915-017-0432-0.
24. Casares, D., Escribá, P. V. & Rosselló, C. A. Membrane Lipid Composition: Effect on Membrane and Organelle Structure, Function and Compartmentalization and Therapeutic Avenues. *International Journal of Molecular Sciences 2019, Vol. 20, Page 2167* **20**, 2167 (2019).
25. Harayama, T. & Riezman, H. Understanding the diversity of membrane lipid composition. *Nature Reviews Molecular Cell Biology 2018 19:5* **19**, 281–296 (2018).
26. Lorent, J. H. *et al.* Plasma membranes are asymmetric in lipid unsaturation, packing and protein shape. *Nature Chemical Biology 2020 16:6* **16**, 644–652 (2020).
27. Shevchenko, A. & Simons, K. Lipidomics: Coming to grips with lipid diversity. *Nat. Rev. Mol. Cell Biol.* **11**, 593–598 (2010).
28. Magalhaes, M. A. O. & Glogauer, M. Pivotal Advance: Phospholipids determine net membrane surface charge resulting in differential localization of active Rac1 and Rac2. *J Leukoc Biol* **87**, 545–555 (2010).
29. Verkleij, A. J. & Post, J. A. Membrane phospholipid asymmetry and signal transduction. *Journal of Membrane Biology* **178**, 1–10 (2000).
30. Grinstein, S. Imaging signal transduction during phagocytosis: Phospholipids, surface charge, and electrostatic interactions. *Am J Physiol Cell Physiol* **299**, 876–881 (2010).
31. Drechsler, R., Chen, S. W., Dancy, B. C. R., Mehrabkhani, L. & Olsen, C. P. HPLC-Based mass spectrometry characterizes the phospholipid alterations in ether-linked lipid deficiency models following oxidative stress. *PLoS One* **11**, 1–22 (2016).
32. Shi, X. *et al.* A Caenorhabditis elegans model for ether lipid biosynthesis and function. *J Lipid Res* **57**, 265–275 (2016).
33. Braverman, N. E. & Moser, A. B. Functions of plasmalogen lipids in health and disease. *Biochimica et Biophysica Acta (BBA) - Molecular Basis of Disease* **1822**, 1442–1452 (2012).
34. Paul, S., Lancaster, G. I. & Meikle, P. J. Plasmalogens: A potential therapeutic target for neurodegenerative and cardiometabolic disease. *Prog Lipid Res* **74**, 186–195 (2019).
35. Watts, J. L. & Ristow, M. Lipid and carbohydrate metabolism in Caenorhabditis elegans. *Genetics* **207**, 413–446 (2017).

36. Andersen, O. S. & Roger E. Koeppe, I. Bilayer Thickness and Membrane Protein Function: An Energetic Perspective. *http://dx.doi.org/10.1146/annurev.biophys.36.040306.132643* **36**, 107–130 (2007).
37. Fuller, N. & Rand, R. P. The Influence of Lysolipids on the Spontaneous Curvature and Bending Elasticity of Phospholipid Membranes. *Biophys J* **81**, 243–254 (2001).
38. Tan, S. T., Ramesh, T., Toh, X. R. & Nguyen, L. N. Emerging roles of lysophospholipids in health and disease. *Prog Lipid Res* **80**, 101068 (2020).
39. Meyer zu Heringdorf, D. & Jakobs, K. H. Lysophospholipid receptors: Signalling, pharmacology and regulation by lysophospholipid metabolism. *Biochimica et Biophysica Acta (BBA) - Biomembranes* **1768**, 923–940 (2007).
40. Merrill, A. H. Sphingolipid and glycosphingolipid metabolic pathways in the era of sphingolipidomics. *Chem Rev* **111**, 6387–6422 (2011).
41. Merrill, A. H. De novo sphingolipid biosynthesis: A necessary, but dangerous, pathway. *Journal of Biological Chemistry* **277**, 25843–25846 (2002).
42. Peng, B. *et al.* A Comprehensive High-Resolution Targeted Workflow for the Deep Profiling of Sphingolipids. *Anal Chem* **89**, 12480–12487 (2017).
43. Shaner, R. L. *et al.* Quantitative analysis of sphingolipids for lipidomics using triple quadrupole and quadrupole linear ion trap mass spectrometers. *J Lipid Res* **50**, 1692–1707 (2009).
44. Gault, C. R., Obeid, L. M. & Hannun, Y. A. An overview of sphingolipid metabolism: From synthesis to breakdown. *Adv Exp Med Biol* **688**, 1–23 (2010).
45. D'Angelo, G., Capasso, S., Sticco, L. & Russo, D. Glycosphingolipids: synthesis and functions. *FEBS J* **280**, 6338–6353 (2013).
46. Surma, M. A. *et al.* Mouse lipidomics reveals inherent flexibility of a mammalian lipidome. *Scientific Reports 2021 11:1* **11**, 1–14 (2021).
47. Han, X. Lipidomics for studying metabolism. *Nature Reviews Endocrinology 2016 12:11* **12**, 668–679 (2016).
48. Lange, M., Ni, Z., Criscuolo, A. & Fedorova, M. Liquid Chromatography Techniques in Lipidomics Research. *Chromatographia 2018 82:1* **82**, 77–100 (2018).
49. Checa, A., Bedia, C. & Jaumot, J. Lipidomic data analysis: Tutorial, practical guidelines and applications. *Anal Chim Acta* **885**, 1–16 (2015).
50. Cajka, T. & Fiehn, O. Toward Merging Untargeted and Targeted Methods in Mass Spectrometry-Based Metabolomics and Lipidomics. *Anal Chem* **88**, 524–545 (2016).
51. Blanksby, S. J. & Mitchell, T. W. Advances in mass spectrometry for lipidomics. *Annual Review of Analytical Chemistry* **3**, 433–465 (2010).
52. Raterink, R. J., Lindenburg, P. W., Vreeken, R. J., Ramautar, R. & Hankemeier, T. Recent developments in sample-pretreatment techniques for mass spectrometry-based metabolomics. *TrAC - Trends in Analytical Chemistry* **61**, 157–167 (2014).
53. Dettmer, K., Aronov, P. A. & Hammock, B. D. Mass spectrometry-based metabolomics. *Mass Spectrom Rev* **26**, 51–78 (2007).
54. Hannich, T. J., Mellal, D., Feng, S., Zumbuehl, A. & Riezman, H. Structure and conserved function of iso-branched sphingoid bases from the nematode: Caenorhabditis elegans. *Chem Sci* **8**, 3676–3686 (2017).

55. Cheng, X. *et al.* Sphingolipidomic analysis of C. elegans reveals development-and environment-dependent metabolic features. *Int J Biol Sci* **15**, 2897–2910 (2019).
56. Xatse, M. A. & Olsen, C. P. Defining the glucosylceramide population of C. elegans. *Front Physiol* **14**, 1244158 (2023).
57. Buescher, J. M. *et al.* A roadmap for interpreting 13C metabolite labeling patterns from cells. *Curr Opin Biotechnol* **34**, 189–201 (2015).
58. Jang, C., Chen, L. & Rabinowitz, J. D. Metabolomics and Isotope Tracing. *Cell* **173**, 822–837 (2018).
59. Vieira, A. F. C. *et al.* Monomethyl branched-chain fatty acids are critical for Caenorhabitis elegans survival in elevated glucose conditions. *Journal of Biological Chemistry* **298**, 101444 (2022).
60. Perez, C. L. & Van Gilst, M. R. A 13C Isotope Labeling Strategy Reveals the Influence of Insulin Signaling on Lipogenesis in C. elegans. *Cell Metab* **8**, 266–274 (2008).
61. Vieira, A. F. C., Xatse, M. A., Murray, S. Y. & Olsen, C. P. Oleic Acid Metabolism in Response to Glucose in C. elegans. *Metabolites* **13**, 1185 (2023).
62. Weijers, R. N. M. Lipid Composition of Cell Membranes and Its Relevance in Type 2 Diabetes Mellitus. *Curr Diabetes Rev* **8**, 390 (2012).
63. Fanning, S. *et al.* Lipidomic Analysis of α-Synuclein Neurotoxicity Identifies Stearoyl CoA Desaturase as a Target for Parkinson Treatment. *Mol Cell* **73**, 1001-1014.e8 (2019).
64. Wang, S. *et al.* Phosphatidylethanolamine deficiency disrupts α-synuclein homeostasis in yeast and worm models of Parkinson disease. *Proc Natl Acad Sci U S A* **111**, E3976–E3985 (2014).
65. Molina, J. A. *et al.* Cerebrospinal fluid levels of non-neurotransmitter amino acids in patients with Alzheimer's disease. *J Neural Transm* **105**, 279–286 (1998).
66. Han, X., Holtzman, D. M. & McKeel, D. W. Plasmalogen deficiency in early Alzheimer's disease subjects and in animal models: molecular characterization using electrospray ionization mass spectrometry. *J Neurochem* **77**, 1168–1180 (2001).
67. Wood, P. L., Barnette, B. L., Kaye, J. A., Quinn, J. F. & Woltjer, R. L. Non-targeted lipidomics of CSF and frontal cortex grey and white matter in control, mild cognitive impairment, and Alzheimer's disease subjects. *Acta Neuropsychiatr* **27**, 270–278 (2015).
68. Su, X. Q., Wang, J. & Sinclair, A. J. Plasmalogens and Alzheimer's disease: A review. *Lipids Health Dis* **18**, 1–10 (2019).
69. Katafuchi, T. *et al.* Effects of plasmalogens on systemic lipopolysaccharide-induced glial activation and β-amyloid accumulation in adult mice. *Ann N Y Acad Sci* **1262**, 85–92 (2012).
70. Fujino, T. *et al.* Efficacy and Blood Plasmalogen Changes by Oral Administration of Plasmalogen in Patients with Mild Alzheimer's Disease and Mild Cognitive Impairment: A Multicenter, Randomized, Double-blind, Placebo-controlled Trial. *EBioMedicine* **17**, 199–205 (2017).
71. Bunney, T. D. & Katan, M. Phosphoinositide signalling in cancer: beyond PI3K and PTEN. *Nature Reviews Cancer 2010 10:5* **10**, 342–352 (2010).
72. Cao, S. *et al.* The biological role and immunotherapy of gangliosides and GD3 synthase in cancers. *Front Cell Dev Biol* **11**, (2023).
73. Peetla, C. *et al.* Breast Cancer Cells : Biophysical Characterization of and Doxorubicin Interactions with Membrane Lipids. *Molecular Pharmaceuticals* **7**, 2334–2348 (2010).

74. Kartal Yandım, M., Apohan, E. & Baran, Y. Therapeutic potential of targeting ceramide/glucosylceramide pathway in cancer. *Cancer Chemother Pharmacol* **71**, 13–20 (2013).
75. Reza, S., Ugorski, M. & Suchański, J. Glucosylceramide and galactosylceramide, small glycosphingolipids with significant impact on health and disease. *Glycobiology* **31**, 1416–1434 (2021).
76. Madigan, J. P. *et al.* A role for ceramide glycosylation in resistance to oxaliplatin in colorectal cancer. *Exp Cell Res* **388**, 111860 (2020).
77. Stefanovic, M. *et al.* Targeting glucosylceramide synthase upregulation reverts sorafenib resistance in experimental hepatocellular carcinoma. *Oncotarget* **7**, 8253–8267 (2016).
78. Liu, Y.-Y. *et al.* A role for ceramide in driving cancer cell resistance to doxorubicin. *The FASEB Journal* **22**, 2541–2551 (2008).
79. La Monica, S. *et al.* Targeting glucosylceramide synthase induces antiproliferative and proapoptotic effects in osimertinib-resistant NSCLC cell models. *Scientific Reports 2024 14:1* **14**, 1–15 (2024).
80. Leonetti, A. *et al.* Resistance mechanisms to osimertinib in EGFR-mutated non-small cell lung cancer. *British Journal of Cancer 2019 121:9* **121**, 725–737 (2019).
81. Ho, Y. S. *et al.* Lipidomic Profiling of Lung Pleural Effusion Identifies Unique Metabotype for EGFR Mutants in Non-Small Cell Lung Cancer. *Scientific Reports 2016 6:1* **6**, 1–13 (2016).
82. Brenner, S. The genetics of behaviour. *Br Med Bull* **29**, 269–271 (1973).
83. Anderson, J. L., Morran, L. T. & Phillips, P. C. Outcrossing and the Maintenance of Males within C. elegans Populations. *Journal of Heredity* **101**, S62–S74 (2010).
84. Kaletsky, R. & Murphy, C. T. The role of insulin/IGF-like signaling in C. elegans longevity and aging. *Dis Model Mech* **3**, 415–419 (2010).
85. Lee, D., Son, H. G., Jung, Y. & Lee, S. J. V. The role of dietary carbohydrates in organismal aging. *Cellular and Molecular Life Sciences* **74**, 1793–1803 (2017).
86. Diot, C. *et al.* Bacterial diet modulates tamoxifen-induced death via host fatty acid metabolism. *Nature Communications 2022 13:1* **13**, 1–15 (2022).
87. Kim, D. H. Bacteria and the Aging and Longevity of Caenorhabditis elegans. *http://dx.doi.org/10.1146/annurev-genet-111212-133352* **47**, 233–246 (2013).
88. Lee, D. *et al.* SREBP and MDT-15 protect C. Elegans from glucose-induced accelerated aging by preventing accumulation of saturated fat. *Genes Dev* **29**, 2490–2503 (2015).
89. Watts, J. L. & Browse, J. Dietary manipulation implicates lipid signaling in the regulation of germ cell maintenance in C. elegans. *Dev Biol* **292**, 381–392 (2006).
90. Deline, M. L., Vrablik, T. L. & Watts, J. L. Dietary supplementation of polyunsaturated fatty acids in Caenorhabditis elegans. *Journal of Visualized Experiments* 1–7 (2013) doi:10.3791/50879.
91. Hillier, L. W. *et al.* Genomics in C. elegans: So many genes, such a little worm. *Genome Res* **15**, 1651–1660 (2005).
92. Kaletta, T. & Hengartner, M. O. Finding function in novel targets: C. elegans as a model organism. *Nature Reviews Drug Discovery 2006 5:5* **5**, 387–399 (2006).
93. Ahringer, J. Reverse genetics. *WormBook* 1–43 (2006) doi:10.1895/wormbook.1.47.1.

94. Singh, J. Harnessing the power of genetics: fast forward genetics in Caenorhabditis elegans. *Molecular Genetics and Genomics 2020 296:1* **296**, 1–20 (2020).
95. Kamath, R. S. & Ahringer, J. Genome-wide RNAi screening in Caenorhabditis elegans. *Methods* **30**, 313–321 (2003).
96. Zhang, H., Abraham, N., Khan, L. A. & Gobel, V. RNAi-based biosynthetic pathway screens to identify in vivo functions of non-nucleic acid – based metabolites such as lipids. **10**, (2015).
97. Yamamoto, S., Kanca, O., Wangler, M. F. & Bellen, H. J. Integrating non-mammalian model organisms in the diagnosis of rare genetic diseases in humans. *Nature Reviews Genetics 2023 25:1* **25**, 46–60 (2023).
98. Kurzchalia, T. V. & Ward, S. Why do worms need cholesterol? *Nature Cell Biology 2003 5:8* **5**, 684–688 (2003).
99. Dou, J., Chen, L., Hu, Y. & Miao, L. Cholesterol and the biosynthesis of glycosphingolipids are required for sperm activation in Caenorhabditis elegans. *Biochimica et Biophysica Acta (BBA) - Molecular and Cell Biology of Lipids* **1821**, 934–942 (2012).
100. Xatse, M. A., Vieira, A. F. C., Byrne, C. & Olsen, C. P. Targeted Lipidomics Reveals a Novel Role for Glucosylceramides in Glucose Response. *J Lipid Res* 100394 (2023) doi:10.1016/J.JLR.2023.100394.
101. Liebisch, G. *et al.* Update on LIPID MAPS classification, nomenclature, and shorthand notation for MS-derived lipid structures. *J Lipid Res* **61**, 1539–1555 (2020).
102. Bodhicharla, R., Devkota, R., Ruiz, M. & Pilon, M. Membrane fluidity is regulated cell nonautonomously by caenorhabditis elegans PAQR-2 and its Mammalian Homolog AdipoR2. *Genetics* **210**, 189–201 (2018).
103. Ma, D. K., Sun, F. & Robert Horvitz, H. Acyl-CoA Dehydrogenase Drives Heat Adaptation by Sequestering Fatty Acids. *Cell* **161**, 1152–1163 (2015).
104. Watts, J. L. Using Caenorhabditis elegans to uncover conserved functions of omega-3 and omega-6 fatty acids. *J Clin Med* **5**, (2016).
105. Klose, C., Surma, M. A. & Simons, K. Organellar lipidomics-background and perspectives. *Curr Opin Cell Biol* **25**, 406–413 (2013).
106. Kniazeva, M., Crawford, Q. T., Seiber, M., Wang, C. Y. & Han, M. Monomethyl branched-chain fatty acids play an essential role in Caenorhabditis elegans development. *PLoS Biol* **2**, (2004).
107. Kniazeva, M., Euler, T. & Han, M. A branched-chain fatty acid is involved in post-embryonic growth control in parallel to the insulin receptor pathway and its biosynthesis is feedback-regulated in C. elegans. *Genes Dev* **22**, 2102–2110 (2008).
108. Entchev, E. V *et al.* LET-767 Is Required for the Production of Branched Chain and Long Chain Fatty Acids in Caenorhabditis elegans * □. **283**, 17550–17560 (2008).
109. Eibler, D. *et al.* Unexpected Formation of Low Amounts of (R)-Configurated anteiso-Fatty Acids in Rumen Fluid Experiments. *PLoS One* **12**, e0170788 (2017).
110. Kniazeva, M., Zhu, H., Sewell, A. K. & Han, M. A Lipid-TORC1 Pathway Promotes Neuronal Development and Foraging Behavior under Both Fed and Fasted Conditions in C.elegans. *Dev Cell* **33**, 260–271 (2015).
111. Zhu, H., Sewell, A. K. & Han, M. Intestinal apical polarity mediates regulation of TORC1 by glucosylceramide in C. elegans. *Genes Dev* **29**, 1218–1223 (2015).

112. Zhu, M. *et al.* Monomethyl branched-chain fatty acid mediates amino acid sensing upstream of mTORC1. *Dev Cell* **56**, 2692-2702.e5 (2021).
113. Li, N. *et al.* A sphingolipid-mTORC1 nutrient-sensing pathway regulates animal development by an intestinal peroxisome relocation-based gut-brain crosstalk. *Cell Rep* **40**, (2022).
114. Zhang, J. *et al.* Mmbcfa c17iso ensures endoplasmic reticulum integrity for lipid droplet growth. *Journal of Cell Biology* **220**, (2021).
115. Simopoulos, A. P. The importance of the omega-6/omega-3 fatty acid ratio in cardiovascular disease and other chronic diseases. *Exp Biol Med* **233**, 674–688 (2008).
116. Simopoulos, A. P. Genetic variants in the metabolism of omega-6 and omega-3 fatty acids: their role in the determination of nutritional requirements and chronic disease risk. *https://doi.org/10.1258/ebm.2010.009298* **235**, 785–795 (2010).
117. Watts, J. L. & Browse, J. Genetic dissection of polyunsaturated fatty acid synthesis in Caenorhabditis elegans. *Proc Natl Acad Sci U S A* **99**, 5854–5859 (2002).
118. Harayama, T. & Shimizu, T. Roles of polyunsaturated fatty acids, from mediators to membranes. *J Lipid Res* **61**, 1150–1160 (2020).
119. Pinot, M. *et al.* Polyunsaturated phospholipids facilitate membrane deformation and fission by endocytic proteins. *Science (1979)* **345**, 693–697 (2014).
120. Vásquez, V., Krieg, M., Lockhead, D. & Goodman, M. B. Phospholipids that Contain Polyunsaturated Fatty Acids Enhance Neuronal Cell Mechanics and Touch Sensation. *Cell Rep* **6**, 70–80 (2014).
121. Hulbert, A. J., Kelly, M. A. & Abbott, S. K. Polyunsaturated fats, membrane lipids and animal longevity. *J Comp Physiol B* **184**, 149–166 (2014).
122. Reis, A. & Spickett, C. M. Chemistry of phospholipid oxidation. *Biochimica et Biophysica Acta (BBA) - Biomembranes* **1818**, 2374–2387 (2012).
123. Deline, M. *et al.* Epoxides Derived from Dietary Dihomo-Gamma-Linolenic Acid Induce Germ Cell Death in C. elegans. *Scientific Reports 2015 5:1* **5**, 1–10 (2015).
124. Walker, A. K. *et al.* A conserved SREBP-1/phosphatidylcholine feedback circuit regulates lipogenesis in metazoans. *Cell* **147**, 840–852 (2011).
125. Ding, W. *et al.* s-Adenosylmethionine Levels Govern Innate Immunity through Distinct Methylation-Dependent Pathways. *Cell Metab* **22**, 633–645 (2015).
126. Wehman, A. M., Poggioli, C., Schweinsberg, P., Grant, B. D. & Nance, J. The P4-ATPase TAT-5 Inhibits the Budding of Extracellular Vesicles in C. elegans Embryos. *Current Biology* **21**, 1951–1959 (2011).
127. Bahmanyar, S. *et al.* Spatial control of phospholipid flux restricts endoplasmic reticulum sheet formation to allow nuclear envelope breakdown. *Genes Dev* **28**, 121–126 (2014).
128. Perez, M. A. *et al.* Ether lipid deficiency disrupts lipid homeostasis leading to ferroptosis sensitivity. *PLoS Genet* **18**, e1010436 (2022).
129. Merrill, A. H. *et al.* Sphingolipidomics: A valuable tool for understanding the roles of sphingolipids in biology and disease. *J Lipid Res* **50**, 97–102 (2009).
130. Quinville, B. M., Deschenes, N. M., Ryckman, A. E. & Walia, J. S. A Comprehensive Review: Sphingolipid Metabolism and Implications of Disruption in Sphingolipid Homeostasis. *International Journal of Molecular Sciences 2021, Vol. 22, Page 5793* **22**, 5793 (2021).

131. Hänel, V., Pendleton, C. & Witting, M. The sphingolipidome of the model organism Caenorhabditis elegans. *Chem Phys Lipids* **222**, 15–22 (2019).
132. Menuz, V. *et al.* Protection of C. elegans from Anoxia by HYL-2 ceramide synthase. *Science (1979)* **324**, 381–384 (2009).
133. Mosbech, M. B. *et al.* Functional Loss of Two Ceramide Synthases Elicits Autophagy-Dependent Lifespan Extension in C. elegans. *PLoS One* **8**, e70087 (2013).
134. Marza, E., Simonsen, K. T., Færgeman, N. J. & Lesa, G. M. Expression of ceramide glucosyltransferases, which are essential for glycosphingolipid synthesis, is only required in a small subset of C. elegans cells. *J Cell Sci* **122**, 822–833 (2009).
135. Nomura, K. H. *et al.* Ceramide glucosyltransferase of the nematode Caenorhabditis elegans is involved in oocyte formation and in early embryonic cell division. *Glycobiology* **21**, 834–848 (2011).
136. Griffitts, J. S. *et al.* Glycolipids as receptors for Bacillus thuringienses crystal toxin. *Science (1979)* **307**, 922–925 (2005).
137. Wang, F. *et al.* Saturated very long chain fatty acid configures glycosphingolipid for lysosome homeostasis in long-lived C. elegans. *Nat Commun* **12**, 1–14 (2021).
138. Mosbech, M. B. *et al.* Functional Loss of Two Ceramide Synthases Elicits Autophagy-Dependent Lifespan Extension in C. elegans. *PLoS One* **8**, e70087 (2013).
139. Menuz, V. *et al.* Protection of C. elegans from Anoxia by HYL-2 ceramide synthase. *Science (1979)* **324**, 381–384 (2009).
140. Lochnit, G., Bongaarts, R. & Geyer, R. Searching new targets for anthelminthic strategies: Interference with glycosphingolipid biosynthesis and phosphorylcholine metabolism affects development of Caenorhabditis elegans. *Int J Parasitol* **35**, 911–923 (2005).
141. Laplante, M. & Sabatini, D. M. An Emerging Role of mTOR in Lipid Biosynthesis. *Current Biology* **19**, R1046–R1052 (2009).
142. Liu, G. Y. & Sabatini, D. M. mTOR at the nexus of nutrition, growth, ageing and disease. *Nat Rev Mol Cell Biol* **21**, 183–203 (2020).
143. Boland, S. *et al.* Phosphorylated glycosphingolipids essential for cholesterol mobilization in Caenorhabditis elegans. *Nature Chemical Biology 2017 13:6* **13**, 647–654 (2017).
144. Zhang, H. *et al.* Apicobasal domain identities of expanding tubular membranes depend on glycosphingolipid biosynthesis. *Nature Cell Biology 2011 13:10* **13**, 1189–1201 (2011).
145. Zhu, H., Shen, H., Sewell, A. K., Kniazeva, M. & Han, M. A novel sphingolipid-TORC1 pathway critically promotes postembryonic development in Caenorhabditis elegans. 1–19 (2013) doi:10.7554/eLife.00429.
146. Saxton, R. A. & Sabatini, D. M. mTOR Signaling in Growth, Metabolism, and Disease. *Cell* **168**, 960–976 (2017).
147. Yin, H., Xu, L. & Porter, N. A. Free radical lipid peroxidation: Mechanisms and analysis. *Chem Rev* **111**, 5944–5972 (2011).
148. Reis, A. & Spickett, C. M. Chemistry of phospholipid oxidation. *Biochimica et Biophysica Acta (BBA) - Biomembranes* **1818**, 2374–2387 (2012).
149. Mitchell, T. W., Buffenstein, R. & Hulbert, A. J. Membrane phospholipid composition may contribute to exceptional longevity of the naked mole-rat (Heterocephalus glaber): A comparative study using shotgun lipidomics. *Exp Gerontol* **42**, 1053–1062 (2007).

150. Xu, L., Davis, T. A. & Porter, N. A. Rate constants for peroxidation of polyunsaturated fatty acids and sterols in solution and in liposomes. *J Am Chem Soc* **131**, 13037–13044 (2009).
151. Greenberg, M. E. *et al.* The Lipid Whisker Model of the Structure of Oxidized Cell Membranes. *Journal of Biological Chemistry* **283**, 2385–2396 (2008).
152. Catalá, A. Lipid peroxidation modifies the picture of membranes from the "Fluid Mosaic Model" to the "Lipid Whisker Model". *Biochimie* **94**, 101–109 (2012).
153. Reis, A. Oxidative Phospholipidomics in health and disease: Achievements, challenges and hopes. *Free Radic Biol Med* **111**, 25–37 (2017).
154. Jiang, X., Stockwell, B. R. & Conrad, M. Ferroptosis: mechanisms, biology and role in disease. *Nature Reviews Molecular Cell Biology 2021 22:4* **22**, 266–282 (2021).
155. Aldrovandi, M., Fedorova, M. & Conrad, M. Juggling with lipids, a game of Russian roulette. *Trends in Endocrinology and Metabolism* **32**, 463–473 (2021).
156. Do, Q. & Xu, L. How do different lipid peroxidation mechanisms contribute to ferroptosis? *Cell Rep Phys Sci* **4**, (2023).
157. Niki, E. Lipid peroxidation: Physiological levels and dual biological effects. *Free Radic Biol Med* **47**, 469–484 (2009).
158. Nakabeppu, Y., Tsuchimoto, D., Yamaguchi, H. & Sakumi, K. Oxidative damage in nucleic acids and Parkinson's disease. *J Neurosci Res* **85**, 919–934 (2007).
159. Bochkov, V. N. *et al.* Generation and biological activities of oxidized phospholipids. *Antioxid Redox Signal* **12**, 1009–1059 (2010).
160. O'Donnell, V. B., Aldrovandi, M., Murphy, R. C. & Krönke, G. Enzymatically oxidized phospholipids assume center stage as essential regulators of innate immunity and cell death. *Sci. Signal* **12**, eaau2293 (2019).
161. Hajeyah, A. A., Griffiths, W. J., Wang, Y., Finch, A. J. & O'Donnell, V. B. The biosynthesis of enzymatically oxidized lipids. *Front. Endocrinol.* **11**, 591819 (2020).
162. Poitout, V. *et al.* Glucolipotoxicity of the pancreatic beta cell. *Biochimica et Biophysica Acta (BBA) - Molecular and Cell Biology of Lipids* **1801**, 289–298 (2010).
163. Rui, L. Energy Metabolism in the Liver. *Compr Physiol* **4**, 177–197 (2014).
164. Petersen, M. C., Vatner, D. F. & Shulman, G. I. Regulation of hepatic glucose metabolism in health and disease. *Nat Rev Endocrinol* **13**, 572–587 (2017).
165. Svensson, E. *et al.* The Adiponectin receptor homologs in C. elegans promote energy utilization and homeostasis. *PLoS One* **6**, (2011).
166. Ruiz, M. *et al.* Membrane fluidity is regulated by the C. Elegans transmembrane protein FLD-1 and its human homologs TLCD1/2. *Elife* **7**, (2018).
167. Wallace, M. *et al.* Enzyme promiscuity drives branched-chain fatty acid synthesis in adipose tissues. *Nat Chem Biol* **14**, 1021–1031 (2018).
168. Vrablik, T. L. & Watts, J. L. Emerging roles for specific fatty acids in developmental processes. *Genes Dev* **26**, 631–637 (2012).
169. Jiang, W. & Ogretmen, B. Autophagy paradox and ceramide. *Biochimica et Biophysica Acta - Molecular and Cell Biology of Lipids* vol. 1841 783–792 Preprint at https://doi.org/10.1016/j.bbalip.2013.09.005 (2014).
170. Haimovitz-Friedman, A., Kolesnick, R. N. & Fuks, Z. Ceramide signaling in apoptosis. *Br Med Bull* **53**, 539–553 (1997).

171. Pattingre, S., Bauvy, C., Levade, T., Levine, B. & Codogno, P. Ceramide-induced autophagy: To junk or to protect cells? *Autophagy* **5**, 558 (2009).
172. Hannun, Y. A. & Obeid, L. M. Many Ceramides *. *Journal of Biological Chemistry* **286**, 27855–27862 (2011).
173. Turpin-Nolan, S. M. & Brüning, J. C. The role of ceramides in metabolic disorders: when size and localization matters. *Nature Reviews Endocrinology 2020 16:4* **16**, 224–233 (2020).
174. Iwabuchi, K., Nakayama, H., Iwahara, C. & Takamori, K. Significance of glycosphingolipid fatty acid chain length on membrane microdomain-mediated signal transduction. *FEBS Lett* **584**, 1642–1652 (2010).
175. Sezgin, E., Levental, I., Mayor, S. & Eggeling, C. The mystery of membrane organization: composition, regulation and roles of lipid rafts. *Nat. Rev. Mol. Cell. Biol.* **18**, 361–374 (2017).
176. Aerts, J. M. F. G., Artola, M., van Eijk, M., Ferraz, M. J. & Boot, R. G. Glycosphingolipids and Infection. Potential New Therapeutic Avenues. *Front Cell Dev Biol* **7**, 324 (2019).
177. Okada, M. *et al.* b-series Ganglioside deficiency exhibits no definite changes in the neurogenesis and the sensitivity to Fas-mediated apoptosis but impairs regeneration of the lesioned hypoglossal nerve. *Journal of Biological Chemistry* **277**, 1633–1636 (2002).
178. Wu, G., Lu, Z. H., Kulkarni, N., Amin, R. & Ledeen, R. W. Mice lacking major brain gangliosides develop Parkinsonism. *Neurochem Res* **36**, 1706–1714 (2011).
179. Hartler, J. *et al.* Automated Annotation of Sphingolipids including Accurate Identification of Hydroxylation Sites Using MS nData. *Anal Chem* **92**, 14054–14062 (2020).
180. Sampaio, J. L. *et al.* Membrane lipidome of an epithelial cell line. *Proc Natl Acad Sci U S A* **108**, 1903–1907 (2011).
181. Shmookler Reis, R. J. *et al.* Modulation of lipid biosynthesis contributes to stress resistance and longevity of C. elegans mutants. *Aging* **3**, 125–147 (2011).
182. Alcántar-Fernández, J., Navarro, R. E., Salazar-Martínez, A. M., Pérez-Andrade, M. E. & Miranda-Ríos, J. Caenorhabditis elegans respond to high-glucose diets through a network of stress-responsive transcription factors. *PLoS One* **13**, 1–24 (2018).
183. Schlotterer, A. *et al.* C. elegans as model for the study of high glucose-mediated life span reduction. *Diabetes* **58**, 2450–2456 (2009).
184. O'Donnell, V. B., Rossjohn, J. & Wakelam, M. J. O. Phospholipid signaling in innate immune cells. *J. Clin. Invest.* **128**, 2670–2679 (2018).
185. Dixon, S. J. & Stockwell, B. R. The hallmarks of ferroptosis. *Annu Rev Cancer Biol* **3**, 35–54 (2019).
186. Kagan, V. E. *et al.* Oxidized arachidonic and adrenic PEs navigate cells to ferroptosis. *Nat Chem Biol* **13**, 81–90 (2017).
187. DeFilippis, A. P. *et al.* Circulating levels of plasminogen and oxidized phospholipids bound to plasminogen distinguish between atherothrombotic and non-atherothrombotic myocardial infarction. *J Thromb Thrombolysis* **42**, 61–76 (2016).
188. Hammad, L. A. *et al.* Elevated levels of hydroxylated phosphocholine lipids in the blood serum of breast cancer patients. *Rapid Communications in Mass Spectrometry* **23**, 863–876 (2009).

189. Wu, R. P. *et al.* Nrf2 responses and the therapeutic selectivity of electrophilic compounds in chronic lymphocytic leukemia. *Proc Natl Acad Sci U S A* **107**, 7479–7484 (2010).
190. Montine, T. J. *et al.* F2-Isoprostanes in Alzheimer and Other Neurodegenerative Diseases. *https://home.liebertpub.com/ars* **7**, 269–275 (2004).
191. Hulbert, A. J., Pamplona, R., Buffenstein, R. & Buttemer, W. A. Life and death: Metabolic rate, membrane composition, and life span of animals. *Physiol Rev* **87**, 1175–1213 (2007).
192. Ni, Z., Angelidou, G., Hoffmann, R. & Fedorova, M. LPPtiger software for lipidome-specific prediction and identification of oxidized phospholipids from LC-MS datasets. *Scientific Reports 2017 7:1* **7**, 1–14 (2017).
193. Spickett, C. M. & Pitt, A. R. Oxidative lipidomics coming of age: Advances in analysis of oxidized phospholipids in physiology and pathology. *Antioxid Redox Signal* **22**, 1646–1666 (2015).
194. Nakanishi, H., Iida, Y., Shimizu, T. & Taguchi, R. Analysis of oxidized phosphatidylcholines as markers for oxidative stress, using multiple reaction monitoring with theoretically expanded data sets with reversed-phase liquid chromatography/tandem mass spectrometry. *Journal of Chromatography B* **877**, 1366–1374 (2009).
195. Yin, H. *et al.* Identification of intact oxidation products of glycerophospholipids in vitro and in vivo using negative ion electrospray iontrap mass spectrometry. *Journal of Mass Spectrometry* **44**, 672–680 (2009).
196. Murphy, M. P. *et al.* Guidelines for measuring reactive oxygen species and oxidative damage in cells and in vivo. *Nature Metabolism 2022 4:6* **4**, 651–662 (2022).
197. Ayala, A., Muñoz, M. F. & Argüelles, S. Lipid peroxidation: Production, metabolism, and signaling mechanisms of malondialdehyde and 4-hydroxy-2-nonenal. *Oxid Med Cell Longev* **2014**, (2014).
198. Yang, B. *et al.* Yin-yang mechanisms regulating lipid peroxidation of docosahexaenoic acid and arachidonic acid in the central nervous system. *Frontiers in Neurology* vol. 10 Preprint at https://doi.org/10.3389/fneur.2019.00642 (2019).
199. Ni, Z., Milic, I. & Fedorova, M. Identification of carbonylated lipids from different phospholipid classes by shotgun and LC-MS lipidomics. *Anal Bioanal Chem* **407**, 5161–5173 (2015).
200. Milic, I., Hoffmann, R. & Fedorova, M. Simultaneous detection of low and high molecular weight carbonylated compounds derived from lipid peroxidation by electrospray ionization-tandem mass spectrometry. *Anal Chem* **85**, 156–162 (2013).
201. Criscuolo, A. *et al.* Analytical and computational workflow for in-depth analysis of oxidized complex lipids in blood plasma. *Nature Communications 2022 13:1* **13**, 1–13 (2022).
202. Wölk, M., Prabutzki, P. & Fedorova, M. Analytical Toolbox to Unlock the Diversity of Oxidized Lipids. *Acc Chem Res* **56**, 835–845 (2023).
203. Kamath, R. S. *et al.* Systematic functional analysis of the Caenorhabditis elegans genome using RNAi. *Nature* **421**, 231–237 (2003).
204. Jenkins, N. L. *et al.* Changes in ferrous iron and glutathione promote ferroptosis and frailty in aging caenorhabditis elegans. *Elife* **9**, 1–28 (2020).
205. Ni, Z., Milic, I. & Fedorova, M. Identification of carbonylated lipids from different phospholipid classes by shotgun and LC-MS lipidomics. *Anal Bioanal Chem* **407**, 5161–5173 (2015).

206. Beydoun, S. *et al.* An alternative food source for metabolism and longevity studies in Caenorhabditis elegans. *Communications Biology 2021 4:1* **4**, 1–9 (2021).
207. Hartler, J. *et al.* Deciphering lipid structures based on platform-independent decision rules. *Nature Methods 2017 14:12* **14**, 1171–1174 (2017).
208. Adams, K. J. *et al.* Skyline for Small Molecules: A Unifying Software Package for Quantitative Metabolomics. *J Proteome Res* **19**, 1447–1458 (2020).
209. Kingsley, S. F. *et al.* Bacterial processing of glucose modulates C. elegans lifespan and healthspan. *Sci Rep* **11**, 1–12 (2021).
210. Kagan, V. E. *et al.* Redox phospholipidomics of enzymatically generated oxygenated phospholipids as specific signals of programmed cell death. *Free Radic Biol Med* **147**, 231–241 (2020).
211. Lamade, A. M. *et al.* Inactivation of RIP3 kinase sensitizes to 15LOX/PEBP1-mediated ferroptotic death. *Redox Biol* **50**, 102232 (2022).
212. Wenzel, S. E. *et al.* PEBP1 Wardens Ferroptosis by Enabling Lipoxygenase Generation of Lipid Death Signals. *Cell* **171**, 628-641.e26 (2017).
213. Rodencal, J. & Dixon, S. J. A tale of two lipids: Lipid unsaturation commands ferroptosis sensitivity. *Proteomics* **23**, 2100308 (2023).
214. López-Otín, C., Blasco, M. A., Partridge, L., Serrano, M. & Kroemer, G. The hallmarks of aging. *Cell* **153**, 1194 (2013).
215. Kenyon, C. J. The genetics of ageing. *Nature* **464**, 504–512 (2010).
216. Johnson, A. A. & Stolzing, A. The role of lipid metabolism in aging, lifespan regulation, and age-related disease. *Aging Cell* **18**, e13048 (2019).
217. Luo, J., Mills, K., le Cessie, S., Noordam, R. & van Heemst, D. Ageing, age-related diseases and oxidative stress: What to do next? *Ageing Res Rev* **57**, 100982 (2020).
218. Chen, T. L. *et al.* Impaired embryonic development in glucose-6-phosphate dehydrogenase-deficient Caenorhabditis elegans due to abnormal redox homeostasis induced activation of calcium-independent phospholipase and alteration of glycerophospholipid metabolism. *Cell Death & Disease 2017 8:1* **8**, e2545–e2545 (2017).
219. Diot, C. *et al.* Bacterial diet modulates tamoxifen-induced death via host fatty acid metabolism. *Nature Communications 2022 13:1* **13**, 1–15 (2022).